Table 4
Recent theoretical calculations of phase stability or phase diagrams.

Type of calculation	Quantities calculated	Typical references
semi-empirical (charge density, size and electronegativity effects)	enthalpy of mixing, ΔH_f	MIEDEMA *et al.* [1980] MIEDEMA and NIESSEN [1988]
Pair potentials	alloy stabilities ΔH_{transf} (at 0 K)	MACHLIN [1981]
Mainly *d*-band effects	maps of related structures and their stability, ΔH_f	PETTIFOR [1986, 1979] WATSON and BENNETT [1979, 1983] YUKAWA *et al.* [1985]
Mainly valence band effects	relative alloy stabilities density of states	MOTT and JONES [1936] BREWER [1968] MASSALSKI and MIZUTANI [1978]
Cluster variation models	ordering energies, order–disorder	DE FONTAINE [1983] R. KIKUCHI [1981]
	ΔH_f (at 0 K) of simple systems	WILLIAMS *et al.* [1982]
First principles calculation using various atomic potentials: DFT, LSDA, KKR-CPA, LMTO	ΔH_{transf} (at 0 K) lattice dynamics, ordered compound stabilities	YIN and COHEN [1982] XU *et al.* [1987] PEI *et al.* [1989]
	simple phase diagrams	STOCKES and WINTER [1984] HAFFNER [1983] TERAKURA *et al.* [1987, 1988]

(ii) Formation of stable intermediate compounds will restrict primary solid solubility. The likelihood of the formation of such compounds in an alloy system is related to the chemical affinity of the participating elements and will be increased the more electronegative one of the elements and the more electropositive the other. The general principle leading to the restriction of solid solubility is illustrated in fig. 4 using hypothetical free-energy curves for a primary solid solution and for an intermediate phase. The width of the shaded area represents the extent of primary solid solubility; it becomes more restricted the greater the stability of the intermediate phase. The above

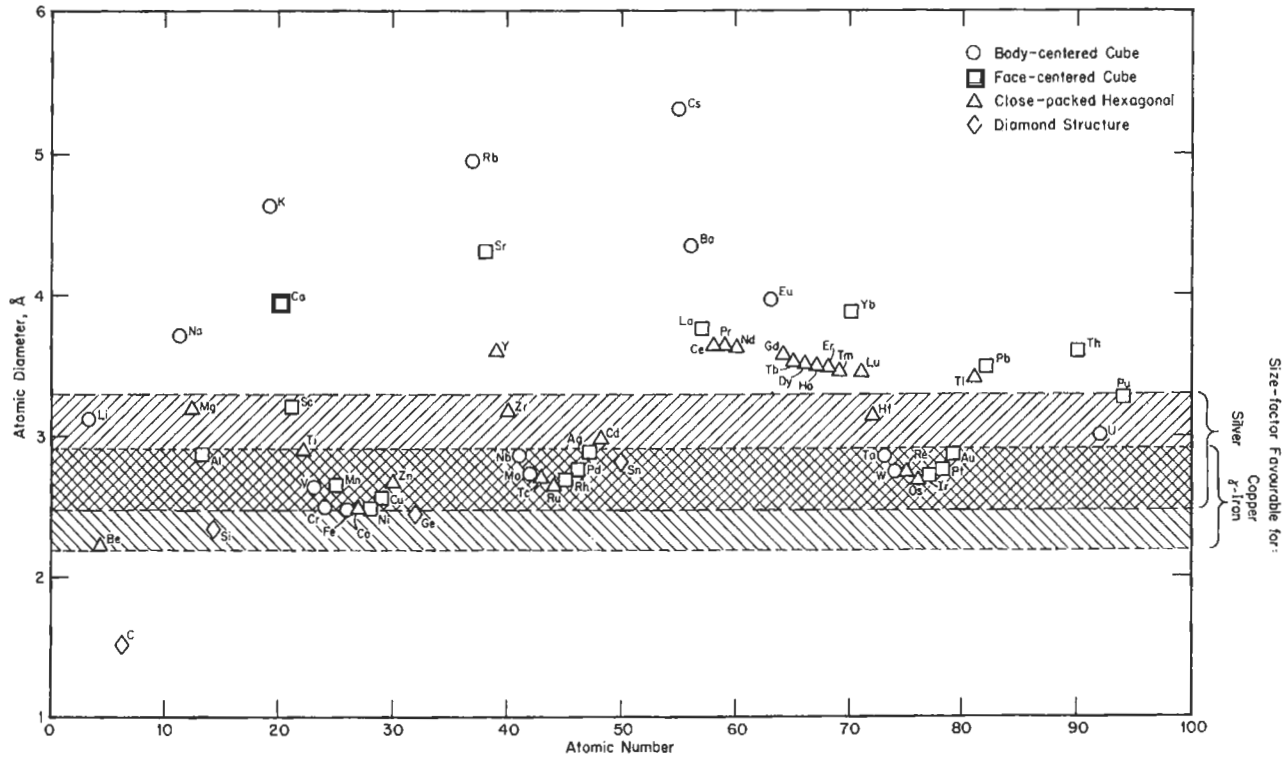

Fig. 3. Illustration of the application of the size-factor principle to solid solutions in copper, silver and γ-iron. The ordinates show the atomic diameters as defined by the closest distance of approach of the atoms in the crystals of elements. The shaded areas show the ranges of favorable size-factor, bounded by the limits ± 15% of the atomic diameters of silver, copper, and γ-iron, respectively. The types of structures involved are indicated by different symbols. (After HUME-ROTHERY [1961a].)

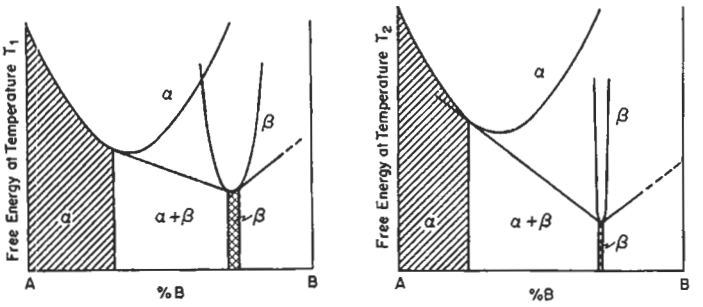

Fig. 4. Restriction of primary solid solubility due to stability of an intermediate phase.

principle has become known as the *electrochemical effect*, which is related to the difference in the electronegativities of the two components.

(iii) Empirical studies have shown that in many alloy systems one of the most important factors determining the extent of solid solubility and the stability of certain intermediate phases is *the electron concentration*. This parameter is usually taken to denote the number of all valence electrons per unit cell provided that all atomic sites within the structure are occupied. Alternatively, electron concentration may be taken as the ratio of all valence electrons to the number of atoms. It is then denoted as e/a.

Following the early investigations by Hume–Rothery and his associates it was also suggested that the mutual solid solubility of two given elements was related to their respective valencies, namely, that the amount of the solid solution in the element of lower valency was always greater than vice versa. This general principle is sometimes known as the *relative valency effect*. It appears to be valid when copper, silver or gold, which are monovalent, are alloyed with the B-subgroup elements of the Periodic Table which possess valencies greater than one. It may be associated in part with the fact that the Brillouin zones of the noble metals are only partially filled with electrons; and, although they are touched by the Fermi surface, they are not overlapped as are the Brillouin zones of the B-subgroup elements. A more likely cause, however, has its origin in the long-range charge oscillations around the impurity atoms as discussed by FRIEDEL [1964] and BLANDIN [1965].

Subsequent appraisals by HUME–ROTHERY [1961a] and GSCHNEIDNER [1980] suggest that the relative valency effect is not really a general principle, and that when two elements which are both of high valency are alloyed together it is often not possible to predict which of the two will form the more extensive solid solution with respect to the other.

5. *The meaning of "electron concentration"*

In the study of alloys it is often convenient to use the electron concentration, rather than atomic or weight composition, as a parameter against which various properties can be plotted. In the case of the alloys of the noble metals, the use of electron concentration has been particularly successful since it almost never fails to bring about interesting

correlations when applied to experimental data. Nevertheless, the physical meaning of electron concentration is by no means as simple as that of chemical composition, and as time progresses it has become increasingly more difficult to "visualize" the process by means of which valence electrons which belong to the solvent and the solute atoms become a common property of the conduction band of an alloy. Usually only the s and p electrons are considered as taking part in such a process, but occasionally the total number of electrons outside the inert-gas core (i.e., s + p + d electrons) has been used to denote the electron concentration (see below). In the B-subgroup elements which follow the noble metals in the respective horizontal rows of the Periodic Table the d bands in the free atoms are fully occupied by electrons. It has been considered for a long time, therefore, that on alloying only the s and p electrons are involved, but the possibility of transfer of electrons from the d band to the conduction band, and the s–d hybridization, makes the situation more complex. There is no doubt that the presence of d-band electrons sufficiently near the Fermi level in alloys of the noble metals and the changes in the energy of the d-band electrons on alloying constitute an important contribution to the electronic structure. This contribution is at present not fully understood but progress continues to clarify the picture. Calculations of the cohesive energy of the noble metals, using the assumption that only the s electrons are important, yield values which are far too low when compared with experimental data. In fact, as pointed recently by COTTRELL [1988], the cohesion of a metal like copper is mainly the result of attraction brought about by the sd hybridized electrons and the positive ions, while that part of the electronic system which corresponds to the classical free-electron gas is actually pushing the atoms apart (see below).

On the other hand, on alloying, even if it is assumed that the d band may be ignored and that certain elements possess a well-defined valence (for example, copper = 1, zinc = 2, gallium = 3, etc.), it is not certain whether all of the (s + p) electrons of a solute element go into the conduction band of the alloy. FRIEDEL [1954a] has suggested that in an alloy some of the s + p electrons may lie in *bound states* near the solute nuclei. According to MOTT [1952] such elements as zinc, gallium, germanium, etc., when dissolved in copper certainly contribute at least one electron to the conduction band. The next electron may or may not be in a bound state, while the additional electrons in gallium and germanium almost certainly are in bound states. Nevertheless, it has been suggested by FRIEDEL [1954a] and others that the valence-electron concentration rules may remain valid if one assumes that the potential acting on conduction electrons in an alloy "subtracts" from the bottom of the conduction band as many bound states as there are electrons in the bound atomic orbitals. Hence, the relationship between the effective conduction electrons and the band structure may be such that the Brillouin-zone effects, associated with the stability of phases and certain other alloy properties, may remain relatively unaltered. For further discussion of this and related subjects see FRIEDEL [1954a], HUME–ROTHERY and COLES [1954], COTTRELL [1988], and the proceedings of recent symposia (RUDMAN *et al.* [1967], BENNETT [1980], GONIS and STOCKS [1989]).

In alloy systems which involve transition elements, rare earths, actinides, lanthanides and transuranic elements, the assessment of valence and the corresponding changes in electron concentration are open to quite wide speculation. Often they depend on the

nature of the particular problem to be considered. Thus, many striking regularities are frequently revealed in a group of related elements, or alloy systems, provided that some valence scheme is adopted against which various properties within the group can be compared. For example, a rather abrupt change occurs in the electronic specific heat, magnetic susceptibility, Hall coefficient, hydrogen absorption, etc., in the transition metals and alloys of the first long period at an electron concentration of about 5.7 (MOTT [1962]) provided that the numbers of electrons outside the inert-gas core are considered to represent their valence, i.e., 4, 5, 6, 7, 8 and 9 for Ti, V, Cr, Mn, Fe and Co respectively. At the same time the valencies of these same elements when in dilute solution in the noble metals or aluminium are usually assessed according to a diffferent scheme in which only the predominantly s electrons are included. Considerations of phase stability (HUME–ROTHERY [1966] and RAYNOR [1956]) and changes of axial ratio (MASSALSKI [1958], MASSALSKI and KING [1960], COCKAYNE and RAYNOR [1961] and HENDERSON and RAYNOR [1962]) suggest that the above transition elements possess much lower, and possibly variable, valencies in the range between 0 and 2.

In a similar way, valence schemes have been suggested for other alloy groups, but will not be discussed here.

5.1. Progress in the electronic theories of metals and alloys

The distinction between metals, semi-metals and insulators, in terms of Brillouin zones, energy bands and the related overlapping or separation of bands, which has been for many years the basis in physics for defining what is a metal, has become somewhat blurred in recent years. COTTRELL [1988] points out that there are many substances that show metallic conductivity (or even superconductivity) even though clearly they are not metals in other aspects. (For example TCNQ, or certain ceramic oxides). When sufficient pressure is applied, electronic clouds of individual atoms are forced to overlap more and more, with the result that additional outer electrons in atoms will cease to belong to any particular atomic orbital and will behave as nearly free, contributing to metallic conductivity and bonding. Thus, the traditional view that the outer electrons (i.e., the valence electrons) become the "bonding glue" when atoms are assembled into crystals has become quite blurred.

In the earlier theories of Brillouin zones and Fermi surfaces the Bloch wavefunctions were used as a basis for calculation. Metals and solid solutions were considered as regular arrays of ions immersed in a "sea" of conduction electrons. The potential in a crystal was considered to be a periodically varying quantity corresponding to the periodicity of the ionic lattice and being more or less atomic (i.e. rapidly falling) in character near each ion. Bloch was able to show that wave functions of the conduction electrons for which the potential energy was modulated by the periodicity of the lattice were valid solutions of the Schrödinger equation. The resulting Bloch model has served as a very successful basis for discussion of the motion of electrons in metals and alloys. Only the conduction electrons, moving without electrostatic interactions with one another, were considered, and their motion was described by one-particle functions. Hence only the kinetic energy of the electrons was involved.

References: p. 199.

Subsequent developments in the electron theory have introduced a number of important modifications to the above model. It was found that the description of electronic properties was more consistent with experimental data if only weak *electron-ion* interactions were assumed, i.e., if the periodical potential was not considered to be atomic in character near each ion but only weakly changing from ion to ion. At the same time the additional problem of having to allow for possible strong *electron-electron* interactions was removed by considering that the Bloch model describes the motion, not of one-electron particles but of more complex entities, called *quasi particles*, introduced by Landau. Quasi particles have an electron at the center, surrounded by a region of electron deficiency (correlation hole) and a further region containing electrons that have been pushed out by the Coulombic repulsion away from the central electron and "flow around it much as water flows around a moving particle" (COHEN [1965]).

The problem of looking realistically at electron-atom interactions in order to reconcile the difference between the atomic and the effective potential in a metallic lattice has been tackled by introducing the notion of a *pseudopotential*. In this treatment the electron wave functions near the ions are ignored to some extent and substituted by pseudo wave functions which have the effect of statistically excluding the valence electrons from regions of space occupied by core electrons. (See ch. 2, § 3.3.) The application of the theory of pseudo-potentials has been very useful to the understanding of some problems in the theory of alloys (HEINE [1967] and STROUD [1980]). Other developments, as already mentioned in section 3, involve calculations of electronic energies "ab initio", and various elaborate treatments of the atomic potentials in solid solutions (see for example, FAULKNER [1982] and COTTRELL [1988]).

6. *Termination of primary solid solubility*

6.1. Electronic theories of primary solid solutions based on noble metals

A survey of binary systems of copper, silver and gold with a large number of elements, and in particular with the B-subgroup elements, has shown that the observed ranges of primary solid solubility may be correlated with electron concentration (HUME–ROTHERY and RAYNOR [1940]). In fig. 5 the maximum ranges* of primary solid solutions based on the three noble metals are indicated as linear plots in terms of e/a for the cases where these solutions are followed by an intermediate phase with a close-packed hexagonal structure (fig. 5a) and, separately, when they are followed by an intermediate phase with the body-centred cubic structure (fig. 5b). Apart from the systems Cu–In and Cu–Sn, the primary solutions followed by the cubic phase reach somewhat higher values of e/a than when followed by the close-packed hexagonal phase.

* It must be remembered that these maximum ranges occur at different temperatures in each system. Strictly speaking the correlation with e/a should apply only at the absolute zero of temperature. The fact that a significant correlation is observed at relatively high temperatures suggests that the electronic factors play a predominant role even at those high temperatures, although entropy considerations undoubtedly also play a role.

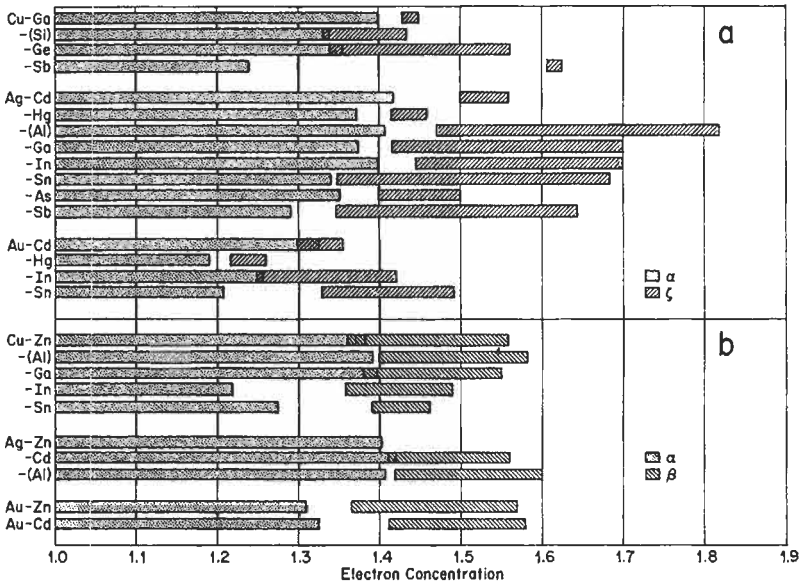

Fig. 5. Extent of the maximum primary solid solubility and of the following intermediate phase in alloys based on the noble metals (see text).

Examination of fig. 5 reveals that in silver-based alloys the primary solid solutions terminate within a fairly close range of values near $e/a = 1.4$, whereas in copper-based alloys the e/a values show a wider scatter, but the range of maximum values is again only a little less than 1.4. In the case of gold-based alloys the primary solid solubility is further restricted ranging between 1.2 and 1.3.

The above correlation between the primary solubility and e/a does not lead to any unique value, but it is quite striking when compared with similar plots drawn as a function of composition. Hence, it has been suspected for a long time that there must be an important link between the primary solid solubility and the electronic structure. During the 1930s an attempt was made by JONES [1937] to calculate the primary solid solubility of alloys based on copper using the theory of Brillouin zones and Bloch functions. This approach, and subsequent developments, are extensively quoted in metallurgical literature and will be discussed briefly below.

The main assumptions of the Jones model were: (i) that the *nearly-free-electron approximation* could be extended from pure metals to random solid solutions, and (ii) that the *rigid-band condition* was applicable on alloying (i.e., that the shape of the density of states curve $N(E)$ for a pure solvent remains unchanged on alloying and that the band gaps in the Brillouin zone do not change in magnitude, the only change being in the number of loosely-bound electrons). The general idea regarding stability of alloy phases was that at certain values of the electron concentration the Brillouin zone of one structure may be associated with a high density of quantum states, $N(E)$, at relatively low values of energy and thus "accommodate" the available electrons within lower total energy than

would be possible in the zone of some other structure. This condition is particularly likely to occur in the range of energies associated with contact between the Fermi surface and Brillouin-zone faces since it results in a peak in the density of states. The connection between phase stability and a peak in the density-of-states curve had been established earlier (JONES [1934a]) for the case of the γ-brass structure.

In 1937 JONES considered in detail the theory of the α–β phase boundary in the Cu–Zn system where the face-centred cubic primary solid solution (α) is succeeded by the body-centred cubic intermediate phase (β). Using the same values of the atomic volume for both α and β phases and making them equal to that of copper, and using the same values of energy gaps as those obtained for copper from optical properties ($\Delta E = 4.1$ eV), Jones calculated the density-of-states curves for both phases in terms of energy expressed in electron volts. The result of the calculation is shown schematically* in fig. 6a. The first peak in the density-of-states curve for the α-phase occurs at about 6.6 eV. When compared with the free electron energy at the center of the {111} faces in the Brillouin zone, 6.5 eV, this suggested that the contact between the Fermi surface and these faces should occur in the α-phase already at an early stage of alloying. Many years later PIPPARD [1958] showed that this contact in fact already exists in pure copper. Interpreted in terms of e/a, the two peaks shown in fig. 6a correspond to $e/a \approx 1.0$ for the α phase and $e/a \approx 1.23$ for the β phase, respectively, and are therefore unlikely to be associated in a simple way with the termination of the primary solid solubility ($e/a \approx 1.4$), or the optimum range of stability for the β phase ($e/a \approx 1.5$). The diagram in fig. 6a is, nevertheless, of interest because of its general emphasis on the relationship between phase stability and the density of states. Actual electronic energy relationships are more likely to be like those shown in fig. 6b, according to which the largest differences between the Fermi energy of free-electron gas and the Fermi energies of electrons in the Brillouin zone of the α and β phases occur at some points to the right of the peaks $\{111\}\alpha$ and $\{110\}\beta$ in the density of states (JONES [1962]). The actual α–β phase boundary will then be determined by the common tangent principle (BLANDIN [1965]). Thus, it appears that while the e/a parameter is indeed important in the α phases, as was thought by Hume–Rothery, their stability ranges also are very strongly influenced by additional factors. For example, each particular range strongly depends on the type of crystal structure that follows a given α phase in a given phase diagram (this is illustrated in fig. 5), as would be expected from phase competition. In addition, it has also been shown by AHLERS [1981] that the part of the configurational cohesive energy in the α phases, which is related to the third nearest neighbor interactions constitutes a large additional part of their total energy. Configurational energy is the difference between the ground state energy (at 0 K) and the heat of formation. While this complicates the simple original picture of α-phase stability in terms of e/a (and the related notions connected with the density of states [$N(E)$] and Fermi surfaces), there is outstanding agreement between the experimentally determined behavior of the electronic specific heats (from

* For actual curves, reference should be made to the original paper (JONES [19371]). Additional discussion may be found in a later review article (MASSALSKI and MIZUTANI [1978]).

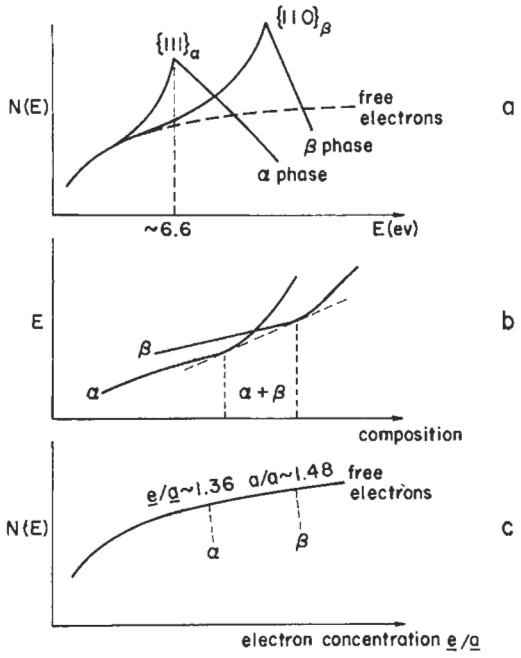

Fig. 6. Schematic models proposed to account for the primary solid solubility of alloys based on copper: (a) Jones model: band gap across the {111} faces of the zone for the fcc structure = gap across the {110} faces of the zone for the bcc structure ≈ 4.1 eV; (b) total electronic energy $E=\int_0^{E_F} N(E)\mathrm{d}E$, corresponding to the density of states as modified by the interactions with the respective Brillouin zones; (c) density of states for free electrons.

which the density of states at the Fermi level can be derived) and the predicted density of states obtained from a parameter-free calculation based on the KKR-CPA approximation (FAULKNER and STOCKS [1981]). This means that the electronic structure of the α phases is now well understood and the path is clear for a detailed stability calculation of these phases in the near future.

Incorporation of the original Jones model into metallurgical literature has led to a good deal of confusion about the relationship between phase stability and the contact between the Fermi surface and the Brillouin-zone faces. One must appreciate the difference between the attempt by Jones to calculate the relative stability of two adjoining phases in terms of the contact between Fermi surfaces and certain Brillouin-zone faces with assumed large energy gaps and in terms of additional thermodynamic quantities, and similar attempts in terms of *spherical* Fermi surfaces. The use of spherical surfaces amounts to merely calculating the electron concentration at which an inscribed *Fermi sphere* would contact the zone faces. In the latter case, the zone faces by implication should possess zero energy gaps. As pointed out by HUME–ROTHERY [1964], this important conclusion has been often overlooked in metallurgical literature. Free-electron calculation shows that contact of a Fermi *sphere* with the Brillouin zone would be obtained in the α phase at 1.36 electrons per atom and in the β phase at 1.48 electrons

per atom (see fig. 6c), and these values are strikingly close to the experimental observation. This, however, must now be regarded as rather fortuitous, at least for the α phases, because it has been proved beyond dispute that the Fermi surface is considerably distorted from a sphere in the [111] direction and touches the set of {111} Brillouin-zone faces in all three noble metals, Cu, Ag and Au (HARRISON and WEBB [1960]). Further comments of developments in this field may be found in a review article by MASSALSKI and MIZUTANI [1978].

6.2. Primary solid solubility in transition metal alloys

Hume–Rothery's further work has shown that electron-concentration principles similar to those established for the noble metals and their alloys apply also to the solid solutions of a number of transition metals, particularly those with the fcc structure (HUME–ROTHERY [1966]). Figure 7 shows the limits of solid solutions in Rh, Pd, Ir and Pt in terms of the *average group number* (AGN) which denotes all electrons outside the rare-gas shell. The general tendency appears to be for the fcc solid solutions to extend back to an AGN value of about 8.4. A similar effect is found for solid solutions of V and Cr in fcc γ-Fe, and in Ni. The behavior in bcc metals has not been generally examined. However, similar correlations may exist. For example, the solid solubilities of Rh and Ru in bcc Mo terminate at a similar value of AGN of about 6.6 (HUME–ROTHERY [1967]).

7. *The atomic size in solid solutions*

On forming a solid solution of element A with element B, two different kinds of atoms come in contact on a common lattice. This inclusion of new centers of disturbance will affect the existing electronic force fields between atoms, both short range and long range; the resulting effects will be of several kinds. On the atomic scale some atoms of the solvent and the solute will be shifted from the mean atomic positions on the lattice and thus suffer a permanent static displacement. The resulting average distance between any two neighboring atoms in a solid solution will depend on whether they are of the like kind, either both solvent or both solute, or of the opposite kind. We may thus talk of the average AA, BB or AB bond distances which may, even for an identical pair of atoms, depend also on the direction in the lattice.

In addition to local displacements, the average distances between lattice planes may also change and we may talk of the change in the *lattice spacings* and, related to them, the volume of the unit cell. Both the lattice spacings and the volume of the unit cell are not related to the actual size of any particular atom.

The relationship between lattice spacings, space lattice and the individual position of atoms may be summarized as follows: the space lattice represents a repetition in space of an elementary unit known as the *unit cell* (fig. 8). The lattice spacings describe the linear dimensions of the unit cell. To a certain extent a unit cell may be chosen quite arbitrarily so that, for example, in the face-centred cubic structure shown in fig. 8b three different unit cells are possible — rhombohedral, face-centred cubic and body-centred tetragonal. The cell which reveals the essential symmetry is cubic; if the X-ray reflections

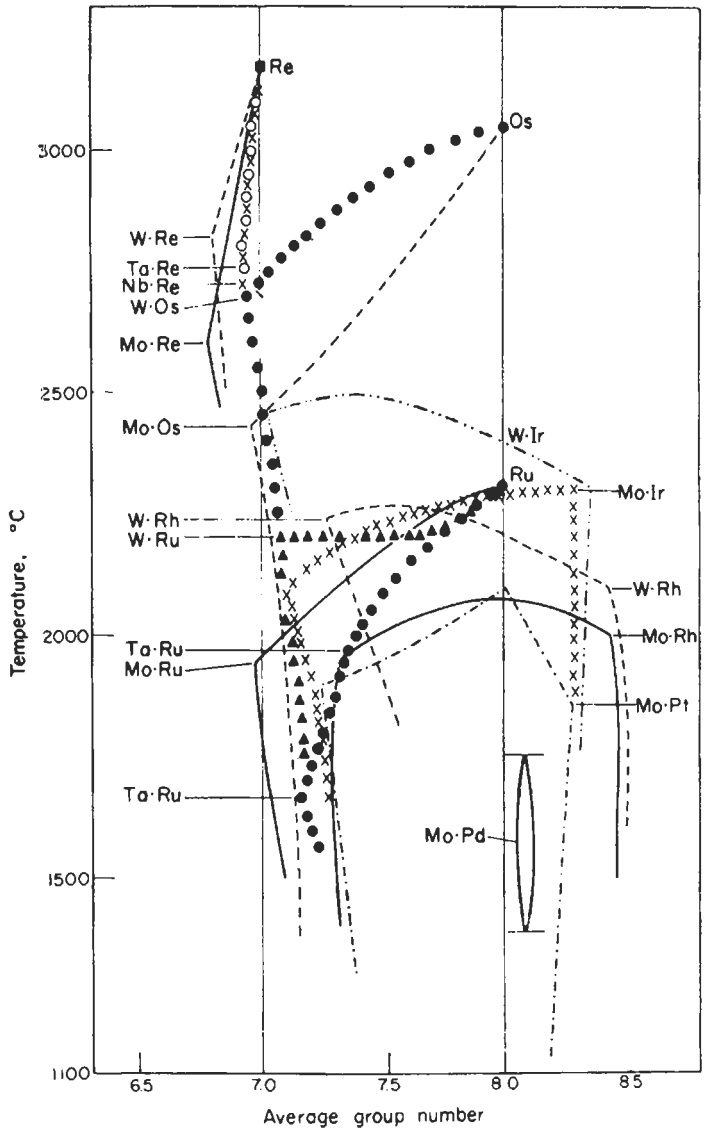

Fig. 7. The composition limits, in terms of AGN, of terminal solid solutions of Nb, Ta, Mo and W in Re, of Mo and W in Os, of Ta, Mo and W in Ru, and of the intermediate σ-phases in the systems Mo–Rh, Mo–Ir, Mo–Pd, Mo–Pt, W–Rh and W–Ir (from HUME–ROTHERY [1966].)

are indexed according to this cell, then the lattice spacing a is associated with the average spacing of atoms located at the corners of the cube and is larger than the spacings between the neighboring atoms within the cube or in other possible unit cells. The a spacing therefore exceeds the closest distance of approach of atoms. For example,

References: p. 199.

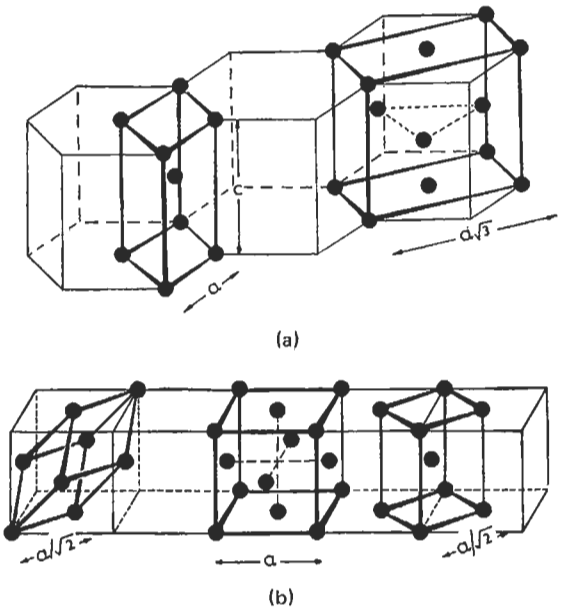

Fig. 8. (a) The close-packed hexagonal structure, showing the tetragonal and orthorhombic unit cells, and (b) the face-centred cubic structure, showing the rhombohedral, the face-centred cubic and the body-centred cubic unit cells.

the *closest distance of approach* of atoms in fig. 8b is $a/\sqrt{2}$. In a simple structure, one can easily calculate this distance from the known dimensions of the unit cell; but this may be very difficult if the structure is complex as, for example, that of γ brass (fig. 16, below).

In some structures there are considerable variations in the distance between pairs of atoms at their closest distance of approach, according to position and direction in the lattice; and in order to study these a more complex analysis, involving all average interatomic spacings, may become necessary. The *cementite* structure (fig. 9) provides a good example. In this structure the iron-carbon distances vary in the unit cell and the determination of spacings between specified pairs of atoms of iron and carbon requires the knowledge of X-ray line intensities in addition to the Debye–Scherrer analysis. (The nature of the bonding in cementile has recently been reexamined by COTTRELL [1993]).

Throughout a range of solid solutions the average "sizes" of individual atoms may be expected to change depending on the degree and nature of local displacements. A change in the average lattice spacings may mean a contraction of solute atoms and expansion of solvent atoms or vice versa, and such local changes may bear little relation to the total macroscopic distortion of the unit cell. Therefore it is very desirable to be able to assess the changes in individual atomic sizes in a solid solution, whenever possible. For this purpose methods involving measurement of diffuse X-ray scattering or changes in the intensity of principal (Bragg) reflections have been developed.

From a materials science point of view, the important questions regarding the atomic size are as follows:

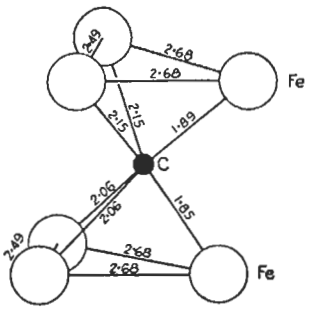

Fig. 9. The variable iron-carbon distances in the structure of cementite, Fe_3C (from GOLDSCHMIDT [1948].)

1) What is the actual size of an atom in a pure element and what are the best ways of estimating and defining that size?

2) Having decided upon atomic sizes of pure elements, which is the best method of estimating the influence of atomic sizes in a solid solution?

3) Can one assess this influence of the disparity between initial atomic sizes without additional measurements in a solid solution?

One would like to know, for example, how successful can be the prediction of the influence of the size difference merely from the knowledge of the atomic sizes of the pure elements and perhaps one other physical property, or whether it is always necessary to perform some kind of a measurement in a solid solution before the importance of the atomic size can be assessed more accurately. Yet another question concerns the relationship between the strain in the crystal lattice and the atomic size. The contribution of the strain energy to the total free energy affects the thermodynamical properties, and recently several attempts have been made to estimate the strain energy using methods of continuum elasticity.

The empirical success of the 15% rule (§ 4) already suggests that initial sizes of atoms can, in some cases, give a guide to the extent of solid solubility on alloying. However, when formulated in this way the atomic-size difference merely provides a guide to the hindrance which it may cause to the formation of extensive primary solid solubility. In some systems, for example in systems Ag-Sn or Ag–Sb, the limits of primary solid solubility are less than average (for silver-based alloys), yet the widths of the close-packed hexagonal intermediate phases are surprisingly large. In both systems the disparity beween atom radii is within the 0–15% range (i.e., the 15% rule is satisfied), and is appears that the actual value of the size difference may be of importance.

7.1. The size factor

The original formulation of the size-factor concept for binary alloy systems involved the assumption that the atomic diameter of an element may be given by the closest

distance of approach of atoms in its structure * (see ch. 1). This approach to estimating atomic size often meets with difficulties when the structures are anisotropic, or complex, or when the coordination numbers are low. For example, when there are several close distances of approach in the structure (as in gallium with $d_1 = 2.437$, $d_2 = 2.706$, $d_3 = 2.736$ and $d_4 = 2.795$ Å), the closest distance of approach, d_1, does not adequately express the size of the gallium atom when in a solid solution. A similar consideration may apply even in the case of an element which crystallizes in a typically metallic structure. For example, in zinc, with the close-packed hexagonal structure but a high value of the axial ratio, four possible values can be considered to represent the size of a zinc atom: spacings between atoms in the basal planes which also correspond to closest packing ($d_1 = 2.6649$ Å); spacings between the nearest neighbors of the adjoining basal planes which strongly depend on the axial ratio ($d_2 = 2.9129$ Å); an atomic diameter derived from the average volume per atom of the unit cell of zinc ($d_3 = 3.0762$ Å); and finally an atomic diameter calculated for a hypothetical structure with coordination number 12 ($d_4 = 2.7535$ Å). For the purpose of the 15% rule, d_1, has been chosen to represent the size of the zinc atom. However, when the behavior of lattice spacings of solid solutions

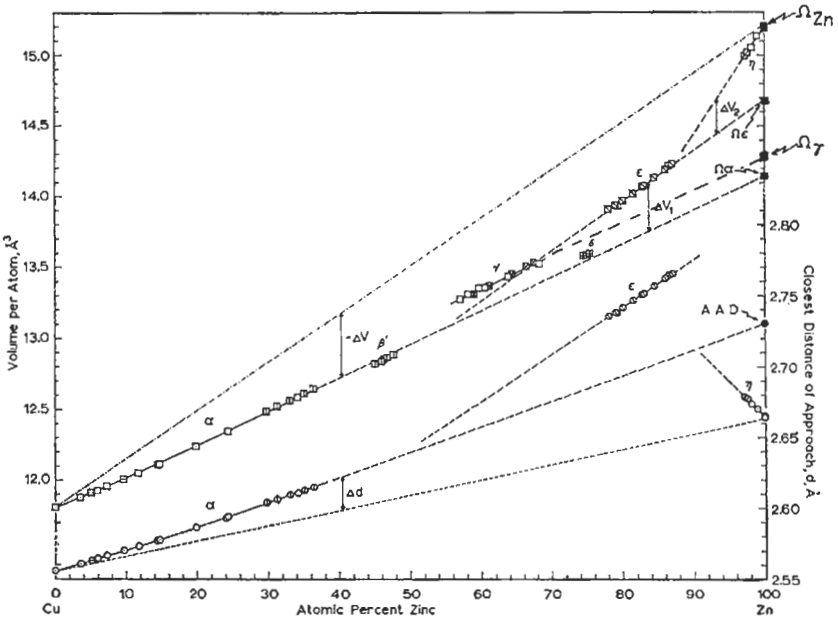

Fig. 10. Trends in lattice spacings and volume per atom in the Cu–Zn system; circles indicate closest distance of approach, d, squares indicate volume per atom. (From MASSALSKI and KING [1961].)

* The size factor is given by $[(d_B - d_A)/d_A] \times 100$ where d_A and d_B are values of the closest distance of approach of atoms in the solvent and solute respectively. For a detailed account of the possible role of the size factor as defined above reference may be made to a review article by RAYNOR [1956].

containing zinc is studied in detail, it appears that frequently the lattice spacings expand, or contract, when an opposite behavior might be expected from the value of the closest distance of approach. In fig. 10 the changes with composition in the closest distance of approach, d, and volume per atom in Cu–Zn alloys are shown. Within the primary solid solution based on copper the lattice spacings follow a curve which indicates that zinc behaves as if it possessed a larger size than that derived from its a spacing, since the lattice spacings of the alloys show a positive deviation from a line joining the closest distances of approach of copper and zinc. On the other hand, within the primary solid solution of copper in zinc, addition of copper to zinc again expands the a spacing of the latter despite the fact that the value of d for copper is indicated to be smaller than that for zinc. Thus, on a finer scale there are often discrepancies between the behavior of lattice spacings in the alloys and the estimated atomic sizes. For such reasons other attempts have been made to derive the average atomic size. For example, in fig. 10 the trend in the α lattice spacing within the α phase may be extrapolated towards pure zinc to give a hypothetical size of a zinc atom for the case where the face-centred cubic structure is maintained throughout the Cu–Zn system and on the assumption that the behavior of lattice spacings is linear. The obtained value is marked AAD in the figure, and it is close to the d_4 value mentioned above. This method of estimating *apparent atomic diameters* (AAD), is due to AXON and HUME–ROTHERY [1948]. Another approach makes use of the trend in the volume per atom (MASSALSKI and KING [1961]). Comparison between the atomic sizes estimated from the volume per atom in the pure elements and the behavior of the volume per atom trends in the Cu–Zn system is shown in the upper portion of fig. 10.

7.2. The measurement of atomic size in terms of volume

By analogy to the use of the apparent atomic diameter, a measure of the size of a solute atom in any particular primary solid solution or an intermediate phase may be obtained by extrapolating to the solute axis the plot of the mean volume per atom within that phase. In fig. 10 such a procedure is illustrated for the α, γ and ε phases of the Cu–Zn system, providing values of the *effective atomic volumes* (MASSALSKI and KING [1961]) or *partial molar atomic volumes*. The different effective atomic volumes estimated in this way for the solute in each phase are independent of the coordination number or the structural anisotropy effects mentioned above. Thus, when the coordination number changes, the atomic volume rather than the interatomic distance tends to remain constant (MOTT [1962]). An extensive study of solid solutions of various B-sub-group metals (Zn, Cd, In, Tl etc.) in late transition elements such as Ni, Pd or Pt has shown that often the initial effective atomic volume of a solute, extrapolated to the pure-solute side, is practically the same in a number of different solvents (ELLNER [1978,1980]). A good example is provided by the behavior of Ga, fig. 11. At the same time, it may be seen from fig. 10 that the effective atomic volumes of zinc in the different phases are smaller than the atomic volume of pure zinc. Since these effective volumes are different in each phase, it appears that the *contribution of the atomic size is variable according to composition* and hence it may be desirable to designate several size

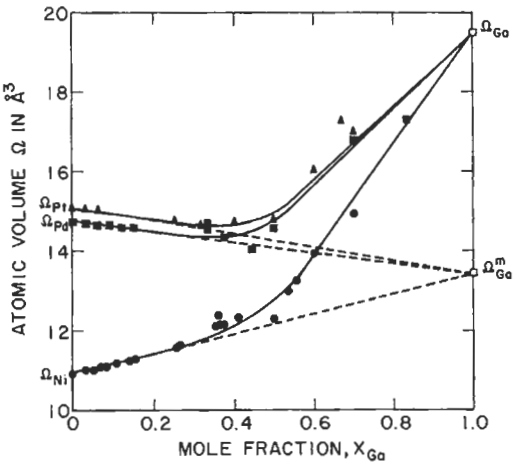

Fig. 11. Changes of atomic volume with composition in the binary Pt–Ga, Pd–Ga and Ni–Ga (from ELLNER [1978].)

Table 5
Effective atomic volume of solutes in electron phases of the noble metals
(from MASSALSKI and KING [1961].)

Sub-group	Solute	Ω_s (Å³)	Effective atomic volume of solute (Å³)					
			Cu ($\Omega_0 = 11.8$)		Ag ($\Omega_0 = 17.05$)		Au ($\Omega_0 = 16.95$)	
			$\Omega_{(\alpha,\beta',\mu)}$	$\Omega_{(\zeta,\varepsilon)}$	$\Omega_{\alpha,\beta',\mu}$	$\Omega_{(\zeta,\varepsilon)}$	$\Omega_{\alpha,\beta',\mu}$	$\Omega_{(\zeta,\varepsilon)}$
II B	Zn	15.2	14.15	14.7	14.7	14.8	14.5	14.8
	Cd	21.6	18.8	–	19.95	20.7	19.25	n.m.
	Hg	23.7	n.m.	–	20.75	22.4	20.2	n.m.
III B	(Al)	16.6	14.2	–	15.5	16.1	15.2	–
	Ga	19.6	14.7	n.m.	16.2	16.7	16.2	–
	In	26.15	20.8[a] 21.3	–	21.4	22.9	21.4[a] 20.5	n.m.
	Tl	28.6	n.m.	–	23.85	–	n.m.	–
IV B	(Si)	20.0	12.5	n.m.	n.m.	–	n.m.	–
	Ge	22.6	15.1	15.8	17.5	–	17.4	–
	Sn	27.05	21.9	–	22.7	23.3	22.2	22.5
	Pb	30.3	n.m.	–	26.7	–	n.m.	–
V B	As	21.5	16.5	n.m.	18.85	n.m.	n.m.	–
	Sb	30.2	22.3	n.m.	24.8	25.5	23.5	–
	Bi	35.4	n.m.	–	29.3	–	n.m.	–

[a] Alternative data

factors in each binary system. The values of the effective atomic volumes, Ω_α, Ω_β, Ω_ζ for solutes in several noble metal electron phases are listed in table 5 together with the atomic volumes of pure solvents, Ω_0, and of pure solutes, Ω_s. An examination of the table shows that without exception all solutes show a decrease of the volume per atom on alloying and that this decrease appears to be greatest with solutes of highest valency. Hence, the atomic sizes of such elements as aluminium, indium, thallium or lead, which are considered to be an exception when measured in terms of the closest distance of approach, are found to be typical of a general trend for the B-subgroup elements with the noble metals when considered in terms of atomic volume (MASSALSKI and KING [1961]). This generalization does not apply to transition elements and other solvents. MOTT [1962] has pointed out that if the volume of a solute atom in the solid solution is nearly the same as in its own pure metal one can expect the heat of solution to be small. Why a solute atom when placed in a hole similar to its own volume in the solvent tends to retain its original energy, even when the valencies of solvent and solute are different, is not altogether clear.

7.3. Combined effects of size and electronegativity

In the early 1950s, DARKEN and GURRY [1953] suggested that the extent of solid solubility in a given solvent metal may be assessed by testing simultaneously both the size and electronegativity differences between solvent and solute elements. They showed that in a combined plot of electronegativity (ordinate) and size (abscissa), which they called a map (see fig. 12) each element can be represented by a point (see also ch. 5, § 1.5). The closer any two points are on the map, the more likely is a high mutual solid solubility between the elements involved. In a typical Darken–Gurry (D–G) plot, as in fig. 12, substantial solubility is usually indicated by an ellipse drawn around a given solvent point. WABER *et al.* [1963] have shown subsequently, following a statistical survey of 1455 systems for which experimental data exists, that over 75% of the systems obeyed the prediction of solid solubility assessed on the basis of a D-G plot. The usefulness of the D–G method is particularly well demonstrated for the actinide metals and rare-earths (GSCHNEIDNER [1980]).

7.4. Strain in solid solutions

A simple model which takes into account the difference between atomic sizes, and which can yield estimates of lattice strain, may be constructed using basic ideas of continuum elasticity. Several such models have been considered (DARKEN and GURRY [1953], ESHELBY [1956] and FRIEDEL [1955]). The general approach is illustrated schematically in fig. 13.

Consider a rubberlike elastic matrix of a large volume V_2 in which a very small cavity has been drilled away of volume V_1. Then, through an infinitesimally small opening (shown as a capillary opening in the figure) an amount of incompressible fluid of volume $(V_1 + \Delta V_1)$ is introduced which, therefore, expands the cavity by the amount ΔV_1. Both the fluid and the matrix are now under stress and the matrix suffers an

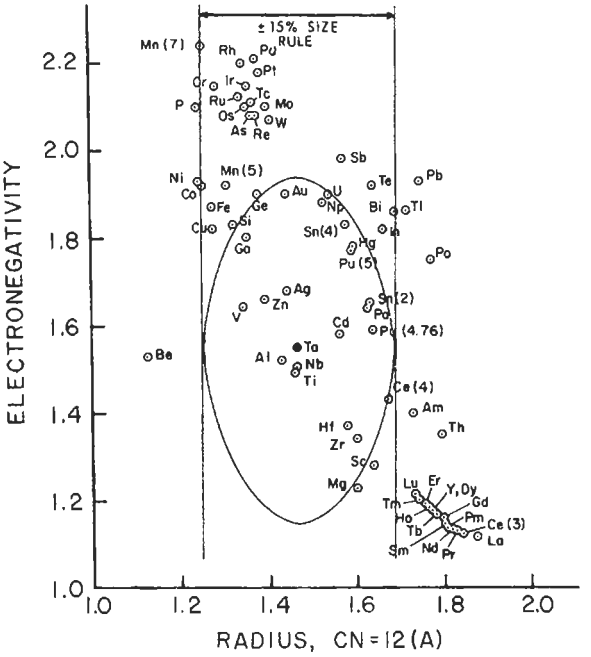

Fig. 12. The Darken–Gurry map with an ellipse drawn about the solvent tantalum. The two vertical lines are the tangents to the ellipse at the termini of the minor axis (±15% of tantalum's radius). (From GSCHNEIDNER [1980].)

expansion ΔV_2, shown in the figure by the shaded portion, which is related to the increase in the volume of the cavity by the relationship

$$\Delta V_2 / \Delta V_1 = 3(1 - \nu)/(1 + \nu), \tag{2}$$

where ν is Poisson's ratio. As pointed out by DARKEN and GURRY [1953], for most metals Poisson's ratio is about 0.3 and hence $\Delta V_2/\Delta V_1$, equals about 1.6, i.e., the volume-increase of a metal bulk will be larger than the increase in the volume of the cavity. The above model can be related to a solid solution in which the expanded cavity is replaced by several solute atoms and the bulk by a metal solvent matrix. In analogy to the expanded volume of the elastic matrix we may expect that in a substitutional solid solution on replacing an atom of the solvent (a cavity) by a somewhat larger-sized atom of the solute (the incompressible fluid) we should obtain a net expansion of the entire unit cell. The estimates of the strain energy associated with such an expansion have enabled a number of authors (DARKEN and GURRY [1953], ESHELBY [1956]) to show a direct link between the limitation of primary solid solubility and Hume–Rothery's 15% rule. Lattice spacing measurements in solid solutions are also in qualitative agreement with the above model, but sometimes a lattice expansion is observed even if the solute atoms are considered to be smaller than those of the solvent. This discrepancy is usually due to the difficulty of being able to assess correctly the sizes of atoms and to the fact

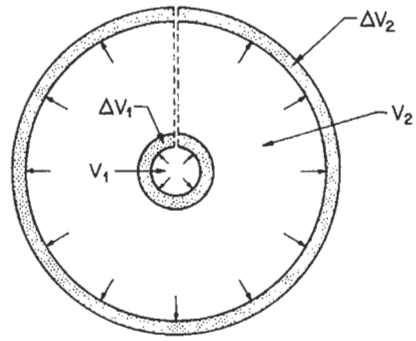

Fig. 13. Model of an incompressible particle in an elastic matrix.

that, on alloying, other factors not included in a crude assessment of size come into play, to mention only that the size of the solute atom in the pure element may differ considerably from its size in solid solution because of such factors as electron concentration, electrochemical effects and static displacements, etc.

Calculations based on simple elastic models permit one to relate the strain energy to composition and atomic volume. A general equation expressing strain energy in a solid solution may be written as (MASSALSKI and KING [1961]):

$$E_S(c) = A\mu\Omega\left(\frac{1}{\Omega}\frac{\partial\Omega}{\partial c}\right)^2 f(c), \tag{3}$$

where A is a numerical constant, μ is the shear modulus, Ω is the mean atomic volume and c the composition. In many alloy phases the variation of atomic volume with composition is nearly linear and hence for dilute solutions (for which $\Omega_0 \approx \Omega$) one may write:

$$\left(\frac{1}{\Omega}\frac{\partial\Omega}{\partial c}\right) \approx \left(\Omega_\alpha - \Omega_0\right)/\Omega_0, \tag{4}$$

where Ω_0 is the atomic volume of the pure solvent and Ω_α the effective atomic volume of the solute in the α phase. The relationship $(\Omega_\alpha - \Omega_0)/\Omega_0$ represents a measure of a volume-size-factor (MASSALSKI and KING [1961]) within a given alloy phase and a comparison of eqs. (3) and (4) shows that the strain energy for dilute alloys is related to the square of the volume-size-factor. Volume-size-factors have been calculated for numerous solid solutions and are available in tabulated form (KING [1966]). It should be pointed out that the use of a volume-size-factor rather than one based on the closest distance of approach necessitates the knowledge of the extrapolated effective atomic volumes of the solute within different phases and hence necessitates additional measurements within solid solutions.

Ellner's studies, for example the plot shown in fig. 11, confirm that in many solid solutions the initial behavior of the atomic volume with composition is practically linear (usually in the composition range up to about 30–40 at% of solute). The corresponding

effective atomic volume obtained from extrapolation to the pure solute side provides a measure of the departure of the atomic volume trend from a possible linear behavior between the atomic volumes of the pure components. If the difference ($\Omega_{solvent} - \overline{\Omega}_{solute}$) is plotted against the difference between the partial molar heats of mixing ($\Delta H_{solvent} - \overline{\Delta H}_{solute}$) obtained from measurements (or calculations), a nearly linear relationship is obtained (ELLNER [1978, 1980]). Thus, size effects find their expression in the corresponding chemical manifestations.

7.5. Deviation from Vegard's law

A study of available systems based on copper, silver and gold with the B-subgroup elements indicates that, when volume-per-atom trends are considered, alloying between any two elements causes a decrease in the volume per atom from a straight line joining the two values for the pure elements. A similar behavior is observed also when various interatomic spacings are measured and plotted within a solid solution, although in such cases the deviation can have positive or negative sign. The trends usually observed are illustrated in fig. 14.

The expected linear dependence on composition of lattice spacing trends, to follow a line joining the values for the pure elements, has come to be known as *Vegard's Law*, although this law has only been found valid for a number of ionic salts (VEGARD [1921, 1928]) and is never quite true in metallic systems. Nevertheless, it is tempting to be able to calculate deviations from assumed linear behavior, without actually performing any measurement in a solid solution, and using solely the knowledge of various parameters in the pure components. Such an attempt has been made by FRIEDEL [1955] for the cases of dilute and concentrated primary solid solutions. Friedel used the atomic volumes,

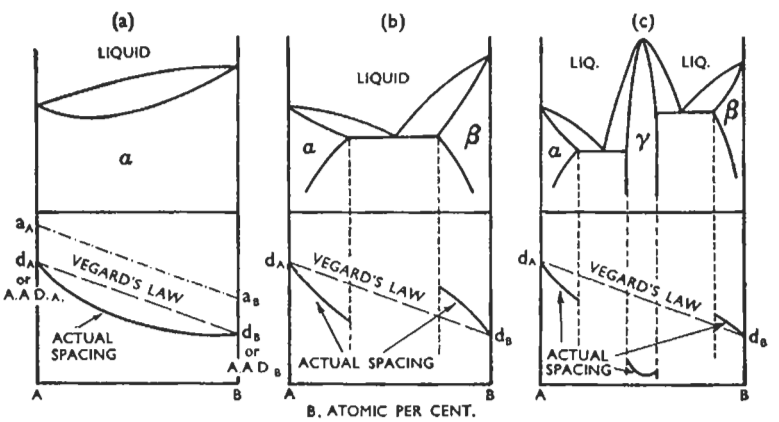

Fig. 14. The commonly observed trends in lattice-spacing-composition curves in three typical binary alloy systems: (a) complete solid solubility; (b) partial solid solubility, A has higher valency than B; (c) presence of an intermediate phase, large electrochemical interaction between A and B. (After MASSALSKI [1958].)

Poisson's ratio, bulk moduli, and compressibilities. The elastic model illustrated in fig. 13 is extended to the case in which both the matrix and the introduced fluid are compressible with compressibility coefficients χ_1 and χ_2. The atoms of solvent and solute are represented by radii r_1, and r_2 which are derived from the atomic volumes of the elements using the relationship $\Omega = \frac{4}{3}\pi r^3$. The holes in the matrix are represented by the atoms of the solvent with radius r_1 and the introduced distortions by atoms of the solute with radius r_2. On replacing an atom of the solvent by an atom of solute both suffer an elastic adjustment which may be represented by an average radius a common to both. Freidel has shown that at *infinite dilution*

$$(a - r_1)/(r_2 - a) = \alpha = (1 + \nu)\chi_1 / 2(1 - 2\nu)\chi_2, \tag{5}$$

where ν is again Poisson's ratio and χ_1, and χ_2 are the compressibilities of the solvent and solute respectively. At a finite concentration c the total volume of the solvent will suffer an increase and the average radius of an atom in the solid solution may now be represented by r (derived from average atomic volume) which will be different from the initial radii r_1 and r_2 of both the solvent and solute. Following Friedel, the initial deviation of the average atomic radius r in a solid solution from a line joining the atomic radii of the solvent and solute, may be expressed-as follows:

$$\frac{r - r_1}{cr_1} = \frac{r_2 - r_1}{r_1} \frac{\alpha + (\chi_1/\chi_2)}{\alpha + 1} \tag{6}$$

Comparison between calculated deviations using the above elastic model and the observed deviations (FRIEDEL [1955]) from the assumed Vegard's Law shows a good general agreement for the cases where the solute atoms are considered to be bigger than the solvent atoms, but usually not vice versa.

7.6. Measurement of actual atomic sizes in solid solutions

The static distortions in a solid solution which can be related to the individual atomic sizes may be estimated from a *modulation in diffuse X-ray scattering* (WARREN *et al.* [1951], ROBERTS [1954] and AVERBACH [1956]) and from a *quasi-temperature reduction in the Bragg reflections* (HUANG [1947], HERBSTEIN *et al.* [1956] and BORIE [1957, 1959]). In the former case the modulations of the diffuse X-ray intensity diffracted by a solid solution are described by coefficients, α_i, related to the nature of local atomic order of atoms, and by size effect coefficients, β_i, related to the differences in the sizes of the component atoms. According to theory,

$$\alpha_i = 1 - P_A^i / X_A \tag{7}$$

and

$$\beta_i = \left(\frac{1}{\eta - 1}\right)\left[-\left(\frac{X_A}{X_B} + \alpha_i\right)\varepsilon_{AA}^i + \left(\frac{X_B}{X_A} + \alpha_i\right)\eta\varepsilon_{BB}^i\right], \tag{8}$$

where

$$\eta = f_B / f_A, \quad \varepsilon^i_{AA} = \left(r^i_{AA} - r_i\right)r_i, \quad \varepsilon^i_{BB} = \left(r^i_{BB} - r_i\right)r_i,$$

and P^i_A = probability of finding an A atom in the i^{th} shell about a B atom; X_A = mol fraction of A atoms; f_A, f_B = scattering factors of A and B atoms; r_i = average interatomic distance to the i^{th} neighbor, calculated from lattice spacings; r^i_{AA} = distance between two A atoms in the i^{th} shell; r^i_{BB} = distance between two B atoms in the i^{th} shell.

8. *Intermediate phases with wide solid solubility*

8.1. The electron phases

Of all intermediate phases which possess wide solid solubility the most typically metallic are the *electron phases.* Their discovery and studies have a historical aspect, and it is of interest to outline this briefly.

In the first quarter of this century, even before X-ray analysis had been applied to the study of such phases as the Cu–Al and Cu–Sn β-brasses, HUME-ROTHERY indicated the possibility that they possessed the same crystallographic structure as that of Cu–Zn β-brass. Systematic and detailed work of Westgren and his collaborators (WESTGREN and PHRAGMEN [1926], WESTGREN [1930]), has subsequently established the validity of this and similar suppositions. The circumstance that the formulas CuZn, Cu_3Al and Cu_5Sn could be ascribed to the three phases with identical β-brass structure caused Hume–Rothery to postulate the principle that the stability of these phases was in some way related to the ratio 3/2 between the number of valence electrons and the number of atoms. Following this empirical formulation many similarities between crystal structures of other intermediate phases have been noted and studied systematically particularly in systems based on copper, silver and gold; and they led to the recognition of the now well-established term *electron compound.* At present it is known that such phases are not compounds in the chemical sense and that they may exist over wide ranges of composition. For this reason they should perhaps be called *electron phases.*

In the Cu–Zn system, which is somewhat typical of systems based on the noble metals, there are three characteristic electron phases commonly known as β-brass, γ-brass and ε-brass. Although these phases possess quite wide ranges of homogeneity, it had been thought originally that their ranges of stability were in each case based upon a characteristic stoichiometric ratio of atoms, and the formulae suggested for the β-, γ- and ε-brasses were CuZn, Cu_5Zn_8 and $CuZn_3$ respectively. From these formulae one obtains the electron/atom values of 3/2, 21/13 and 7/4 (1.50, 1.62 and 1.75) which have become widely accepted as characteristic of greatest stability of electron phases despite the fact that in some cases these values fall outside the range of stability of known electron phases.

Following mainly the work of JONES [1934a,b, 1937, 1952], the stability of electron phases has been linked via a simple electronic theory of metals with possible interactions between the Fermi surface and the Brillouin zones, with the emphasis on the influence of such interactions on the density of states $N(E)$ at the Fermi surface. The β-, γ- and ε-brasses possess the body-centred cubic, complex cubic and hexagonal close-packed

structures respectively; and it can be shown that at the onset of contact between the Fermi surface of free electrons and the principal faces of the respective Brillouin zones the zones are relatively full. The values of e/a associated with the free-electron concept of the Fermi surface are: $e/a = 1.48$ for contact between the Fermi surface and the zone for β-brass, $e/a = 1.54$ for contact between the Fermi surface and the {300} and {411} faces of the large zone for γ-brass, and $e/a = 1.75$ associated with the filling of the inner zone of ε-brass. These electron/atom values based on the Brillouin zone models bear similarity to the original e/a ratios based on chemical formulae (compare 1.5, 1.62 and 1.75 with 1.48, 1.54 and 1.75), but it must be remembered that in both cases the actual values are derived from particular models put forward to interpret the stability of electron phases. The chemical formulae are now known not to be applicable, and the simple Brillouin-zone models suffer from the limitation already mentioned before that for the e/a values quoted above the band gaps across the Brillouin zone must be assumed to be zero or near zero. Thus, as in the case of the theory of primary solid solutions, we are left with two possibilities: (i) The band gaps in the Brillouin zones are relatively large, and the Fermi surfaces are not spherical, but the stability may be described qualitatively by

Table 6
Typical electron phases based on noble metals, zinc and cadmium, and some transition elements.

Phases with cubic symmetry						Phases with hexagonal symmetry (hcp)	
disordered bcc structure e/a range 1.36–1.59			γ-brass structure e/a range 1.54–1.70		β-Mn structure e/a range 1.40–1.54	$c/a = 1.633$ e/a range 1.22–1.83	$c/a = 1.57$ e/a range 1.65–1.89
β			γ		μ	ζ	ε
Cu–Be	Ag–Zn	Au–Al	Cu–Zn	Mn–Zn	Cu–Si	Cu–Ga	Cu–Zn
Cu–Zn	Ag–Cd		Cu–Cd	Mn–In	Ag–Al	Cu–Si	Ag–Zn
Cu–Al	Ag–Al		Cu–Hg	Fe–Zn	Au–Al	Cu–Ge	Ag–Cd
Cu–Ga	Ag–In		Cu–Al	Co–Zn	Co–Zn	Cu–As	Au–Zn
Cu–In			Cu–Ga	Ni–Zn		Cu–Sb	Au–Cd
Cu–Si			Ci–In	Ni–Cd		Ag–Cd	Li–Zn
Cu–Sn			Cu–Si	Ni–Ga		Ag–Hg	Li–Cd
Mn–Zn			Cu–Sn	Ni–In		Ag–Al	
			Ag–Li	Pd–Zn		Ag–Ga	
			Ag–Zn	Pt–Zn		Ag–In	
			Ag–Cd	Pt–Cd		Ag–Sn	
			Ag–Hg			Ag–As	
			Ag–In			Ag–Sb	
			Au–Zn			Au–Cd	
			Zu–Cd			Au–Hg	
			Au–Ga			Au–In	
			Au–In			Au–Sn	
						Mn–Zn	

References: p. 199.

a model as that shown in fig. 6b which points to the existence of a relationship between the density of states and phase stability. (ii) The band gaps in the Brillouin zone are variable with composition and are small in the range of electron phases so that the nearly spherical model of the Fermi surface describes the situation adequately. Experimental estimates of the Fermi surfaces in alloys are still limited, but some measurements have been made in both dilute and concentrated solid solutions, and they indicate that the Fermi surface is distorted from the spherical shape, but not substantially (see for example PEARSON [1967], Massalski and MIZUTANI [1978] and KOLKE *et al.* [1982]). Although the details are still not clear, one is left with indisputable experimental correlations that show e/a to be an important factor in the stability of electron phases. Modelling of such stability in terms of electronic energy alone suggests that very small differences of the order of a few hundred cal/mole are involved between respective competing electron phases (MASSALSKI and MIZUTANI [1978]).

A list of typical electron phases is shown in table 6 in which are also shown the experimentally established ranges of stability of these phases.

8.2. Electron phases with cubic symmetry

The range of stability of the β-phases is shown in fig. 5b, above. The disordered β-phases are stable only at high temperatures and upon cooling or quenching they usually decompose, unless they become ordered as in the Cu–Zn system. In all cases the range of homogeneity of the disordered β-phases decreases with the fall of temperature, causing the phase fields to have the characteristic V-shape as illustrated in fig. 15. The electronic structure of the β-phases appears to be closely linked with the Brillouin zone for the bcc structure formed by 12 {110} faces, which constitute a rhombic dodecahedron. As mentioned in the preceding section, in the free electron approximation a spherical Fermi surface would just touch these faces at $e/a = 1.48$ (see fig.6c). If the

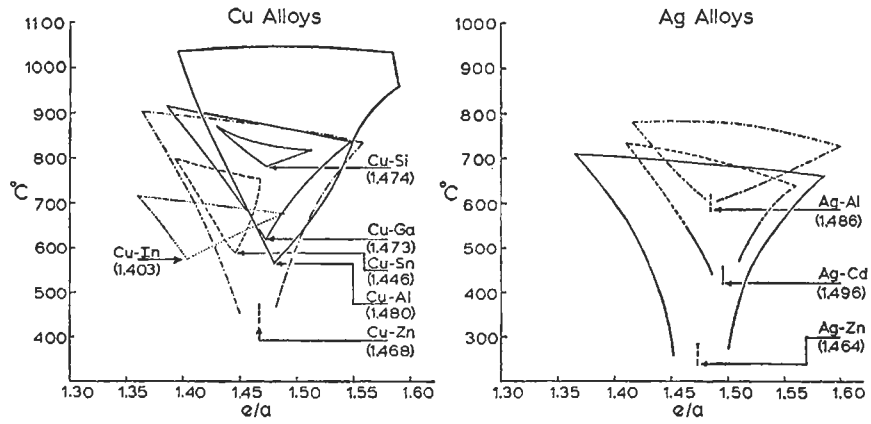

Fig. 15. The typical V-shaped phase fields of the disordered β-phases (from MASSALSKI and KING [1961].)

Brillouin-zone faces have a finite discontinuity, the density-of-states curve should show a peak near the value of e/a associated with the contact between the Fermi surface and the Brillouin zone. This possibility has been made the basis of a theory of the occurrence and stability of the β-phases (JONES [1937, 1952]). However, as pointed out above, if the gap across the faces of the Brillouin zone is assumed to be about 4.2 eV, the position in terms of e/a of the calculated peak in the density-of-states curve appears to occur at relatively low values of e/a and bears no relation to the actual ranges of stability. Nevertheless, it is remarkable that the most stable compositions of the β-phases, represented by eutectoid points at the tips of the V-shaped portions of the phase fields (see fig. 15), very nearly correspond to electron-concentration values associated with the free-electron model. More recent developments have centered on the measurement of properties, such as electronic specific heats, or the de Haas van Alphen effect (dHvA), that can be more directly related to the electronic structure. They show that the band gaps in the Brillouin zone are relatively small (~ 3.5 eV), and that the Fermi surface contours approximate a free-electron sphere. However, the stability of the β-phases is undoubtedly related to the total electronic energy integrated from the density-of-states trends from the bottom of the energy band to the Fermi level, and not just to some specific condition such as an initial contact between the Fermi surface and the Brillouin zone (MASSALSKI and MIZUTANI [1978]).

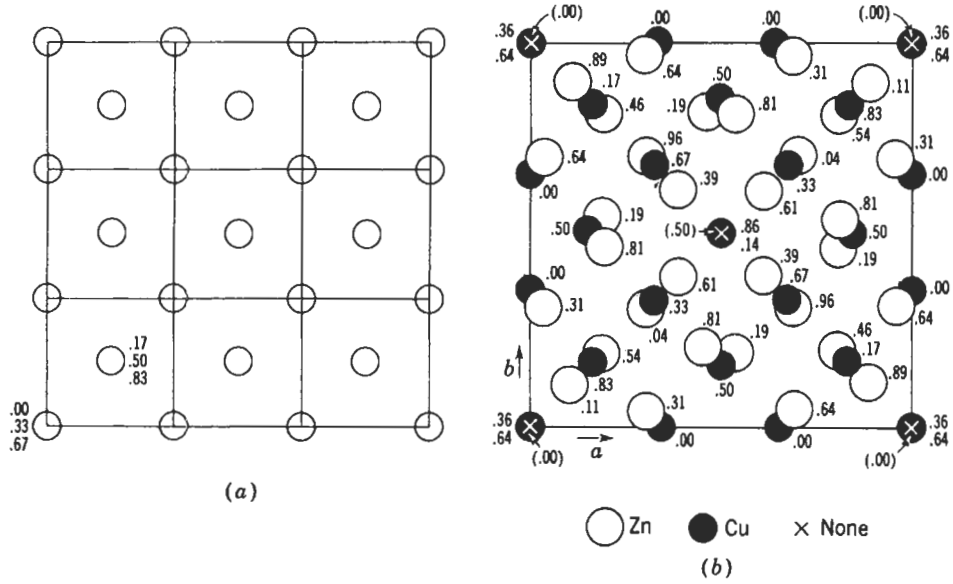

Fig. 16. The structure of γ-brass. (a) Planar view. The structure is built up from 27 bcc cells stacked in three dimensions. Distances above the projection plane are indicated in terms of the large cell edge. (b) The gamma-brass structure derived from (a) by removing the corner and central atoms and displacing others. (From BARRETT and MASSALSKI [1966].)

References: p. 199.

The range of stability of the γ-phases appears to be associated with no particular single value of electron concentration (see table 6) although there does seem to be a strong connection between the stability of γ-phases and the *large (Brillouin) zone* (see JONES [1934a, b, 1960]). The γ-phases have a complex bcc structure with approximately 52 atoms per cell (see fig. 16). They are usually ordered, certain related atomic sites being occupied by solute atoms and others by solvent atoms. The electronic structure of the γ-phases and certain of their physical properties have been reviewed by MASSALSKI and KING [1961] and MASSALSKI and MIZUTANI [1978]. On the whole, the γ-phases are brittle and they are therefore of no primary metallurgical interest. However, from the point of view of electronic theories the γ-phases are of historical interest because they were the first to be identified with a possible peak in the density-of-states curve associated with the contact of the Fermi surface with the Brillouin zone. Detailed calculations show that actually two closely positioned peaks are involved, corresponding to small band gaps, of the order of 1–2 eV. It is not surprising, therefore, that the Fermi surface associated with the γ-phases appears to be nearly spherical. The interaction of such a spherical Fermi surface with a Brillouin zone which itself resembles a sphere (the zone is bounded by 48 faces), should produce a rapid decrease in the density of states once contact has occurred between the Fermi surface and the zone. This is indeed confirmed by experimental measurements of electronic specific heats which show a rapid decrease of the electronic specific heat coefficient γ with composition. A similar effect is also observed in the cubic μ-phases which possess the β-Mn structure (MASSALSKI and MIZUTANI [1978]).

8.3. Electron phases with hexagonal symmetry

Apart from the more complex σ-, μ- and certain other phases which possess cubic symmetry (see, e.g., MASSALSKI and KING [1961]), the remaining group of electron phases possess the close-packed hexagonal structure. These phases are most numerous of all intermediate phases based on the noble metals, and they may occur anywhere within the electron-concentration range between 1.32 and 2.00 except for the narrow region 1.89–1.93. Together with the close-packed hexagonal primary solid solutions of zinc and cadmium with the noble metals (the η-phases) the close-packed hexagonal phases fall into three natural groups and are usually denoted by the Greek symbols ζ, ε and η on the basis of electron concentration, axial ratio and solute content. The known ε-phases always contain zinc or cadmium as their principal constituents (MASSALSKI and KING [1961]) and their range of stability varies between $e/a = 1.65$ and $e/a = 1.89$ (see table 6). The stability of close-packed hexagonal electron phases again appears to be intimately linked with both contact and overlap of electrons across the Brillouin zone.

The Brillouin zone for the close-packed hexagonal structure is shown in fig. 17 for an ideally close-packed structure. This zone is bounded by twenty faces, six of the {10.0} type, two of the {00.2} type, and twelve of the {10.1} type. The energy discontinuity vanishes across certain lines in the {00.1} faces (JONES [1960]) unless the structure is ordered, and hence these planes do not form a part of the energy zone. However, the {00.1} faces together with the {10.1} faces may be used to obtain a

slightly smaller zone for the structure as described by JONES [1960]. Many of the measured electronic properties in hcp structures may be related to the Brillouin zone. The dHvA (de Haas van Alphen) data for pure hcp metals, for instance, are often interpreted in terms of the reduced zone scheme, while the low-temperature specific heat data can be more conveniently discussed in terms of the extended zone. If the extended "roofs" formed beyond the {10.0} planes by the intersection of the {10.1} planes are removed, the resulting zone is still surrounded by energy discontinuities in all directions except along the lines of intersection between the {10.1} and {10.0} zone planes (line HL in fig. 17a). This smaller zone is sometimes known as the *Jones zone* and its electron content per atom is:

$$e/a = 2 - \frac{3}{4}\left(\frac{a}{c}\right)^2\left[1 - \frac{1}{4}\left(\frac{a}{c}\right)^2\right], \tag{9}$$

where c/a is the axial ratio.

The importance of the electron concentration, e/a, as the major parameter controlling the properties and behavior of the hcp phases became clearly evident only after the relationship between c/a and e/a was established in detail. When e/a is constant, for example in a ternary system, c/a also remains constant. However, when e/a is allowed to change c/a changes accordingly. In binary systems, the axial-ratio trends of all known ζ and ε phases conform to a general pattern as shown in fig. 18. Consideration of this

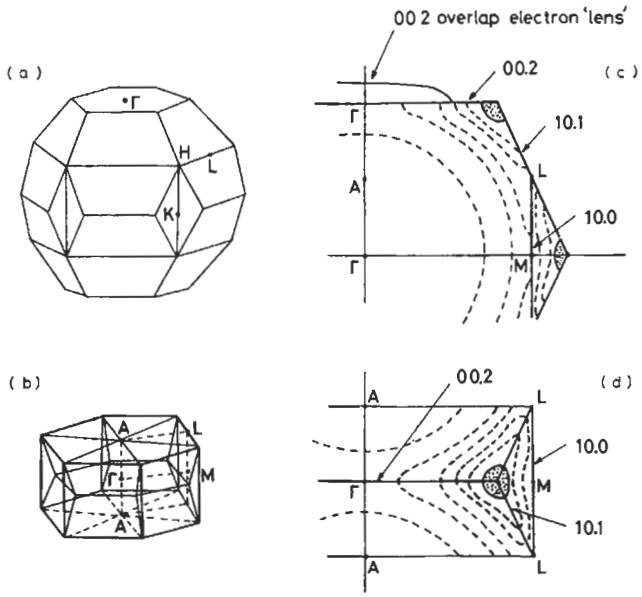

Fig. 17. The Brillouin zone of the hcp structure in the extended scheme (a) and in the reduced scheme (b). The possible contours of the Fermi surface in the vertical section of the corresponding Brillouin zone are shown in (c) and (d). The shaded areas correspond to the holes in pure Zn. The hole in (d) is known as a portion of the "monster". (After MASSALSKI *et al.* [1975].)

References: p. 199.

behavior suggests a direct dependence of the structural parameters a and c on the interaction between Fermi surface and Brillouin zone (FsBz interaction): as the electron concentration increases, the resulting contacts and overlaps of the Fermi surface with respect to different sets of zone planes cause a distortion of the Brillouin zone. This in turn affects the lattice parameters in real space. The earlier models of the electronic structure of the hcp phases have been derived mainly from the interpretation of the trends in lattice parameters, but more recently the electronic structure has also been explored by additional techniques using, e.g., electronic specific heat, superconductivity, magnetic

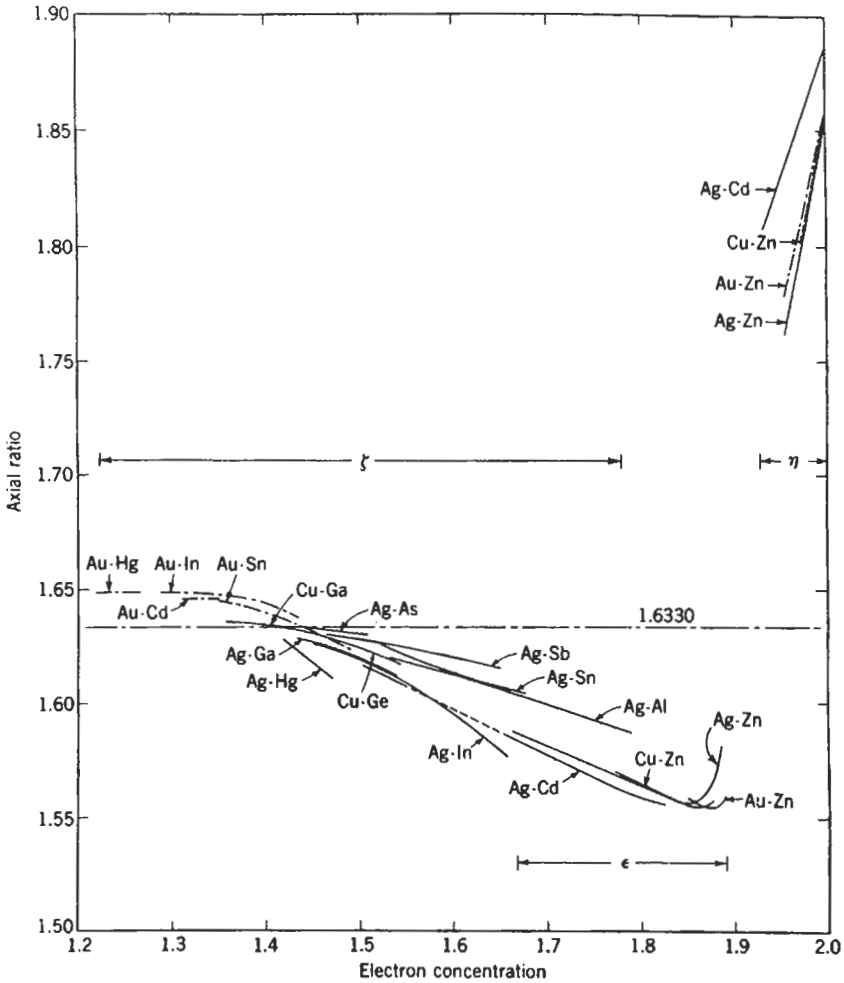

Fig. 18. The trend of the axial ratio as a function of the electron concentration in various hcp alloy systems (from MASSALSKI and MIZUTANI [1978].)

susceptibility, thermodynamic activity and positron annihilation.

The distance from the origin to the respective zone plane in k-space is given by:

$$k_{10.0} = \frac{2\pi}{\sqrt{3}a}, \quad k_{00.2} = \frac{2\pi}{c} \quad \textit{and} \quad k_{10.1} = \frac{2\pi}{\sqrt{3}a}\left(1 + \frac{3}{4}\left(\frac{a}{c}\right)^2\right)^{1/2}, \tag{10}$$

and hence depends on the axial ratio. In the range of c/a higher than $\sqrt{3}$, the {00.2} zone planes are closest to the origin, leading to the sequence $k_{00.2} < k_{10.0} < k_{10.1}$ which holds in the η-phases, where c/a exceeds 1.75. The sequence $k_{10.0} < k_{00.2} < k_{10.1}$ holds for all ζ- and ε-phase structures. The corresponding Jones zone holds, at most, only 1.75 electrons per atom. Therefore, overlaps of electrons from the Jones zone into higher zones are expected at relatively low values of e/a. The interpretation of the lattice-spacing trends in the ζ-phase Ag-based alloys, whose axial ratios vary between 1.63 and 1.58, strongly suggests that overlaps of electrons across the {10.0} zone planes already occur at about 1.4 electrons per atom. The occurrence of possible overlaps across the {00.2} zone plane within the range of the ε-phases has been inferred from measurements of the lattice spacings, electronic specific heat coefficient, the Debye temperature, the superconductivity transition temperature, the magnetic susceptibility and the thermodynamic activity (MASSALSKI and MIZUTANI [1978]). This is shown in fig. 19. In each case the onset of electron overlaps across the {00.2} zone planes has been proposed for the range of e/a exceeding approximately 1.85 electrons per atom. All such measurements imply the occurrence of FsBz interactions that should be reflected also in the corresponding density-of-states changes on alloying.

The available calculated density-of-states curves for the hcp structure are at the moment limited to several pure metals, such as Mg, Zn or Be. All these metals have two valence electrons per atom and may be represented by relatively similar features in the corresponding density-of-state curves. The positions of peaks and subsequent declining slopes occur more or less at the same electron concentration for all three cases, in spite of a large difference in the axial ratios, atomic volumes and electronic interactions. This strongly indicates that the main features of the respective density-of-states curves originate from the FsBz interactions in which e/a plays an essential role. From this, one can conclude that a density-of-states curve for a disordered hcp alloy may also have essentially the same characteristic features. This is confirmed by experiments involving the measurement of electronic specific heats, which are directly proportional to the density of states at the Fermi level (fig. 20).

The experimental coefficients γ plotted in fig. 20 as a function of e/a show that, irrespective of the solute or solvent species, all available γ_{exp} values follow a very similar general trend over a wide range of electron concentrations. An increasing trend is evident in the lower e/a range, culminating in a broad maximum at about 1.5 electrons per atom, and followed by a decreasing trend at higher e/a values. The theoretical density-of-states curve for the hcp Zn, shown in units of mJ/mole K^2 in the same figure allows a direct comparison between a relevant calculation and the experimental data. This shows that the large peak in the theoretical curves more or less coincides with the experimental peak on the abscissa.

References: p. 199.

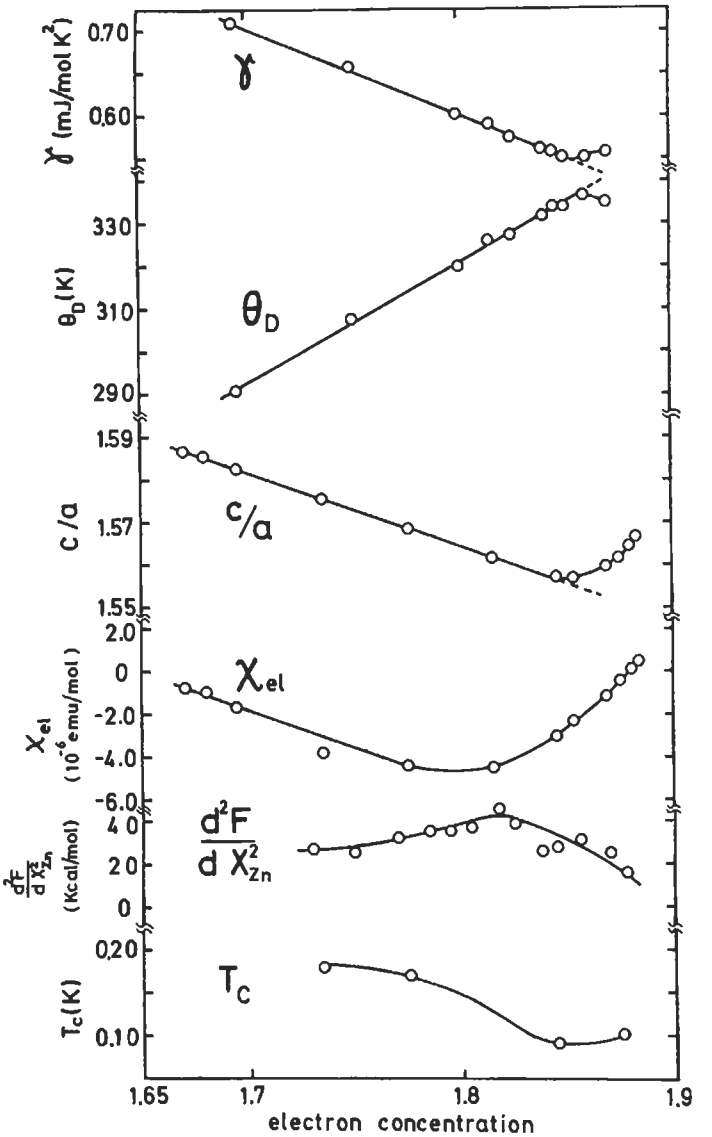

Fig. 19. Behavior of various physical properties in the ε-phase Ag–Zn alloy system: electronic specific heat coefficient γ; Debye temperature θ_D; axial ratio c/a; magnetic susceptibility due to conduction electrons χ_{el}; second derivative of the free energy with respect to concentration (d^2F/dX_{Zn}^2) (in units of 4.2 kJ/mol); superconducting transition temperature T_c. (From MASSALSKI and MIZUTANI [1978].)

The combination of contacts and overlaps with respect to a large number of zone planes is clearly responsible for the large peak in the $N(E)$ curve in hcp metals. The distance of the {10.1} planes from the origin of the zone is relatively insensitive to the

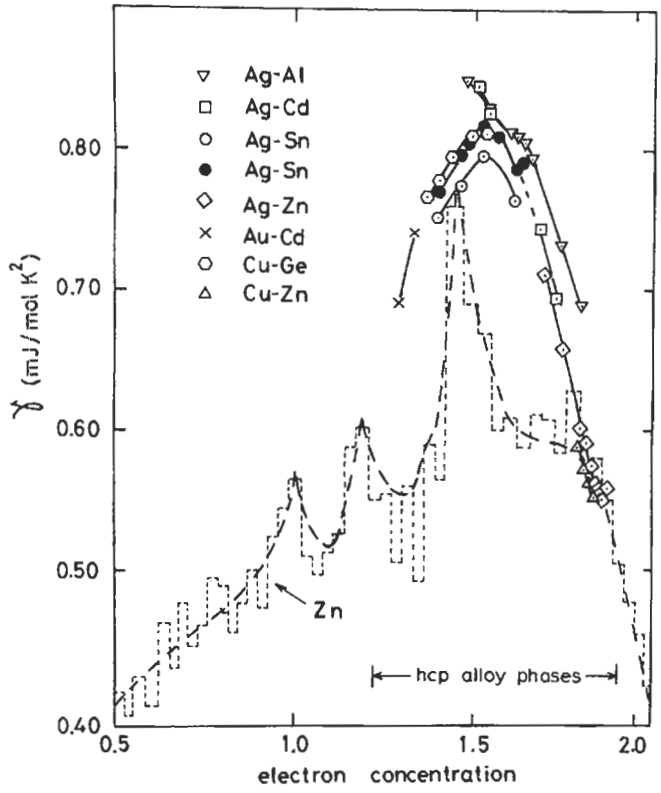

Fig. 20. Trends of electronic specific heat coefficients as a function of electron concentration for hcp Hume–Rothery alloys, shown against the band calculation for pure Zn (from MASSALSKI and MIZUTANI [1978].)

axial ratio (eq. 9). Hence, the large peak may be expected to occur at similar e/a values in most hcp structures. Once contact with the {10.1} planes occurs, additional electrons will be allocated in the remaining hole regions of the Brillouin zone until overlaps across the {10.1} or {00.2} zone planes become possible. Thus, until a sufficiently high e/a is reached, a progressive decrease in the $N(E)$ curve is expected as is actually seen in fig. 20. Based on the above interpretation the likely Fermi surface topography for a typical hcp Hume–Rothery phase may be expected to be like that shown in fig. 21. The recent positron-annihilation studies of the Fermi surface in the ζ-phase Cu–Ge alloys, by SUZUKI *et al.* [1976] and KOIKE *et al.* [1982] are entirely consistent with the conclusions drawn from the electronic specific heat data and earlier work on lattice spacings and axial ratios. Indeed, because of zone contacts and overlaps that are likely to occur in all hcp alloy phases, this particular group of alloys offers a most challenging research area for the positron-annihilation method. For the first time it has become possible to provide

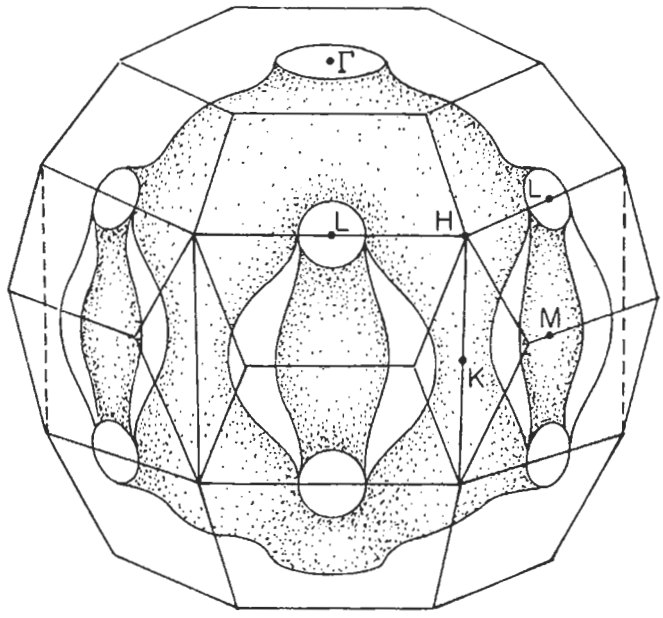

Fig. 21. A very likely Fermi surface topography in an hcp Hume–Rothery electron phase alloy. The 101 contact and 100 overlap are assumed to be present. (From MASSALSKI and MIZUTANI [1978].)

a direct evidence for the existence of the Fermi-surface concept in disordered electron phases, precisely along the lines predicted by numerous earlier interpretations based on indirect data.

8.4. Laves phases

An important group of related intermediate phases is obtained by alloying of elements whose atomic diameters, d_{AA} and d_{BB}, are approximately in the ratio 1.2 to 1. The exact lattice geometry requires that d_{AA}/d_{BB} should be 1.225, but in known examples of this type of intermediate phases the ratio varies from about 1.1 to about 1.6. Much of the original work concerning the above phases is due to Laves and his co-workers. For this reason they are often called *Laves phases* (see ch. 4).

Laves phases are close packed, of approximate formula AB_2, crystallizing in one of the three structural types:

1) C_{14} structure, typified by the phase $MgZn_2$, hexagonal, with packing of planes of atoms represented by the general sequence ABABAB etc;

2) the C_{15} structure, typified by the phase $MgCu_2$, cubic, with packing ABCABCABC;

3) the C_{36} structure, typified by the phase $MgNi_2$, hexagonal, with packing ABACABAC.

The main reason for the existence of Laves phases appears to be one of geometrical origin — that of filling space in a convenient way. However, within the given range of atomic diameters which satisfy the space-filling condition, it appears that often the choice as to which particular modification will be stable is determined by electronic considerations. The evidence

for this is particularly striking in the magnesium alloys studied by LAVES and WITTE [1935, 1936]. The experimental results concerning the three modifications occurring in several ternary systems based on magnesium are shown in fig. 22 and are plotted in terms of electron concentration. Witte and his co-workers have carried out experiments suggesting that the phase boundaries on the electron-rich side of typical Laves structures occur at very nearly the same e/a, suggesting that the homogeneity of a particular structure may be restricted by an appropriate Brillouin zone. Measurements of the changes in magnetic susceptibility and hydrogen solubility of several alloys within the pseudobinary sections $MgCu_2$–$MgZn_2$, $MgNi_2$–$MgZn_2$, $MgCu_2$–$MgAl_2$ and $MgZn_2$–$MgAl_2$, appear to support this hypothesis. The changes of the magnetic susceptibility in the pseudo-binary $MgCu_2$–$MgZn_2$ system are shown in fig. 23. KLEE and WITTE [I954] proposed that they may be interpreted in terms of interactions between the Fermi surface and the Brillouin zone, the dip in the susceptibility prior to the termination of solid solubility indicating a dip in the density of states.

Measurements of the electronic specific heats, that can be related to the density of states at the Fermi surface, have provided a further evidence of the importance of electronic factors in Laves phases. Examination of the trends of the electronic specific heat coefficient γ, as it varies in pseudobinary systems of $MgCu_2$ with polyvalent metals such as Zn, Al and Si, has shown that a sharp decrease of the density of states occurs near the phase boundary before the $MgCu_2$ structure is replaced by a two-phase field. A possible interpretation of this is that an appropriate Brillouin zone becomes filled with electrons. In this respect the electronic specific heat data and the magnetic susceptibility data shown in fig. 23 are very similar (SLICK *et al.* [1965]).

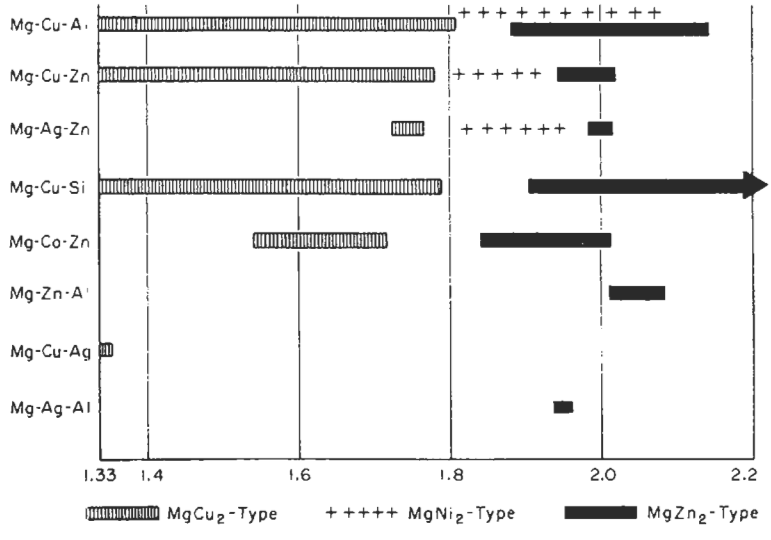

Fig. 22. The ranges of homogeneity in terms of electron concentration of several ternary magnesium alloys which possess the three typical Laves structures (from MASSALSKI [1956] after LAVES and WITTE [1936].)

References: p. 199.

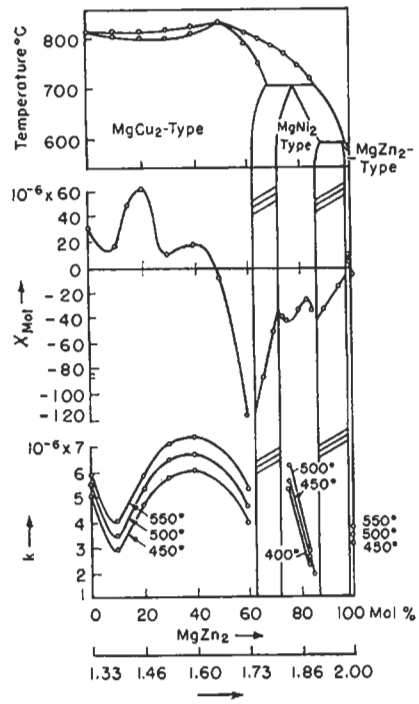

Fig. 23. Variation of hydrogen solubility and magnetic susceptibility with electron concentration in quasi-binary systems $MgCu_2$–$MgZn_2$ (from MASSALSKI [1956] after KLEE and WITTE [1954].)

8.5. Phases with wide solubility formed by the transition elements

A number of intermediate phases formed by the transition elements possess wide ranges of solid solubility. They are often designated by various Greek or Latin symbols such as σ, μ, δ, χ, P or R. For details reference may be made to TAYLOR [1961], NEVITT [1963] and ch. 5 which deals specifically with alloy compounds.

The σ-phase, the unit cell of which is tetragonal with $c/a \approx 0.52$ and 30 atoms per cell, has received much detailed attention, chiefly because of the detrimental effect which the formation of this phase has on mechanical properties of certain steels. In the system Fe–Cr, for example, the σ-phase separates out of the ferritic matrix and causes brittleness, but in more complex steels such as Fe–Cr–Mn σ-phases can also precipitate from the austenite phase.

X-ray and neutron diffraction studies have shown that many of the phases listed above are structurally related to one another because they can be built up from layers that show close similarities. Thus, undoubtedly, atomic packing plays an important role in determining their stability. At the same time studies of stability ranges, particularly in ternary systems, have shown that the contours of the phase fields of the above phases often bear relation to the value of the average group number (AGN). Hence, much

speculation has been advanced about the electronic nature of their stability that might be similar to the electron phases of the noble metals. In fig. 24 the ternary phase relationships of some 19 ternary systems are shown at various temperatures as collected by NIEMIEC [1967]. The relationship between AGN and the contours of the σ-phase fields is particularly noticeable. It must be kept in mind however, that since the d-electrons

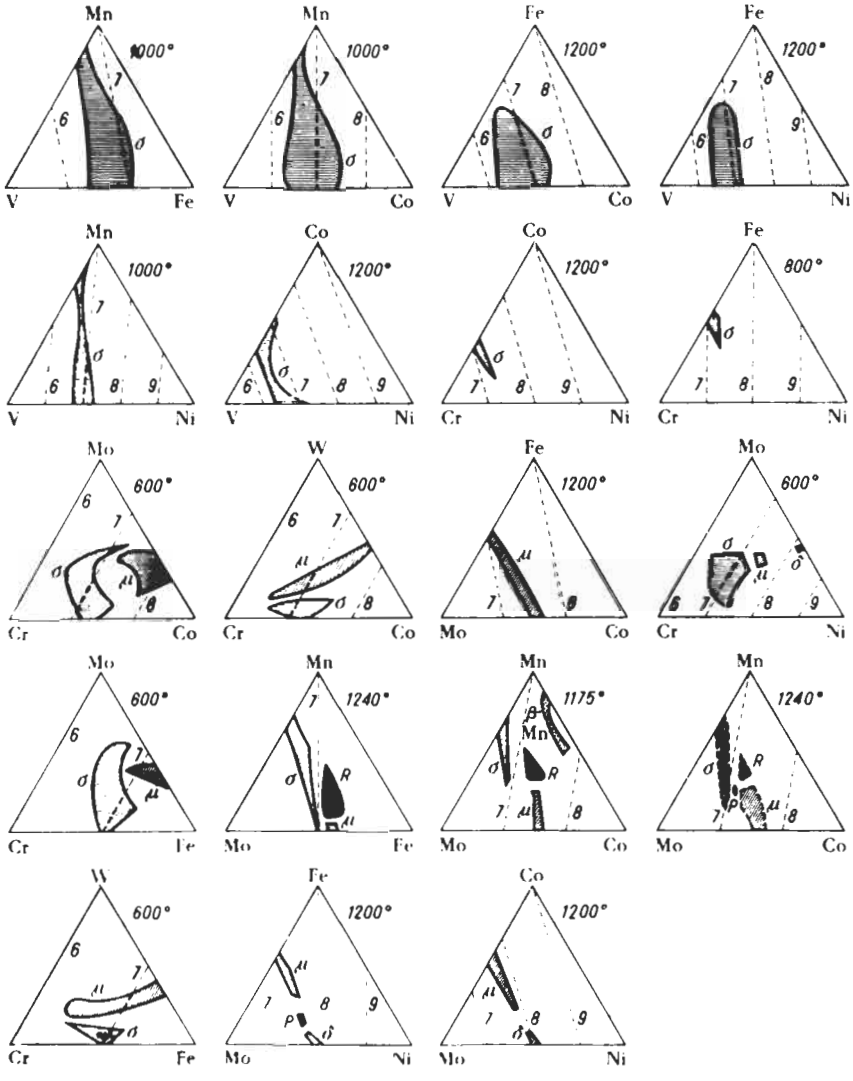

Fig. 24. Isothermal sections through a number of ternary phase diagrams between transition elements showing phase fields of phases with wide solid solubility. Values of average group number are indicated by dashed lines. (From NIEMIEC [1966].)

unquestionably contribute to e/a in these phases, and since the d-bands are incompletely filled, the details of possible electronic interactions are bound to be complex and not necessarily related solely to some simple Brillouin-zone-Fermi-surface effects. For example, some of the bonding forces may be highly directional, or the number of "d-band vacancies" rather than electrons, may play a role.

9. *Lattice spacings in solid solutions*

The measurement of precise values of lattice spacings in solid solutions has contributed to the understanding of a number of factors which influence their stability and properties. Since the introduction of the Debye–Scherrer powder method some sixty years ago, the interest in the knowledge of lattice spacings in alloys has developed in three distinct directions:

1) in connection with precision measurements of lattice parameters for studies of systematic structural similarities between related alloy phases;

2) in connection with studies of relationships between lattice spacings, composition, electronic structure, size effects, local order, magnetic effects and numerous other properties of solid solutions;

3) in connection with the use of the lattice-spacing method as a tool for determining phase boundaries in alloy systems.

Detailed measurements of lattice spacing trends within individual alloy phases date back to the early 1930s. They were done mostly in terminal solid solutions of the noble metals and a few intermediate phases *. Today the available data fill large volumes (PEARSON [1958, 1967]), and further additions are rapidly growing. The importance of the behavior of lattice spacings in hcp electron phases, in connection with their electronic structure, has already been discussed in § 8.3. Some additional aspects are discussed below.

9.1. Lattice spacings in primary solid solutions

The problem of lattice distortion in primary solid solutions of the *monoralent noble metals* has been considered by Hume–Rothery and by Owen and their associates (HUME–ROTHERY [1964] and OWEN [1947]). The relationships obtained by OWEN [1947] between the percentage lattice distortion and the solute valency in binary systems based on a common solvent are shown in figs. 25 and 26. The importance of valence difference is clearly demonstrated in the figures, but there appear to be departures from the general trends which have not been explained. In order to gain further insight into the particular role of the difference beween valencies of the component elements, RAYNOR [1949a] attempted to eliminate size contributions by assuming that the electronic and size effects in certain solid solutions are additive and can be analyzed separately. Raynor's analysis was based on the assumption that a linear Vegard's Law may be applied to the sizes of

* For a review of some of these measurements see MASSALSKI [1958].

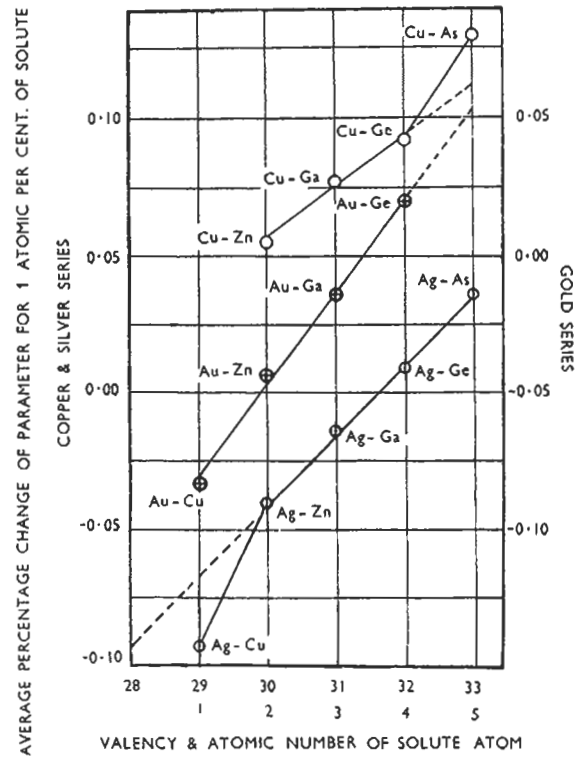

Fig. 25. Percentage lattice distortion as a function of solute valency in solid solutions. Cu, Ag and Au with Zn, Ga, Ge and As. (From PEARSON [1958] after OWEN [1947].)

atoms as given by the closest distance of approach and is therefore open to some doubt (MASSALSKI and KING [1961]).

Nevertheless, a detailed analysis of numerous solid solutions has shown that, after the assumed size contribution has been subtracted, the remaining lattice-spacing variation appears to be proportional to $(V_{so} - V_{bv})^2$ for solutes (so) and solvents (sv) of the same period, and to $(V_{so} - V_{sv})^2 + (V_{so} - V_{sv})$ for solutes and solvents from different periods. Subsequently, PEARSON [1982] has shown that a more general correlation is obtained, valid for a larger number of systems, if a size-effect correction, $\overline{D}$, is calculated from a relationship of the form $a = f\overline{D} + k$, where a is the lattice parameter, $\overline{D}$ is the average atomic diameter calculated from a linear relationship involving initial atomic diameters based on coordination 12, and f and k are constants. If an additional assumption is made that Ga, Ge, Sn, As, Sb and Bi contribute only two electrons to the conduction-electron concentration when alloyed with the noble metals, fifteen more systems appear to obey a uniform correlation.

Studies of binary systems have been extended to *ternary systems* where it is found that lattice spacings of ternary alloys may often be calculated from binary data using empirical additive relationships. An example of a linear relationship between lattice

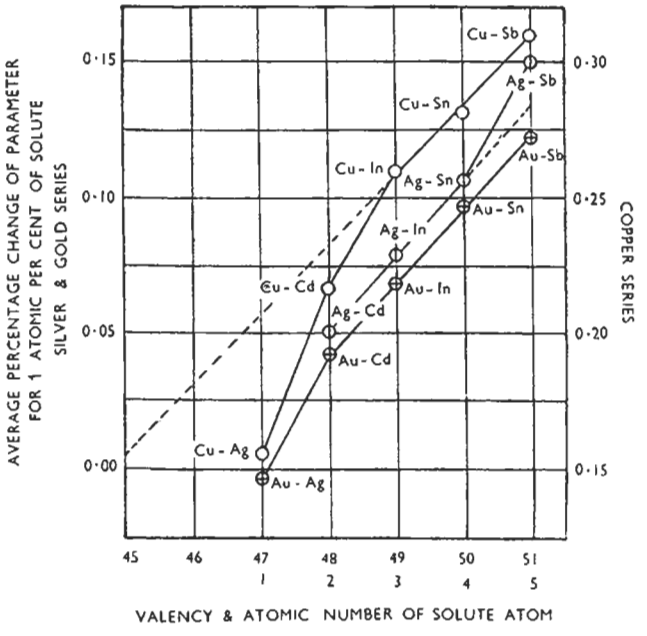

Fig. 26. Percentage lattice distortion as a function of solute valency in solid solutions. Cu, Ag and Au with Ag, Cd, In, Sn and Sb. (From PEARSON [1958] after OWEN [1947].)

spacings and composition in the system Cu–Al–In (STIRLING and RAYNOR [1956]) is shown in fig. 27. ARGENT and WAKEMAN [1957] have shown that the expansion of the copper lattice by additions of zinc and gallium or zinc and germanium is additive in the respective ternary systems. Similar results hold also for additions of gallium and germanium to copper. Additive linear behavior suggests that in simple ternary solid solutions there is no appreciable solute–solute interaction, at least in dilute solutions where atoms of copper can effectively prevent contact beween solutes. Even in the system Ag–Mg–Sb (HILL and AXON [1956–7]) the strictly additive behavior of lattice spacings is still observed despite the fact that strong electrochemical differences between magnesium and antimony, and the tendency towards compound formation (Mg_3Sb_2), might be expected to favor clustering of magnesium and antimony atoms which should lead to the contraction of the lattice. However, when magnesium and silicon are dissolved in an aluminium lattice, contractions are observed which point to electrochemical interactions (HILL and AXON [1954–5]).

The lattice spacings of solid solutions of lithium, magnesium, silicon, copper, zinc, germanium and silver *in aluminium* have been studied and discussed by AXON and HUME-ROTHERY [1948] whose data are plotted in fig. 28. It may be seen from the figure that apart from silver, which produces virtually no change of lattice spacings, the aluminium lattice is expanded by magnesium and germanium and contracted by lithium, silicon, copper and zinc. Aluminium is an example of a trivalent solvent with a face-centered cubic structure. The first Brillouin zone can hold only two electrons per atom and must therefore be overlapped; but it has been shown (HARRISON [1959] and HARRISON

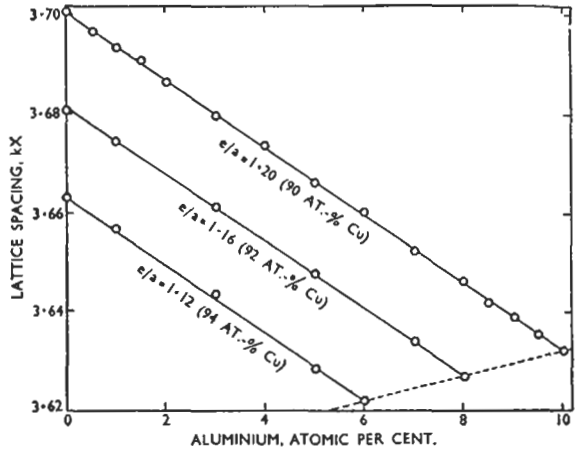

Fig. 27. Lattice spacings of α solid-solution alloys in the Cu–Al–In system along lines of constant copper content (from MASSALSKI [1958] after STIRLING and RAYNOR [1956]).

and WEBB [1960]) that the various portions of the overlapped and unoverlapped Fermi surface, when assembled together, resemble a free electron sphere. Hence, although overlaps exist in the aluminium structure and its alloys, their influence upon lattice spacings may be small.

AXON and HUME-ROTHERY [1948] have shown that the extrapolated AAD (§ 6.1) values for various elements dissolved in aluminium are influenced by the interplay of a number of factors such as relative volume per valence electron in the crystals of the solvent and the solute, the relative radii of the ions, and the relative difference in the electrochemical affinities.

The changes in the lattice spacings in the system *magnesium–cadmium* at temperatures at which complete solid solubility occurs in this system (see fig. 1) have been studied by HUME-ROTHERY and RAYNOR [1940]. When magnesium is alloyed with cadmium, no change occurs in the nominal electron concentration, both elements being two-valent. The initial additions of cadmium to magnesium cause a contraction of the a lattice spacing but only a very slight increase in the axial ratio because the c lattice spacing decreases at about the same rate as does the a lattice spacing. When magnesium is added to cadmium at the opposite end of the phase diagram, both a and c also decrease, but c more rapidly, causing a rapid decrease of c/a. The presence of at least two electrons per atom in this system means that there must exist overlaps from the first Brillouin zone (see fig. 17) since the alloys are conductors of electricity. It is now known from direct measurements of the Fermi surface that in both pure cadmium and pure magnesium overlaps exist across the horizontal and vertical sets of planes in the Brillouin zone, and although the amounts of these overlaps are different in both cases the nature of the overlaps is similar. Hence the relationship between overlaps and trends in the lattice spacings and the axial ratio in the Mg–Cd system is open to speculation.

In a similar way, because of the complexity of factors involved, the interpretation of

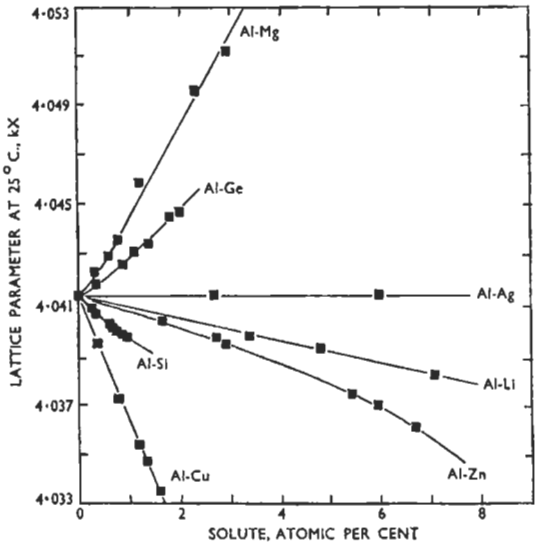

Fig. 28. The lattice-spacing-composition curves of alloys based on aluminium as solvent (from MASSALSKI [1958] after AXON and HUME-ROTHERY [1948].)

the lattice spacings of alloys of transition elements may be expected to meet formidable difficulties. The inner-core d-band shells are incomplete, and it is known that electrons from these shells can contribute both to bonding and to conductivity.

The trends in the lattice spacings of the *transition elements* of the Second Long Period (zirconium, niobium, molybdenum, rhodium and palladium), when dissolved in the hexagonal close-packed ruthenium, have been studied by HELLAWELL and HUME-ROTHERY [1954]. In all cases the parameters c and c/a are increased by the formation of a solid solution and, at equal percentages of each solute, the increases are in the order zirconium → niobium → molybdenum → palladium → rhodium. The a parameters are diminished by zirconium and rhodium and increased by palladium, niobium and molybdenum. The axial ratio of ruthenium (1.5824) is considerably less than the ideal value (1.633), and the interatomic distance in the basal plane is greater than the distance between an atom and its nearest neighbor in the plane above or below. Hellawell and Hume-Rothery interprete the observed lattice spacings on the basis of "size differences" between component atoms as expressed by the minimum distance of approach between atoms in the pure elements and by a possible directional sharing of the electron cloud of zirconium which may take place on alloying.

9.2. The relationship between lattice spacings and magnetic properties

A survey of the lattice spacings of transition metal alloys as a function of composition shows (PEARSON [1958]) that there are many inflections in the lattice spacing curves reflecting changes in the magnetic properties. The magnetic properties of metals and

alloys depend on the arrangement and separation of atoms in a structure, and therefore such changes as the ferromagnetic-paramagnetic transition might be expected to be related to some changes in the lattice spacings and the volume of the unit cell.

The ferromagnetic–paramagnetic changes (F–P) and the antiferromagnetic–paramagnetic changes (A–P) are *second-order transitions* in which the ordering of the spin orientation develops gradually on cooling below the transition temperature, T_c. Such changes are usually accompanied by a sharp change in the slope of the lattice-spacing curve as a function of temperature, such that the derivative da/dT is discontinuous at T_c (WILLIS and ROOKSBY [1954]). Ferromagnetic-antiferromagnetic changes (F-A), on the other hand, are a first-order transition involving a discontinuous change of electron spin orientation and are accompanied by a discontinuous change in lattice spacing (WILLIS and ROOKSBY [1954]). The second order F–P and A–P changes are truly reversible while the first order changes are accompanied by the usual thermal hysteresis in the transition region.

An example of the lattice-spacing changes accompanying an F–P transition is shown in fig. 29a for the system Mn-Sb (WILLIS and ROOKSBY [1954]). In cases of a first-order transition at the Curie point, the discontinuous change in the lattice spacings may also be associated with some displacements of the different types of atoms in a structure, so that in such a case the change in the lattice spacing represents two processes occurring at the same time. According to ROBERTS [1956], the first-order transition at the Curie point is associated with a movement of about 10% of the manganese atoms into interstitial positions. The actual trend in the lattice spacings with temperature in the Mn-Bi system as determined by WILLIS and ROOKSBY [1954] is shown in fig. 29b.

A definite anomaly is found in the temperature variation of the lattice spacings accompanying the F–P transition of pure nickel, but no pronounced anomalies are observed in the slope of the lattice spacings as a function of composition in nickel alloys at compositions at which the F–P change should occur (PEARSON [1958]). COLES [1956]

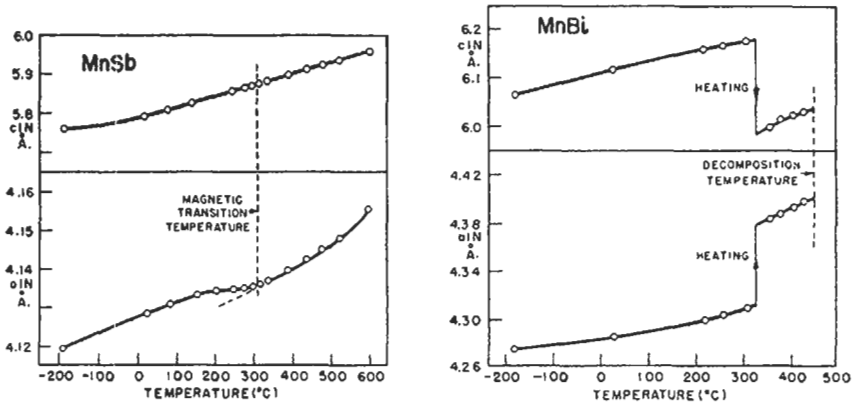

Fig. 29. (a) Lattice spacing of MnSb, which has a $B8_1$ type of structure as a function of temperature. (b) Lattice spacing of MnBi, which has a $B8_1$ type of structure as a function of temperature. (From PEARSON [1958] after WILLIS and ROOKSBY [1954].)

References: p. 199.

has reported a slight change of slope accompanying the F–P change in an alloy of nickel–35at. copper. This composition corresponds to alloys in which the Curie point occurs at room temperature.

10. Defect structures

In addition to the occurrence of clustering or ordering of atoms, which constitutes a departure from randomness, solid solutions can contain various imperfections which can be of three general types: point-, line- and surface imperfections, according to whether they are vacant sites or interstitial atoms, various types of dislocations, stacking faults, or small-angle boundaries. The nature of dislocations, their interactions and their properties are discussed in ch. 20. Below we shall briefly consider some aspects of vacancies in solid solutions and the presence of various stacking disorders.

From the point of view of energy relationships, the presence of vacant sites in solid solutions may enhance stability, owing to their association with the entropy, the strain energy, or the electronic energy. Vacancies may be introduced by quenching from higher temperatures where their equilibrium number, due to entropy considerations, is higher than at lower temperatures, or they may be introduced by various irradiation processes, plastic deformation or, finally, by alloying. The calculation of the energy associated with the formation of vacancies or interstitials in a solid solution at finite concentrations presents several difficulties (see, for example, FUMI [1955], FRIEDEL [1954b], BROOKS [1955] and MANN and SEEGER [1960]). The subject is presented in great detail in ch. 18.

10.1. Vacancies and vacant sites in structures of alloys

From the point of view of the theory of alloys, vacancies are believed to be produced on alloying under certain conditions when the number of electrons per atom is kept constant or reduced. Evidence of this is provided by terminal solutions or electron phases with lattice defects. With the increase or decrease in the number of solute atoms a change can occur in the number of atoms per unit cell in a way which produces vacant lattice sites. It is believed that this takes place in order to maintain optimum electronic energy. Such vacancy populations, determined by composition and not by temperature, are distinguished as *constitutional vacancies.* (CAHN [1979], AMELINCKX [1988]).

The work of BRADLEY and TAYLOR [1937] and TAYLOR and DOYLE [1972] on Ni–Al, and of LIPSON and TAYLOR [1939] on some ternary alloys based on this phase, are first-known examples of this phenomenon. The Ni–Al alloy may be regarded as an electron phase analogous to β-brass if nickel, a transition element, is assumed to have zero to near zero valency. At 50 at% this phase possesses a Cs–Cl ordered structure in which one kind of atoms, say nickel, occupy cube centers and the other kind of atoms, cube corners. The diameter of a nickel atom is smaller than that of an aluminium atom and hence, if nickel content is increased above 50 at%, the lattice parameter of the structure decreases in the expected manner while the density is increased. However, when the aluminium content is increased above 50 at%, an anomalous behavior is observed since

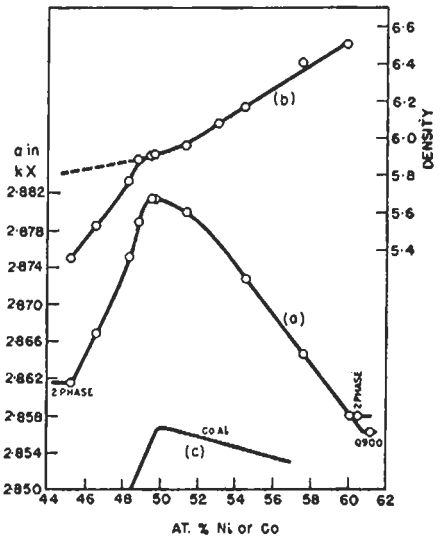

Fig. 30. (a, b) Lattice spacing and density of β-AlNi as a function of composition. (c) Lattice spacing of β-AlCo as a function of composition. (From PEARSON [1958] after original work of BRADLEY and TAYLOR [1937] and BRADLEY and SEAGER [1939].)

the lattice spacing of the Ni–Al phase does not increase but actually decreases, and the fall in the density is much more rapid than would be expected from the replacement of nickel atoms by aluminium. This behavior is shown in fig. 30 in which the lattice spacing data for Co-Al (BRADLEY and SEAGER as quoted by PEARSON [1958]) are also included. BRADLEY and TAYLOR [1937] concluded that the observed anomalies could be explained if one supposed that in the aluminium-rich alloys there are less than two atoms per unit cell and that omission of atoms occurs from some lattice points with the creation of vacancies. On the nickel-rich side, the extra nickel atoms substitute in the usual way for aluminium atoms on the aluminium sublattice. The aluminium-rich side, however, is quite different: hardly any aluminium substitutes on the nickel sublattice; instead nickel atoms disappear from the nickel sublattice, leaving nickel vacancies. For instance, according to the most recent measurements (KOGACHI *et al.* [1992, 1995]) at 46 at% Ni, 10% of the nickel sites are vacant, most of the aluminium sites are filled. In this way the number of electrons per unit cell is kept constant and equal to approximately 3, corresponding to an e/a ratio of 3/2 characteristic of the β-brass structures. Several other studies showed that a stoichiometric β-NiAl quenched from a high temperature (as opposed to that slowly cooled) contained a high concentration of *thermal* vacancies; the most recently cited figure is 1.08% of vacancies at 1600°C. This is a very much larger thermal vacancy concentration than is found in other metals or alloys, even just below the melting temperature; so large that on cooling the vacancies will separate out into a population of voids visible in the electron microscope (EPPERSON *et al.* [1978]). 50/50 NiAl containing such vacancies, all on the nickel sublattice, must also contain substitutional defects – that is some nickel atoms in the aluminium sublattice, also called

References: p. 199.

nickel antistructure atoms — to preserve the overall chemical composition: specifically, two vacancies must be accompanied by one substitutional defect. Such a trio of linked defects is now termed a triple defect. Parallels for the behavior of the NiAl alloys at high temperatures are found in other systems isomorphous with NiAl (see CAHN [1979]).

The conclusion related to the dependence of constitutional vacancies on electron concentration has been criticized on the basis that the omission of atoms could also be interpreted in terms of size-effects. Since there is only one atom of aluminium in the unit cell of the Ni–Al alloy, it appears possible that the omission of atoms with addition of aluminium in excess of 50% occurs as a result of an inability to squeeze an additional large aluminium atom in the place of a small nickel atom. A possible differentiation between an interpretation in terms of electronic considerations and one in terms of size considerations could be made by introduction of a further element into the Ni–Al alloy. The size-effect spatial theory requires that the loss of atoms should take place when the concentration of aluminium exceeds more than one per unit cell whereas the electronic theory requires that it should occur when a definite electron concentration, approximately 1.5, is exceeded. LIPSON and TAYLOR [1939] have shown that in two ternary systems, Fe–Ni–Al and Cu–Ni–Al, the general shape of the phase field of the ternary alloys based on Ni–Al falls into the composition regions which indicate that electron concentration, rather than size, is the main factor determining the phase stability. A detailed analysis of constitutional vacancies in Ni–Al based on band energies has just been published by COTTRELL [1995].

The interpretation of the lattice spacings and density behavior in alloys based on Ni–Al is limited by the fact that nickel, a transition element, must be assumed to possess zero valency in order to make it possible to assume that the above phase is an electron phase of the 3/2 type. However, further evidence of omission of atoms from sites in a unit cell has also been obtained in the study of some γ-brasses (HUME–ROTHERY *et al.* [1952]) and Al—Zn primary solid solutions (ELLWOOD [1948, 1951–2]), in which no transition elements are involved so that the valence of the participating atoms is more definite. In the case of γ-brass two particular binary systems were studied, Cu–Al and Cu–Ga (HUME–ROTHERY *et al.* [1952]). In the former system, lattice spacing work and density data show that the number of atoms in the unit cell of the γ-phase remains constant at about 52 as aluminium is increased to approximately 35.3 at%, after which the number steadily decreases. A similar effect has been observed in the Cu–Ga γ-brass to occur at about 34.5 at% gallium. The data for Cu–Al and Cu–Ga alloys are shown in fig. 31. HUME–ROTHERY *et al.* [1952] have interpreted the creation of vacant sites in γ-brass structures in terms of the Brillouin zone of the γ-brasses, suggesting that both the normal and the defect y-structures can hold no more than about 87–88 electrons per cell in order not to exceed an electron concentration of about 1.68–1.70. It appears that the high-temperature δ-phase in the Cu–Zn system resembles a defect γ-brass structure in that it possesses numerous lattice defects and vacant atomic sites. Other constitutional vacancies in brass-type alloys have been discussed by NOVER and SCHUBERT [1980].

Creation of lattice defects in which vacancies or excess atoms are involved occurs in intermediate phases probably more frequently than it was thought likely in the past. For example, in intermediate phases which crystallize in structures closely related to the NiAs structure, the basic structure, corresponding to the formula AB, can gradually

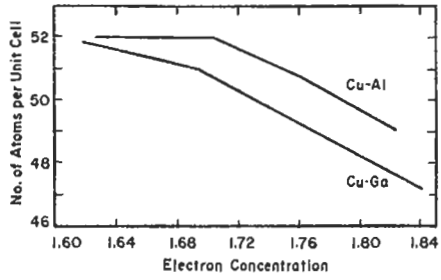

Fig. 31. The number of atoms per unit cell in the γ-phases of the system Cu–Ga and Cu–Al as a function of electron concentration (after HUME-ROTHERY *et al.* [1952].)

change in the direction of compositions A_2B by a gradual filling of certain vacant spaces* in the structure by the excess atoms of one of the components. In the series of phases such as NiS → NiSe → NiAs → Ni_3Sb_2 → Ni_3Sn_2 → Ni_2Ge → Ni_2In. The number of nickel atoms becomes greater than 50 at% and X-ray work has shown that this is accomplished by nickel atoms gradually filling certain interstitial positions in the ideal NiAs structure. The typical NiAs structure may be regarded as based on a close-packed hexagonal lattice of metalloid atoms in which the metal atoms occupy the octahedral spaces between the close-packed hexagonal layers (see ch. 5). As the structure becomes filled with the excess of the more metallic atoms, it gradually acquires a pseudo-cubic symmetry and the metallic character increases considerably so that, for example, in the series quoted above the Ni_2In phase is almost indistinguishable from the Cu–Al or Cu–Ca γ-brasses.

Constitutional vacancies in large concentrations have also been found in a number of oxides, especially those of the transition metals, and in some hydrides (e.g., TiH_x) and carbides. In some instances there is also evidence of vacancy ordering.

10.2. Stacking faults

The possibility of the formation of stacking faults in typically metallic solid solutions has recently come to play an ever-increasing role in the understanding of many properties of solid solutions, particularly those with the face-centred cubic and the close-packed hexagonal structures. Such phenomena, for example, as the changes in electrical resistivity, work-hardening, recrystallization, creep, deformation texture, crystallography of phase transformations, corrosion, phase morphology and a number of others have been shown to be related to the presence of stacking faults and therefore to the *stacking-fault energy.*

The face-centred cubic and close-packed hexagonal structures are closely related and, being both close packed, differ essentially only in the way in which the closest-packed planes are stacked together. It has been shown originally by BARRETT [1950] that stacking disorders exist in a cold-worked metal. Subsequently, several authors (PATERSON

* These are analogous to the octahedral, tetrahedral and other vacant spaces which exist in the simple metallic structures as discussed in ch. 2.

[1952], WARREN and WAREKOIS [1955], WAGNER [1957], WILKENS [1957] and JOHNSON [1963]) developed theories which relate the effect of the presence of various types of stacking faults to the changes in the X-ray diffraction pattern of the face-centred cubic structure. The normal sequence of {111} planes in a face-centred cubic structure can be described as ABCABCABC using the usual A, B, C notation. The three typical stacking errors are illustrated by the characteristic stacking patterns shown in fig. 32. They are: (1) the *intrinsic fault*, corresponding to the removal of a close-packed layer of atoms, (2) the *extrinsic fault*, corresponding to the insertion of an extra close-packed layer of atoms, and (3) the *twin (growth) fault*, produced at the interface between two perfect crystallites which are in twin relation (see READ [1953]). The intrinsic faults have received the most attention, and calculations based upon idealized models suggest that such faults should produce broadening and shifts in X-ray peak positions. This prediction has been verified experimentally in a number of pure metals (Cu, Au, Ag, Pb, Ni, etc.) and alloy systems (mostly based on the noble metals Cu, Ag and Au). Theoretical considerations of the influence of twin faults and extrinsic faults indicate that the corresponding X-ray line-broadening should be asymmetric in both cases and that the peak shifts resulting from the presence of extrinsic faults should occur in a direction opposite to the shift produced by intrinsic faulting (JOHNSON [1963]). Published work to date indicates that in metals intrinsic faults predominate. However in other materials, for example in silicon (AERTS *et al.* [1962a, b]), the stacking-fault energy of intrinsic and extrinsic faults may be of about equal magnitude. If, in addition, one considers the less idealized cases in which the distribution of stacking-fault density is variable in a specimen, the prediction of the over-all X-ray pattern becomes very complex (see for example, BARRETT and MASSALSKI [1966] p. 464). Nevertheless, the X-ray work has served as a useful means for comparison between various metals and alloys and for the studies of trends in faulting probability with composition and temperature.

In addition to the above mentioned X-ray analysis a direct estimate of stacking-fault energy γ can also be made by studies of certain annealing or deformation features in metals and alloys and their changes with temperature, by studies of twinning frequency in metallographic samples (FULLMAN [1951] and BOLLING and WINEGARD [1958a, b]), by interpretation of dissociated dislocations (nodes) in transmission electron photomicrographs (HOWIE and SWANN [1961] and CHRISTIAN and SWANN [1965]) and other features such as cross-slip, creep, texture etc. [GALLAGHER [1970]).

The possibility of the existence of stacking faults in hcp and bcc structures has been

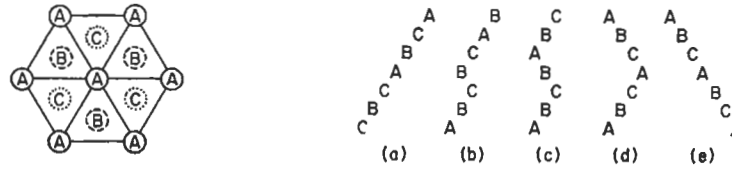

Fig. 32. Planar view of atomic positions and stacking sequences for: (a) perfect fcc crystal; (b) intrinsic fault; (c) extrinsic fault; (d) twin fault; (e) twin crystal. (After JOHNSON [1963].)

considered in a number of publications both from the experimental and the theoretical point of view. In bcc and hcp metals stacking faults do not produce line shifts (see WARREN [1959a]). In hexagonal metals they produce broadening of certain reflections, which has been observed experimentally, particularly in the case of cobalt (EDWARDS and LIPSON [1942]).

A number of attempts have been made to elucidate the factors which influence the changes of stacking-fault energy upon alloying. Although all such factors must be electronic in nature, it appears at the moment that a detailed interpretation is not possible. In a number of publications the changes of stacking-fault energy have been related to the electron concentration, certain size effects, the changes in the density of stat.es, and the changes in the topology of the Fermi surface (See GALLAGHER [1970].)

In the case of fcc *metals*, recent measurements of the rate of loop annealing, the stability of tetrahedra introduced by deformation, of faulted dipoles, and of texture developed by rolling have led to the availability of quite precise information on the magnitude of γ for materials in which extended nodes or extrinsic-intrinsic fault pairs cannot be observed. Thus, it is no longer essential to estimate the fault energy of such metals as Cu, Au, Al, and Ni by extrapolating node data or normalized X-ray faulting probability results, although the extrapolation procedures, too, have been improved and now lead to more reliable results. Reasonable estimates of γ, probably accurate to ±20%, are: $\gamma_{Ag} = 21.6$ mJ/m^2, $\gamma_{Ph} = 30$ mJ/m^2, $\gamma_{Au} = 50$ mJ/m^2, $\gamma_{Cu} = 55$ mJ/m^2, $\gamma_{Al} = 200$ mJ/m^2 and $\gamma_{Ni} = 250$ mJ/m^2. Estimates of γ in other elements from scaled rolling-texture data are subject to rather larger errors, but are the best values available at the present time: $\gamma_{Ce} <$ 5 mJ/m^2, $\gamma_{Yb} < 10$ mJ/m^2, $\gamma_{Th} = 70$ mJ/m^2, $\gamma_{Pt} = 75$ mJ/m^2, $\gamma_{Pd} = 130$ mJ/m^2 and $\gamma_{Rh} = 330$ mJ/m^2 (GALLAGHER [1970]). Advances have been made in theoretical estimates of γ for pure materials (BLANDIN *et al.* [1966]), but difficulties are still experienced in applying the treatments to noble metals on account of their complex electronic structure.

In fcc *solid solutions*, a satisfactory amount of numerically accurate information is now available for the variation of γ (effective) with alloying, particularly in systems with copper, silver, and nickel as solvents. The form of the variation with B-group solutes in all cases follows the pattern established in the earliest studies in that γ decreases with increasing solute concentration, and a considerable normalization of the data is achieved in plots with the electron/atom ratio as abscissa.

Several authors have noted that straight-line relationships for the change of γ with alloying can be obtained if γ is plotted on a log scale and the abscissa is expressed in terms of a composition-dependent function $[c/(1+c)]^2$, where $c =$ (alloying concentration)/(solubility limit) at high temperatures. Expressing the abscissa in this form appears to provide a normalizing effect similar to that which arises by using the e/a ratio, but with the advantage that the solubility limit is in some systems more accurately known than is the effective valence of the solute. The relationship obtained for the fcc Cu–Si alloys is shown in fig. 33. Recent studies also suggest that in alloys of two fcc elements having complete mutual solubility, all compositions have γ intermediate in value between the fault energies of the component metals. Such noble-metal–transition-metal alloys as have been studied have γ of the same order as in the pure noble metal. Contrary to early studies, considerable extrinsic–intrinsic faulting has recently been observed in copper-,

References: p. 199.

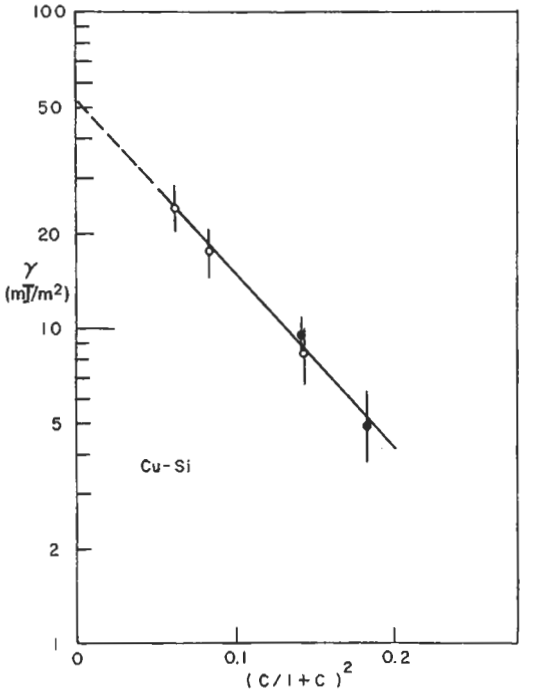

Fig. 33. Semi-log plot of γ versus $[c/(1+c)]^2$ in the Cu–Si series (from GALLAGHER [1970]).

silver-, and gold-base alloys, and measurements on fault pairs have revealed that the extrinsic and intrinsic fault energies are approximately equal (GALLAGHER [1970]).

10.3. Metastable structures*

Many solid solutions whose properties have been outlined in the preceding sections can exist in a metastable condition at temperatures which fall outside the equilibrium range of stability but at which the rate of approach to equilibrium is so slow as to be negligible. One of the most frequently used methods for producing metastability is rapid quenching from a high temperature. During quenching a single-phase solid solution may be retained untransformed, or it may transform by changing its crystal structure, either by a martensitic or a "massive" process (see BARRETT and MASSALSKI [1966]). Metastable solid solutions have also been obtained by a rapid cooling from the liquid state, using the "splat" or "crusher" cooling techniques (DUWEZ [1965, 1967]), by a rapid cooling from the vapor state, using vacuum deposition techniques (MADER *et al.* [1963]) or sputtering (MASSALSKI and RIZZO [1988]), by various methods involving the quenching of liquid metals on a rapidly revolving copper wheel, and by surface melting methods

* See also chapter 19.

using laser beams, electron beams, etc. (See DUWEZ [1978] and also ch. 7, § 9.1.).

Following these procedures, enhanced solubilities, non-equilibrium phases and unusual crystalline and amorphous structures have been obtained. For example, a continuous series of *metastable solid solutions* can be obtained in the Cu–Ag system in place of the well-known eutectic phase diagram corresponding to equilibrium conditions. In other instances solid solutions have been obtained that are *amorphous,* resembling a frozen liquid. A large number of metastable phases obtained by the various rapid-cooling techniques have most unusual crystalline (or non-crystalline) electrical, semiconducting, superconducting, magnetic and thermal properties. The research area of metallic glasses, in particular, has seen very rapid growth during the past two decades and numerous symposia and reviews on this subject have been published (see, e.g., MASUMOTO and SUZUKI [1982], PEREPEZKO and BOETTINGER [1983]; TURNBULL [1981]; JOHNSON [1986]). In order to produce a metallic glass, crystallization has to be prevented during rapid cooling of the liquid. Cooling rates exceeding 10^6 K/s are usually needed to achieve this, and the most likely regions in phase diagrams where metallic glasses can be produced are the deep eutectic regions. The reason for this has been discussed in numerous publications. One of the possibilities is that, in deep eutectics, the crystallization competing with metallic-glass formation must be of a multi-phase form, which is kinetically difficult. Here, the T_0 concept provides a very useful guide to the search for glass formation regions in metallic systems (MASSALSKI [1982]). Hence, the chilled liquid becomes more and more viscous without crystallization until a glass transition temperature is reached when the liquid becomes a solid. The subject is discussed more fully in ch. 7, § 9.1.

11. Order in solid solutions

The phenomena related to order–disorder (O–D) changes in solid solutions comprise a very extensive literature and a detailed review of these is beyond the scope of this chapter. Nevertheless, the tendency for unlike atoms to occupy adjoining sites of a crystalline lattice, leading towards formation of superlattices, is a very prominent feature of many solid solutions; and we shall briefly consider this subject from the structural point of view.

On the basis of thermodynamics (see ch. 5) it can be shown that an ordered arrangement of atoms in an alloy may produce a lower internal energy compared to a disordered arrangement, particularly if the segregation of atoms to designated atomic sites occurs at relatively low temperatures where entropy, associated with randomness, plays a lesser role. The condition of perfect order, such that the like atoms are never nearest neighbors, could be achieved only in a perfect single crystal with a simple metallic lattice and at compositions corresponding to stoichiometric ratios of atoms like AB, AB_2, AB_3, etc. Actually, the presence of various imperfections and grain boundaries precludes this possibility in most cases. In addition, it is known that an ordered solid solution consists of *ordered domains* which may be perfectly ordered within themselves but which are *out of step* with one another. This results in more contact between like atoms at the boundaries of adjacent domains. Ordered domains are sometimes called *antiphase domains* and

usually their number is quite large within each grain of the material. With the development of electron microscopy techniques, the presence of antiphase domains has been confirmed by direct observation in thin films (GLOSSOP and PASHLEY [1959], SATO and TOTH [1961]).

A further departure from maximum order occurs in solid solutions whose compositions deviate from the optimum stoichiometric ratios of atoms. This is often associated with the fall of the ordering temperature on both sides of the ideal composition and by the change of other properties such as hardness, electrical resistivity, etc.

When the interaction between unlike atoms is very strong, the critical temperature T_c, at which disordering occurs, may lie above the melting point of the material. Alloys with this characteristic closely resemble chemical compounds. When the interaction forces are less intense, an ordered solid solution may become disordered at a critical temperature even though the composition corresponds to a stoichiometric compound-like formula. Many typical alloy phases show this behavior with temperature. Finally, if the ordering forces are weak, as for example at low atomic concentrations in terminal solid solutions, the critical temperature may lie below the temperature at which attainment of equilibrium is possible within a reasonable time. One may then speak of the disordered state being frozen in. It has been found that the activation energy necessary to switch atoms into disordered positions in a fully ordered alloy is of the same order of magnitude as the heat of activation for diffusion or for recovery from cold work, usually about 1.5–2 eV. References to recent work on long range order in alloys are given by LAUGHLIN [1988].

11.1. Types of superlattices

Simple superlattices in binary alloys with cubic structure occur near compositions corresponding to formulas A_3B, AB and AB_3. The Cu–Au system (see fig. 1b, above) provides a well-known prototype of ordered solid solutions based on the fcc structure. The superlattices Cu_3Au, CuAu and $CuAu_3$ have been investigated in great detail. In the case of Cu_3Au the low-temperature structure, (fig. 34a) is cubic, but in the case of CuAu (fig. 34c) alternate (002) planes contain either all copper or all gold atoms and a contraction occurs in the c direction, presumably as a result of attraction between atoms in these planes. This results in a tetragonal fcc structure with c/a ratio of 0.92.

Order in bcc alloys again depends on composition. At 50 at% of solute the AB type of order results in the well-known CsCl structure (fig. 34b) which occurs, for example, in ordered β-brass. When the composition is between approximately 25 and 50 at% of solute, a sequence of ordered structures based on the simple body-centred cube sometimes becomes possible and such structures have been studied in detail (e.g., RAPACIOLI and AHLERS [1977], for β-Cu, Zn, Al). The superlattices that occur in the Fe–Al system (fig. 34d) and the *Heusler alloys* (Cu_2MnAl), which are ordered when in the ferromagnetic condition, have received particular attention (see, for example, TAYLOR [1961]). With solute contents exceeding 50 at% the γ-brass type of order and other more complex superlattices are possible.

By analogy with the cubic structures, ordered superlattices occur frequently in close-packed hexagonal solid solutions. For example, in the Mg–Cd system the continuous

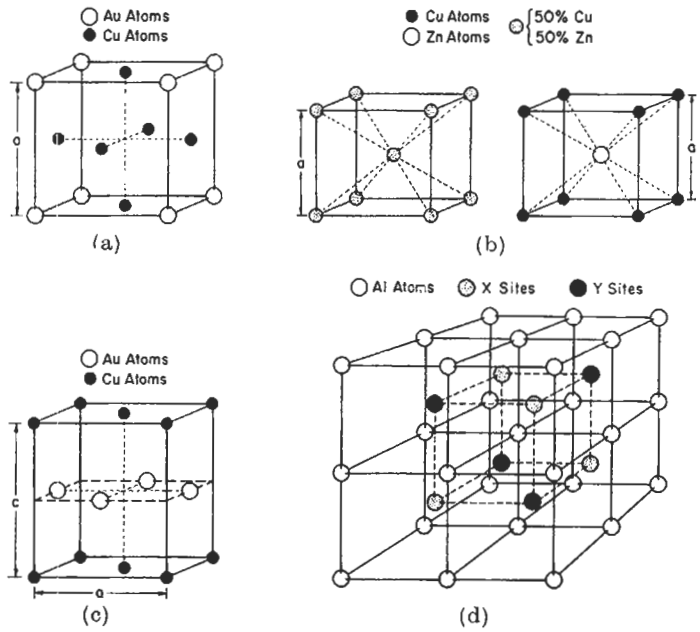

Fig. 34. Various types of ordered superlattices: (a) ordered cubic superlattice Cu_3Au; (b) disordered and ordered structures of β-brass; (c) the tetragonal superlattice of AuCu; (d) the structure of Fe_3Al and FeAl: Al atoms fill the X sites in Fe_3Al and the X and Y sites in FeAl.

series of solid solution at high temperatures is broken at lower temperatures by the formation of ordered superlattices at compositions $MgCd_3$, MgCd and Mg_3Cd (see fig. 1d, above). $MgCd_3$ orders to form the DO_{19} type of structure which is distorted from close-packed hexagonal, while the Mg_3Cd is closepacked hexagonal but with the a axis doubled and the basal layers so arranged that each cadmium atom is in contact with three magnesium atoms in the adjacent layers. Cooling of alloys in the MgCd composition region produces an ordered orthorhombic structure.

11.2. Long-period superlattices

As mentioned in the previous section, the low-temperature annealing of CuAu alloys (below 380°C) produces a face-centred tetragonal structure whose unit cell is shown in fig. 34b. This structure is usually referred to as CuAu I. In the temperature interval between 380–410°C another ordered structure has been detected (by JOHANSSON and LINDE [1936]) which is often described as CuAu II. The superlattice CuAu II is a modification of CuAu I and the unit cell of this structure is orthorhombic as shown in fig. 35a. The long cell is obtained by stacking five CuAu I unit cells in a row in the direction of one of the long-cell edges ($\boldsymbol{b}$) and then repeating this unit at five cell intervals with a simultaneous *out-of-step* shift at the boundary through a distance equal to the vectorial distance $\frac{1}{2}(\boldsymbol{a}+\boldsymbol{c})$. The distance between each antiphase boundary may thus

References: p. 199.

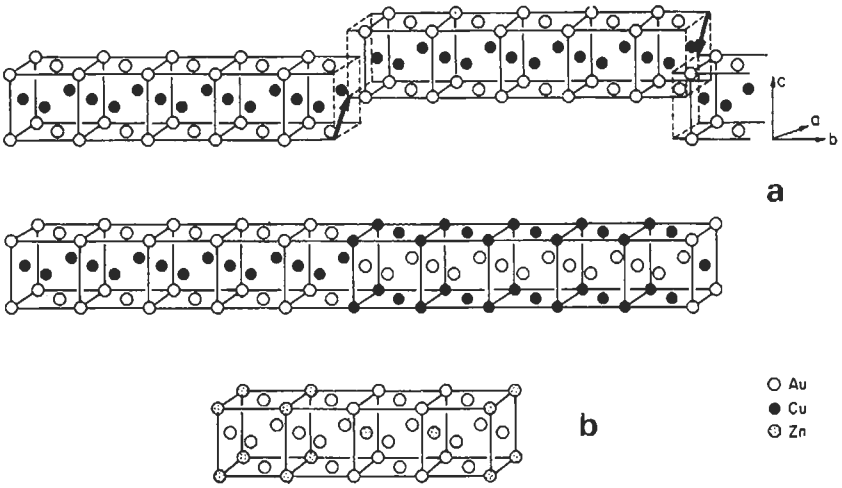

Fig. 35. Long-period superlattices: (a) the structure of CuAu II; (b) the structure of Au–Zn. (After SCHUBERT *et al.* [1955].)

be specified by $M \times b$ where M denotes the domain size *or the period.* For CuAu II, $M = 5$. This superlattice is therefore called a *one-dimensional long-period superlattice* with a period equal to five. OGAWA and WATANABE [1954] have shown that a repulsive force arises at the junction of the long antiphase domains, which leads to a small local lattice-parameter increase in the direction of the long axis. This has the effect of a small periodic error in the diffracting lattice in this direction, and in electron-diffraction patterns it produces "satellite" reflections around the normal reflections.

Many other long-period superlattices have been discovered in cubic alloys, particulary at the A3B compositions. Long-period superlattices have also been reported in hexagonal alloys (SCHUBERT *et al.* [1955]). The structure shown in fig. 35b corresponds to the orthorhombic structure Au_3Zn. This long-period superlattice is based on Cu_3Au and consists of four face-centred cells stacked together with a half-diagonal shift as shown in the figure. Most of the long-period superlattices at compositions A_3B retain the cubic symmetry of atomic distribution and they can be either one-dimensional long-period superlattices or two-dimensional superlattices. Much of the recent work in this field is due to SCHUBERT *et al.* [1955] and to SATO and TOTH [1961, 1962, 1965].

The discovery of the long-period superlattices has presented a challenge to the theory of alloys because the usual atom-pair interaction models adopted for explanation of the order-disorder phenomena cannot be used unless one assumes extremely long-distance interactions. The most successful interpretation at the moment appears to be that such superlattices are a result of a complex interaction between the Fermi surface and the Brillouin zone (SATO and TOTH [1961, 1962, 1965]) and is therefore connected with the collective behavior of the free electrons. The Brillouin zone for the CuAu alloys is shown in fig. 36. The thin lines represent the zone for the disordered fcc structure. This zone is bounded by the octahedral {111} and cubic {200} faces and can hold two

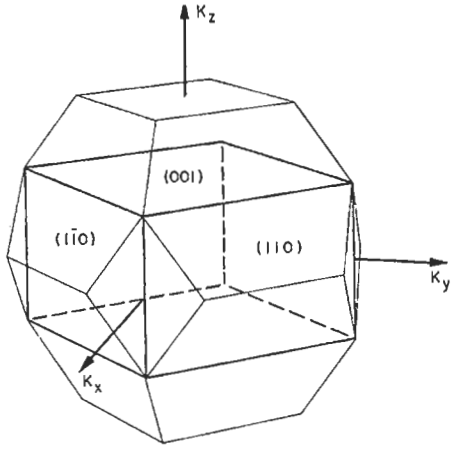

Fig. 36. The Brillouin zone of the disordered (thin lines) and ordered (thick lines) fcc structures (from SATO and TOTH [1962].)

electrons per atom. The thick lines represent the zone for the ordered CuAu I superlattice. This zone, as a result of order in the lattice, is now bounded by the {001} and {110} faces and is therefore no longer symmetrical, the {100} faces being much closer to the origin than the {110} faces. The free-electron energies at the centers of the {100} and {110} faces are 2.4 eV and 4.8 eV respectively, while the energy at the Fermi surface corresponding to one electron per atom (Cu–Au system) is 6.5 eV. Therefore electrons should overlap into the larger zone. The existence of "satellite" reflections around the normal reflections in the *b* direction, corresponding to the long-range periodicity in the CuAu II superlattice, suggests that the Brillouin zone would show a slight splitting of certain faces. This is illustrated in fig. 37b and c which represents a horizontal section in the reciprocal lattice throught the zone shown in fig. 36. SATO and

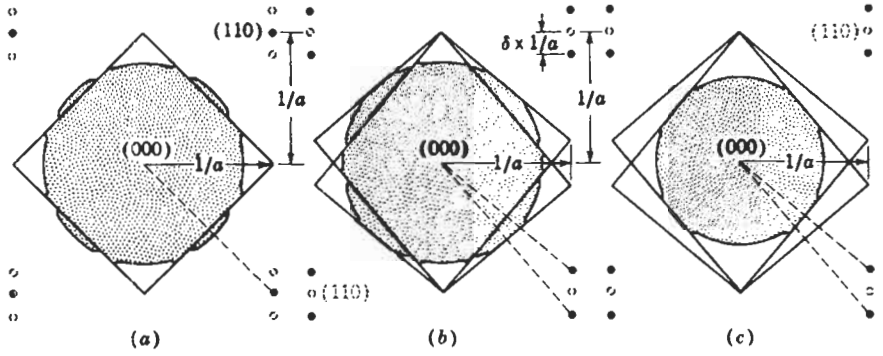

Fig. 37. Horizontal section in reciprocal space through the Brillouin zone of fig. 36, showing possible Fermi surface contours for the Cu–Au superlattice: (a) CuAu I; (b,c) CuAu II. (From BARRETT and MASSALSKI [1966].)

TOTH [1962] have proposed that at one electron per atom, the Fermi surface comes rather close to the {110} faces and, when the CuAu II superlattice is formed, the interaction between the Fermi surface and these split faces produces extra stabilization of the long-period structure. Since the period M governs the extent to which the satellite spots are separated in the reciprocal lattice, there should be a relationship between M and the electron concentration which governs the volume of the Fermi "sphere". It can be shown that as e/a increases, the Fermi "sphere" would fit better with respect to the {110} faces if their splitting were increased. This requires that the period M should decrease. SATO and TOTH [1961] have shown that additions of alloying elements to the CuAu II superlattice, resulting in changes of e/a, also poduce changes of the long-range period in the direction suggested by the above model. Furthermore, the model makes also possible the explanation of other characteristics of the long-period superlattices such as the nature of the distortion of the lattice, the concentration and temperature dependence of the distortion and of the periods, and the question whether or not the superlattice will be one-dimensional or two-dimensional. (Ordering in CuAu is treated by RAPSON [1995].)

11.3. Long-range order and short-range order

Attempts to formulate a theory of ordering date back to the 1930s and are associated with the names of Borelius, Johansson and Linde, Dehlinger, Bragg and Williams, Bethe, Peierls, Takagi and others. Several comprehensive reviews exist on both the mechanisms of ordering and on various treatments of the subject, and they may be consulted for details; for example, those of NIX and SHOCKLEY [1938], LIPSON [1950] and GUTTMAN [1956].

The essential condition for a solid solution of suitable composition to become ordered is that dissimilar atoms must attract each other more than similar atoms in order to lower the free energy upon ordering. In terms of interaction energies between pairs of atoms of two atomic species A and B this condition is usually expressed as follows:

$$E_{AB} < \tfrac{1}{2}\left(E_{AA} + E_{BB}\right), \tag{11}$$

where E_{AA} and E_{BB} represent energies of like pairs of atoms and E_{AB} represents the energy of the unlike pair. If this condition is satisfied for a given alloy of a stoichiometric composition, then at some suitably low temperature the structure will become perfectly ordered, the A and B atoms occupying designated sites in the lattice, which may be called the α and β sites. On warming up the energy will be supplied in the form of heat and will cause some A atoms to migrate into "wrong" β sites and vice versa, causing the atomic distribution to become more *random*. With perfect order at a low temperature the mathematical probability of finding an A atom on an a site and a B atom on a β site is unity. At higher temperatures, however, the probability that an a site is occupied by an A atom will be reduced to a fraction of unity, say p. BRAGG and WILLIAMS [1934] have used this description to define the *long-range order parameter*, S,

$$S = (p - r)/(1 - r), \tag{12}$$

where r is the fraction of A atoms in the alloy. According to eq. (11), S varies from one to zero as order decreases.

The order-disorder change, like the magnetic change, is a *cooperative phenomenon*. As more atoms find themselves in "wrong" atomic sites due to thermal agitation the energy difference indicated by eq. (10) decreases and it becomes easier to produce further disorder. Eventually a critical temperature is reached, T_c, at which all distinction between different sites is lost.

The simple approach as outlined above does not allow for the possibility of the existence of magnetic domains and other types of interruptions in the ordered array of atoms that may cause a departure from perfect order (as mentioned in a previous section) which makes it possible for a high degree of local order to exist even though its perfection is not absolute on a large volume scale. In order to describe such situations an alternative method of defining the state of order is possible which, instead of considering the probability of finding A or B atoms on designated α or β lattice sites, takes into acount the number of unlike nearest neighbors around a given atom. For example, the BETHE [1935] *short-range order parameter*, σ, is defined by:

$$\sigma = (q - q_r)/(q_m - q_r), \tag{13}$$

where q denotes the fraction of unlike nearest neighbors at a given temperature and q_r and q_m correspond to the fractions of unlike nearest neighbors at conditions of maximum randomness and maximum order. As may be seen, σ is defined in such a way that it would become unity for perfect order and zero for randomness.

Actually, instead of reaching zero on disordering, σ usually remains a definite value above T_c. In terms of the relationship between atoms, σ measures the state of order in the immediate vicinity of a given atom unlike the long-range order parameter, S, of Bragg and Williams which deals with the whole lattice. The description of the immediate surroundings of a given atom can be extended further to include several successive concentric shells corresponding to the first, second, third, etc., nearest neighbors (COWLEY [1950]).

References

AAERTS, E., P. DELAVIGNETTE, R. SIEMS and S. AMELINCKX, 1962a, Electron Microscopy (Academic, New York).

AAERTS, E., P. DELAVIGNETTE, R. SIEMS and S. AMELINCKX, 1962b, J. Appl. Phys. **33**, 3078.

AHLERS, M., 1981, *J. Phys. F* **11**, 1775.

AMELINCKX, S., 1988, in: Encyclopedia of Materials Science and Engineering, Supp. Vol. 1, ed. R.W. CAHN, Pergamon Press, Oxford, p. 77.

ARGENT, B.B., and D.W. WAKEMAN, 1956–7, J. Inst. Metals **85**, 413.

AVERBACH, B.L., 1956, in: Theory of Alloy Phases (ASM, Metals Park, OH).

AXON, H.J., and W. HUME-ROTHERY, 1948, Proc. Roy. Soc. **A193**, 1.

BARRETT, C.S., 1950, Trans. AIME **188**, 123.

BARRETT, C.S., and T.B. MASSALSKI, 1966, Structure of Metals, 3rd Ed. (McGraw-Hill, New York).

BENNETT, L.H., ed., 1980, Proc. Conf. on theory of Alloy Phase Formation (AIME, Warrendale, PA).

BETHE, H.A., 1935, Proc. Roy. Soc. (London) **A150**, 552.

BLANDIN, A., 1965, in: Alloying Behavior and Effects in Concentrated Solid Solutions, ed. T. B. MASSALSKI (Gordon and Breach, New York).
BLANDIN, A., and J. FRIEDEL and G. SAADA, 1966, J. Phys. Suppl. C3, **27**, 128.
BOLLING, G. F., and W. C. WINEGARD, 1958a, J. Inst. Metals **86**, 492.
BOLLING, G. F., and W. C. WINEGARD, 1958b, Acta Metall. **6**, 288.
BOLLING, G. F., T. B. MASSALSKI and C. J. MCHARGUE, 1965, Phil. Mag. **6**, 491.
BORIE, B. S., 1957, Acta Cryst. **10**, 89.
BORIE, B. S., 1959, Acta Cryst. **12**, 280.
BRADLEY, A. J., and A. TAYLOR, 1937, Proc. Roy. Soc. (London) **A159**, 56.
BRAGG, W. L., and E. J. WILLIAMS, 1934, Proc. Roy. Soc. (London) **A145**, 669.
BREWER, L., 1968, Science, **161**, 115.
BROOKS, H., 1955, in: Impurities and Imperfections, ASM Seminar (ASM, Metals Park, OH).
CAHN, R. W., 1979, Nature **279**, 579.
CHRISTIAN, J. W., and P. R. SWANN, 1965, in: Alloying Behavior and Effects in Concentrated Solid Solutions, ed. T. B. MASSALSKI (Gordon and Breach, New York) p. 105.
COCKAYNE, B., and G. V. RAYNOR, 1961, Proc. Roy. Soc. **A261**, 175.
COHEN, M. H., 1965, in: Alloying Behavior and Effects in Concentrated Solid Solutions, ed. T. B. MASSALSKI (Gordon and Breach, New York).
COLES, B. R., 1956, J. Inst. Metals **84**, 346.
COTTRELL, A. H., 1988, Introduction to the Modern Theory of Metals, Institute of Metals, London.
COTTRELL, A. H., 1993, Mat. Sci and Tech. **9**, 277.
COTTRELL, A. H., 1995, Intermetallics **3**, 341.
COWLEY, J., 1950, Phys. Rev. **77**, 669.
DARKEN, L. S., and R. W. GURRY, 1953, Physical Chemistry of Metals (McGraw-Hill, New York).
DE FONTAINE, D., 1983, M. R. S. Symp., vol. 19, p. 149.
DUWEZ, P., 1965, in: Alloying Behavior and Effects in Concentrated Solid Solutions, ed. T. B. MASSALSKI (Gordon and Breach, New York).
DUWEZ, P., 1967, Trans. ASM **60**, 607.
DUWEZ, P., ed., 1978, Metallic Glasses, ASM seminar (ASM, Metals Park, OH).
EDWARDS, Os., and H. LIPSON, 1942, Proc. Roy. Soc. **A180**, 208.
ELLNER, M., 1978, J. Less-Common Met. **60**, 15.
ELLNER, M., 1980, J. Less-Common Met. **75**, 5.
ELLWOOD, E. C., 1948, Nature, **163**, 772.
ELLWOOD, E. C., 1951–2, J. Inst. Metals **80**, 217.
EPPERSON, J. E., K. W. GERSTENBERG, D. BRENER, G. KOSTORZ and C. ORTIZ, 1978, Phil. Mag. **A38**, 529.
ESHELBY, J. D., 1956, Solid State Phys. **3**, 79.
FAULKNER, J. S. and G. M. STOCKS, 1981, *Phys. Rev. B*, **23**, 5628.
FAULKNER, J. S. , 1982, Prog. Mater. Sci. **27**, 1.
FRIEDEL, J., 1954a, Adv. Phys. **3**, 446.
FRIEDEL, J., 1954b, Les Electrons dans les Métaux, 10th Solvay Conference (ed. R. STOOPS, Bruxelles, 1955).
FRIEDEL, J., 1955, Phil. Mag. **46**, 514.
FRIEDEL, J., 1964, Trans. AIME **230**, 616.
FULLMAN, R. L., 1951, J. Appl. Phys. **22**, 488.
FUMI, F., 1955, Phil./ Mag. **45**, 1007.
GALLAGHER, P. C. J., 1970, Metallurg. Trans. **1**, 2450.
GLOSSOP, A. B., And D. W. PASHLEY, 1959, Proc. Roy. Soc. **A250**, 132.
GOLDSCHMIDT, H. J., 1948, J. Iron Steel Inst. **160**, 345.
GSCHNEIDNER, K. A., 1980, in: Theory of Alloy Phase Formation, ed. L. H. BENNETT (AIME, Warrendale, PA).
GUTTMAN, L., 1956, Solid State Phys. **3**, 145.
HAFNER, J., 1983, in: Mat. Res. Soc. Symp. Proc., Vol. 19, eds. H. BENNETT, T. B. MASSALSKI and B. C. GIESSEN, Elsevier Science Publ. Co., p. 1.
HARRISON, W. A., 1959, Phys. Rev. **116**, 555; 1960, **118**, 1190.
HARRISON, W. A., and M. B. WEBB, eds., 1960, The Fermi Surface (Wiley, New York).

HEINE, V., 1967, in: Phase Stability in Metals and Alloys, eds. P. S. RUDMAN, J. STRINGER and R. I. JAFFEE (McGraw-Hill, New York).
HELLAWELL, A., and W. HUME–ROTHERY, 1954, Phil. Mag. **45**, 797.
HENDERSON, B., and G. RAYNOR, 1962, Proc. Roy. Soc. **A267**, 313.
HERBSTEIN, F. H., B. S. BORIE and B. L. AVERBACH, 1956, Acta Cryst. **9**, 466.
HILL, R. B., and H. J. AXON, 1954–5, J. Inst. Metals **83**, 354.
HILL, R. B., and H. J. Axon, 1956–7, J. Inst. Metals **85**, 102.
HOWIE, A., and P. R. SWANN, 1961, Phil. Mag. **6**, 1215.
HUANG, K., 1947, Proc. Roy. Soc. **A190**, 102.
HUME–ROTHERY, W., 1955, Atomic theory for the Students of Metallurgy (The Institute of Metals, London); enlarged edition, 1960.
HUME–ROTHERY, W., 1961a, Elements of Structural Metallurgy (The Institute of Metals, London) Monograph and Report Series, no. 26).
HUME–ROTHERY, W., 1961b, J. Inst. Metals **9**, 42.
HUME–ROTHERY, W., 1964, The Metallurgist, p. 11.
HUME–ROTHERY, W., 1966, The Structure of Alloys of Iron (Pergamon Press, Oxford).
HUME–ROTHERY, W., 1967, in: Phase Stability in Metals and Alloys, eds. P. S. RUDMAN, J. STRINGER and R. I. JAFFEE (McGraw-Hill, New York).
HUME–ROTHERY, W., and B. R. COLES, 1954, Adv. Phys. **3**, 149.
HUME–ROTHERY, W., and G. V. RAYNOR, 1949), Proc. Roy. Soc. **A174**, 471.
HUME–ROTHERY, W., J. O. BETTERTON and J. REYNOLDS, 1952, J. Inst. Metals **80**, 609.
HUME–ROTHERY, W., R. E. SMALLMAN and C. W. HAWORTH, 1969, The Structure of Metals and Alloys , 5th edn. (The Institute of Metals, London), p. 349.
JOHANNSON, C. H., and J. O. LINDE, 1936, Ann. Phys. **25**, 1.
JOHNSON, C. A., 1963, Acta Cryst. **16**, 490.
JOHNSON, W. L., 1986, Prog. Mat. Sci. **30**, 81.
JONES, H., 1934a, Proc. Roy. Soc. **A144**, 225.
JONES, H., 1934b, Proc. Roy. Soc. **A147**, 396.
JONES, H., 1937, Proc. Roy. Soc. **A49**, 250
JONES, H., 1952, Phil. Mag. **43**, 105.
JONES, H., 1960, The Theory of Brillouin Zones and Electronic States in Crystals (North-Holland, Amsterdam).
JONES, H., 1962, J. Phys. Radium **23**, 637.
KIKUCHI, R., Physica, 1981, **103B**, 41.
KING, H. W., 1966, J. Mater. Sci. **1**, 79.
KING, H. W., and T. B. MASSALSKI, 1961, Phil. Mag. **6**, 669.
KLEE, H., and H. WITTE, 1954, Z. Phys. Chem. **202**, 352.
KOGACHI, M., S. MINAMIGAWA and K. NAKAHIGASHI, 1992, Acta Metall. et Mater. **40**, 1113.
KOGACHI, M., Y. TAKEDA and T. TANAHASHI, 1995, *Intermetallics*, in press.
KOIKE, S., M. HIRABAYASHI and To. SUZUKI, 1982, Phil. Mag. **45**, 261.
LAVES, F., and H. WITTE, 1935, Metallwirtschaft **14**, 645.
LAVES, F., and H. WITTE, 1936, Metallwirtschaft **15**, 840.
LAUGHLIN, D. E. , 1988, "Long-Range Order in Alloys", Encyclopedia of Materials Science and Engineering, Supp. Vol. 1, (Pergamon Press, Oxford) pp. 263–268.
LIESER, K. H., and H. WITTE, 1954, Z. Phys. Chem. **202**, 321.
LIPSON, H., 1950, Prog. Metals Phys. **2**, 1.
LIPSON, H., and A. TAYLOR, 1939, Proc. Roy. Soc. (London) **A173**, 232.
LOMER, 1967, in: *Phase Stability in Metals and Alloys*, eds. P. S. RUDMAN, J. STRINGER and R. I. JAFFEE, McGraw Hill, New York.
MACHLIN, E. S., 1981, CALPHAD vol. 5, p. 1.
MANN, E., and A. SEEGER, 1970, J. Phys. Chem. Solids **12**, 314.
MASSALSKI, T.B., 1958, Met. Rev. **3**, 45.
MASSALSKI, T.B., and H. W. KING, 1961, Prog. Mater. Sci. **10**, 1.
MASSALSKI, T.B., and U. MIZUTANI , 1978, Prog. Mater. Sci. **22**, 151.

MASSALSKI, T.B., U. MIZUTANI and S. NOGUCHI, 1975, Proc. Roy. Soc. **A343**, 363.
MASSALSKI, T.B., 1982, in: Proceedings of RQ4 Conference, T. MASUMOTO and U. SUZUKI, eds. Jap. Inst. of Metals, p. 203.
MASSALSKI, T. B., and H. F. RIZZO, 1988, Proc. of JIMIS-5 on Non-Equilibrium Solid Phases of Metals and Alloys, Suppl. to Trans. JIM, vol. 29, p. 217.
MASSALSKI, T. B., 1989 , The Campbell Lecture, Metallurgical Transactions, **20A**, 1295; and **20B**, 445.
MASSALSKI, T. B., 1990, Binary Alloy Phase Diagrams, second edition, T. B. MASSALSKI editor-in-chief, H. OKAMOTO and L. KACPRZAK, editors, American Society for Metals.
MIEDEMA, A. R., P. F. DE CHATEL and F. R. DE BOER, 1980, *Physica*, **100B**, 1.
MIEDEMA, A. R., and A. K. NIESSEN, 1988, *Proc. JIMIS-5*, "Non-Equilibrium Solid Phases of Metals and Alloys", JIM Suppl. vol. 29, p. 209.
MOHRI, T., K. TERAKURA, T. OGUCHI and K. WATANABE, 1988, Acta Metall., **36**, 547.
MORINAGA, M., N. YUKAWA and H. ADACHI, 1985,J. Phys. F, **15**, 1071.
MOTT, N. F., and H. Jones, 1936. The Theory of the Properties of Metals and Alloys (Oxford University Press).
MOTT, N. F., 1952, Prog. Met. Phys. **3**, 76.
MOTT, N. F., 1962, Rept. Prog. Phys. **25**, 218.
NEVITT, M., 1963, in: Electronic Structure and Alloy Chemistry of Transition Elements, ed. P. A. BECK (Wiley, New York).
NIEMIEC, J., 1966, in: Fizykochemia Ciala Stalego, ed. B. STALINSKI (Panstwowe Wydawnictwo Naukowe, Warsaw).
NIX., F. C., and W. SHOCKLEY, 1938, Rev. Mod. Phys. **10**, 1.
NOVER, R. G., and K. SCHUBERT, 1980, Z. Metallk. **71**, 329.
OGAWA, S., and D. WATANABE, 1954, Acta Cryst. **7**, 377.
OWEN, E. A., 1947, J. Inst. Metals, **73**, 471.
PATERSON, M. S., 1952, J. Appl. Phys. **23**, 805.
PEARSON, W. B., 1958 and 1967, A Handbook of Lattice Spacings and Structures of Metals and Alloys (Pergamon Press, London and New York) vol. 1, 1958; vol. 2, 1967.
PEARSON, W. B., 1967, in: Phase Stability in Metals and Alloys, P. S. RUDMAN, J. STRINGER and R. I. JAFFEE, eds., McGraw Hill, New York.
PEREPEZKO, J. H. and W. J. BOETTINGER, 1983, in Alloy Phase Diagrams, L. H. BENNETT, T. B. MASSALSKI and B. C. GIESSEN, eds. MRS Symposium, Vol. 19, p. 223. Elsevier Publ., Inc.
PEI, S., T. B. MASSALSKI, W. M. TEMMERMAN, P. A. STERNE and G. M. STOCKS, 1989, Physical Review B, **39**, 5767.
PETTIFOR, D. G., 1979, Phys. Rev. Letters **42**, 846.
PETTIFOR, D. G., 1986, J. Phys. C, **19**, 285.
PIPPARD, A. B., 1957, Phil. Trans. Roy. Soc. **A250**, 325.
RAPACIOLI, R., and M. AHLERS, 1977, Scripta Metall. **11**, 1147.
RAPSON, W. S., 1995, in: Intermetallic Compounds — Principles and Practice, eds. J. H. Westbrook and R. L. Fleischer (Wiley, Chichester), Vol. 2, p. 559.
RAYNOR, G. V., 1949a, Trans. Farad. Soc. **45**, 698.
RAYNOR, G. V., 1949b, Prog. Met. Phys. **1**, 1.
RAYNOR, G. V., 1956, The Theory of Alloy Phases, (ASM, Metals Park, OH), p. 321.
READ, W. T., Jr., 1953, Dislocations in Crystals (McGraw-Hill, New York).
ROBERTS, R. W., 1954, Acta Metall. **2**, 597.
ROBERTS, B. W., 1956, J. Metals **8**, 1407, Phys. Rev. 104, 607.
ROBINSON W. M., and M. B. BEVER, 1967, Metallurgical Transactions, **239**, p. 1015.
RUDMAN, P. S., J. STRINGER and R. I. JAFFEE, eds. 1968, Phase Stability in Metals and Alloys, (McGraw Hill, New York).
SATO, H., and R. S. TOTH, 1961, Phys. Rev. **124**, 1833.
SATO, H., and R. S. TOTH, 1962, Phys. Rev. Lett. **8**, 239.
SATO, H., and R. S. TOTH, 1965, in: Alloying Behavior and Effects in Concentrated Solid Solutions, ed. T. B. MASSALSKI (Gordon and Breach, New York).
SCHUBERT, K., B. KIEFER, M. WILKENS and R. HAUFLER, 1955, Z. Metallk. **46**, 692.

STIRLING, P. H., and G. V. RAYNOR, 1956, J. Inst. Metals, **84**, 57.
SLICK, P. I., C. W. MASSENA and R. S. CRAIG, 1965, J. Chem. Phys. **43**, 2792.
STOCKS, G. M., and H. WINTER, 1984, The Electronic Structure of Complex Systems, eds. P. PHARISEAU and W. M. TAMMERMAN, Plenum Press, New York.
STOCKS, G. M. and A. GONIS, Eds., 1989, NATO Symposium on "Alloy Phase Stability", Kluwer Academic Publishers, vol. 163, series E.
STROUD, D., 1980, in: Proc. Conf. on Theory of Alloy Phase Formation, ed. L. H. BENNETT, (AIME, Warrendale, PA), p. 84.
SUZUKI, To., M. HASEGAWA and M. HIRABAYASHI, 1976, J. Phys. **F6**, 779.
TAYLOR, A., 1961, X-Ray Metallography (Wiley, New York).
TAYLOR, A., and N. J. DOYLE, 1972, J. Appl. Cryst. **5**, 201.
TERAKURA, K., T. OGUCHI, T. MOHRI and K. WATANABE, 1987, Phys. Rev. B, **35**, 2169.
TURNBULL, D., 1980, Met. Transactions **12A**, p. 695.
VEGARD, L., 1928, Z. Cryst. **67**, 239.
WABER, J. T., K. A. GSCHNEIDNER, A. C. LARSON and M. Y. PRINCE, 1963, Trans. AIME **227**, 717.
WAGNER, C. N. J., 1957, Acta Metall. **5**, 427 and 477.
WARREN, B. E., B. E. AVERBACH and B. W. ROBERTS, 1951, J. Appl. Phys. **22**, 1943.
WARREN, B. E., and E. P. WAREKOIS, 1955, Acta Metall. **3**, 473.
WARREN, B. E., 1959a, Acta Cryst. **12**, 837.
WARREN, B. E., 1959b, Prog. Met. Phys. **8**, 147.
WATSON, R. E., and L. H. BENNETT, 1979, Phys. Rev. Letters, **43**, 1130.
WATSON, R. E., and L. H. BENNETT, 1983, in: Alloy Phase Diagrams, MRS Symposium, L. H. BENNETT, T. B. MASSALSKI and B. C. GIESSEN, eds. Vol. 19, p. 99.
WESTGREN, A., and G. PHRAGMEN, 1926, On the Chemistry of Metallic Compounds, Z. Metallk. **18**, 279.
WESTGREN, A., 1930, Z. Metallk. **22**, 368.
WILKENS, M., 1962, Phys. Stat. Sol. **2**, 692.
WILLIAMS, A. R., C. D. GELATT and V. L. MORUZZI, 1980, Phys. Rev. Lett. **44**, 429.
WILLIS, M., and H. F. ROOKSBY, 1954, Proc. Phys. Soc. **B67**, 290.
XU, J. H., T. OGUCHI and A. J. FREEMAN, 1987, Phys. Rev. **B35**, 6940.
YIN, M. T., and M. L. COHEN, 1982, Phys. Rev. **26B**, 3259.

Further reading

(a) In the present chapter the main emphasis has been placed on solid solutions and structures with wide solid solubility. However, this subject is closely bound with the much wider area of the stability of all alloy phases and crystal structures. Further reading on early ideas on the theories of alloy phases may be found in: ASM Symposium on the Theory of Alloy Phases (ASM, Metals Park, OH, 1956) and the Symposium on Metallic Solid Solutions, Orsay, France, eds. J. FRIEDEL and A. GUINIER (Benjamin, New York, 1963). More recent symposia or reviews include:

AIME Symposium on The Alloying Behavior and Effects in Concentrated Solid Solutions, ed. T. B. MASSALSKI, Gordon and Breach, New York (1965).

Battelle Inst. Symposium on Phase Stability in Metals and Alloys, eds. P. S. RUDMAN, J. STRINGER and R. I. JAFFEE, eds., McGraw Hill, (1967).

Structure of Metals, 3rd edition, C. S. BARRETT and T. B. MASSALSKI, McGraw-Hill, New York (1966).

A discussion of the theories of alloys based on the noble metals, Cu, Ag and Au, is given by:

W. HUME-ROTHERY, J. Inst. Metals **9** (1961–2) 42. T. B. MASSALSKI and H. W. KING, Prog. Mater. Sci. **10** (1961) 1. T. B. MASSALSKI and U. MIZUTANI, Prog. Mater. Sci. **22** (1978) 151.

(b) Problems concerning the transition elements and their alloys are discussed in:

AIME Symposium on Electronic Structure and Alloy Chemistry of Transition Elements, ed. P. A. BECK, Wiley, New York (1963).

Electrons in Transition Elements, by N. F. MOTT, Adv. Phys. **13** (1964) 325.

Battelle Inst. Symposium on Phase Stability in Metals and Alloys, eds. P. S. RUDMAN, J. STRINGER and R. I. JAFFEE, McGraw Hill (1967.

(c) Relations between phase stability and phase diagrams are discussed in:
T. B. MASSALSKI, the Campbell Lecture, Metallurgical Transactions, **20A**, 1295; and **20B**, 445 (1989).

(d) Size effects in alloy phases are discussed by:
H. W. KING, in: AIME Symposium (1965) listed above.
F. LAVES, in: Advances in X-ray Analysis, eds. W. M. MUELLER and M. F. FAY, **6** (1962) 43. For electron theory connections to size effects see F. J. PINSKI, B. GINATEMPO, D. D. JOHNSON, J. B. STAUNTON, G. M. STOCKS and B. L. GYOFFRY, 1991, Phys. Rev. Lett., **66**, 766.

(e) Long-period superlattices and stacking faults are discussed by H. SATO and R. S. TOTH, and J. W. CHRISTIAN and P. SWANN, respectively, in the AIME Symposium (1965) listed above under (a), and more recently in the NATO Symposium on Alloy Phase Stability listed under (g).

(f) Stability and electronic structure of metallic glasses are discussed by:
U. MIZUTANI, Prog. Mater. Sci. **28** (1983).

(g) Recent concepts related to the electronic interactions in metals and alloys are discussed in a NATO Symposium on "Alloy Phase Stability" G. M. STOCKS and A. GONIS, eds., Kluwer Academic Publishers, vol. 163, series E, (1989); and in a book by Alan H. COTTRELL, "Introduction to the Modern Theory o Metals", Institute of Metals, London (1988). Interested readers should perhaps consult first the chapter on electronic theories in this book.

CHAPTER 4

STRUCTURE OF INTERMETALLIC COMPOUNDS AND PHASES

RICCARDO FERRO AND ADRIANA SACCONE

Istituto di Chimica Generale
Università di Genova
Genova, Italy

R. W. Cahn and P. Haasen†, eds.
Physical Metallurgy; fourth, revised and enhanced edition

1. Introduction

1.1. Preliminary remarks and definition of an intermetallic phase

In the field of solid state chemistry an important group of substances is represented by the intermetallic compounds and phases. A few general and introductory remarks about these substances may be presented by means of figs. 1 and 2. In binary and multicomponent metal systems, in fact, several crystalline phases (terminal and intermediate, stable and metastable) may occur.

Simple schematic phase diagrams of binary alloy systems are shown in fig. 1. In all of them the formation of solid phases may be noticed. In fig. 1a we observe the formation of the AB_x phase (which generally crystallizes with a structure other than those of the constituent elements) and which has a negligible homogeneity range. Thermodynamically, the composition of any such phase is variable. In a number of cases, however, the possible variation in composition is very small (invariant composition phases or stoichiometric phases, or "compounds" proper, also called "point compounds" in binary alloys).

In fig. 1b and 1c, on the contrary, we observe that solid phases with a variable composition are formed (non-stoichiometric phases). In the reported diagrams we see examples both of terminal (1b, 1c) and intermediate phases (1c). These phases are characterized by homogeneity ranges (solid solubility ranges) which, in the case of the terminal phases, include the pure components and which, generally, have a variable temperature-dependent extension. (In the older literature, stoichiometric and non-stoichiometric phases were often called "daltonides" and "berthollides", respectively. These names, however, are no longer recommended by the Commission on the Nomenclature of Inorganic Chemistry (IUPAC), LEIGH [1990].

More complex situations are shown in fig. 2, where some typical examples of isobarothermal sections of ternary alloy phase diagrams are presented. In the case of a ternary system, such as that reported in fig. 2a, we notice the formation of several, binary and ternary, stoichiometric phases. In the case shown in fig. 2b, different types of variable composition phases can be observed. We may differentiate between these phases by using terms such as: "*point compounds*" (or *point phases*), that is, phases represented in the composition triangle, or, more generally, in the composition simplex by points, "*line phases*", "*field phases*", etc.

As a summary of the aforementioned considerations, we may notice that several types of substances may be included in a preliminary broad *definition of an intermetallic phase*. Both *stoichiometric (compounds) phases* and *variable-composition (solid solutions) phases* may be considered and, as for their structures, both fully ordered or (more or less completely) disordered phases.

For all the intermetallic phases the identification (and classification) requires information about their chemical composition and structure. To be consistent with the other field of descriptive chemistry, this information should be included in specific chemical (and structural) formulae built up according to well-defined rules. This task, however, in the specific area of the intermetallic phases (or more generally in the area of solid state chemistry) is much more complicated than for other chemical compounds.

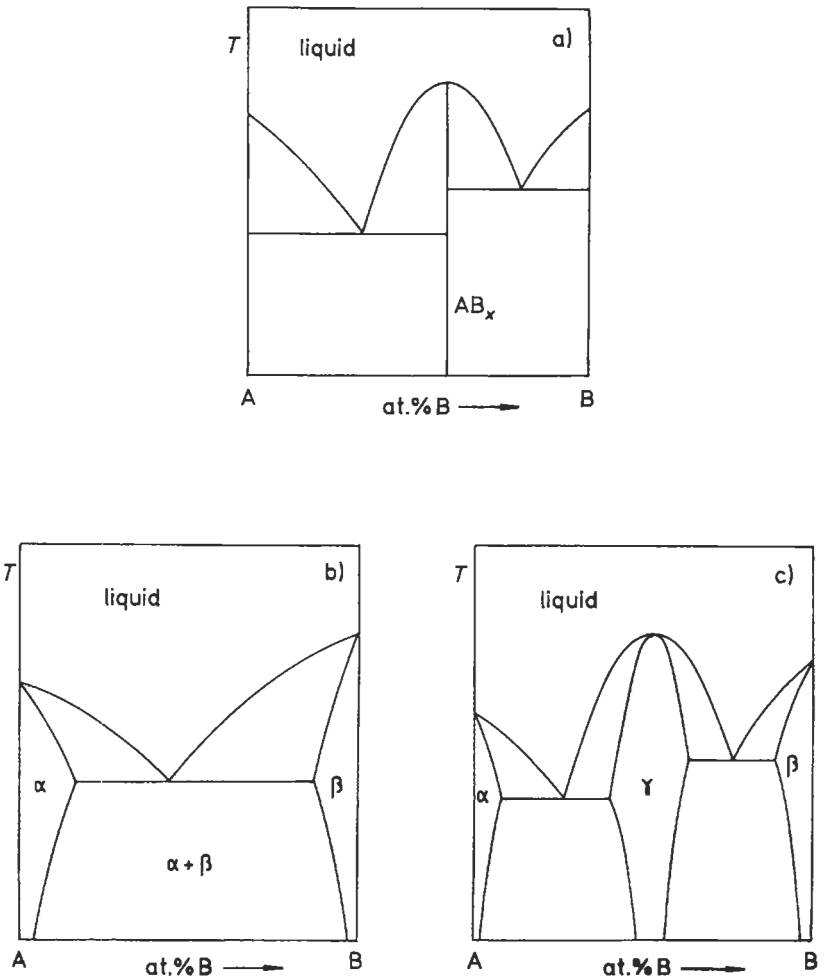

Fig. 1. Examples of simple binary diagrams.

a) A stoichiometric, congruently melting, compound is formed at the composition corresponding to the AB_x formula.

b) No intermediate phase is formed. The components show a certain limited mutual solid solubility.

c) The two components show limited mutual solid solubility (formation of the α- and β-phases). Moreover, an intermediate phase (γ) is formed: it is homogeneous in a certain composition range.

This complexity is related both to the chemical characteristics (formation of variable composition phases) and to the structural properties (the intermetallic compounds are generally non-molecular in nature, while the conventional chemical symbolism has been mainly developed for the representation of molecular units). As a consequence there is not a complete, or generally accepted, method of representing the formulae of intermetallic compounds.

References: p. 363.

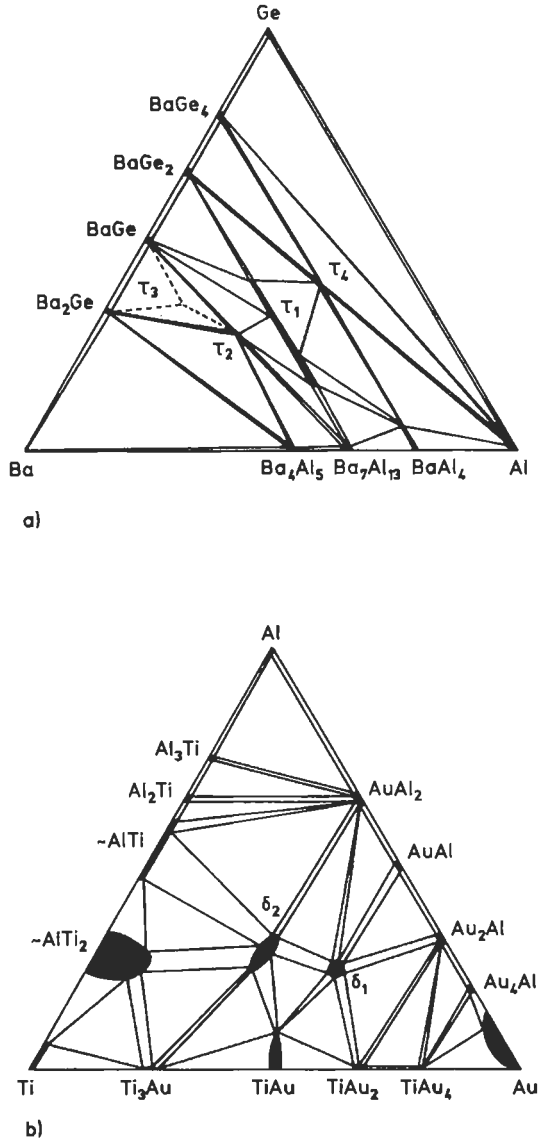

Fig. 2. Isobarothermal sections of actual ternary systems (from "Ternary Alloys", PETZOW and EFFENBERG, [1988 *et seg.*]).

a) Ba–Al–Ge system. A number of binary compounds are formed in the side binary systems. Moreover, a few ternary phases have been observed.
τ_1: $\approx Ba(Al_xGe_{1-x})_2$, line phase, stable for $0.41 < x < 0.77$;
τ_2: $Ba_3Al_2Ge_2$, τ_3: $Ba_{10}Al_3Ge_7$, τ_4: $BaAl_2Ge_2$, point phases.

b) Ti–Au–Al system. The binary systems show the formation of several intermediate phases, generally characterized by certain composition ranges (ideal simple formulae are here reported). Two ternary field phases are also formed. Their homogeneity ranges are close to $TiAu_2Al$ (δ_1) and TiAuAl (δ_2), respectively.

Some details on these points will be given in the next sections. These will then be used for a description of selected common phases and a presentation of a few characteristic general features of intermetallic crystallochemistry. For an exhaustive description of all the intermetallic phases and a comprehensive presentation and discussion of their crystallochemistry, general reference books and catalogues, such as those reported in the list of references, should be consulted. More references to specific topics will be reported in the following sections.

Those who are interested in the historical development of the intermetallic compound concept and science may refer to the review written by WESTBROOK [1977] on the past and future potential of intermetallic compounds. In this review Westbrook selected the following topics for the examination of their historic roots:

a) the development of the modern concept of the intermetallic compound;
b) the development of the phase diagram;
c) the role of electron concentration in determining intermetallic phase stability;
d) the role of geometrical factors in determining intermetallic phase stability;
e) the point defect concept and its relation to non-stoichiometric compounds;
f) the unusual role of grain boundaries in intermetallic compounds.

He reported information on the chronological growth in the number of binary metallic phase diagrams studied (starting from the year about 1830 with the systems Pb–Sn, Sn–Bi, etc.,) and of the intermetallic compounds.

The first problems encountered while studying these substances are pointed out: typically that simple valence concepts were not applicable for rationalizing compound formulation and that several compounds seemed to exist over a range of composition and not at some specific ratio as with ordinary salts. The development of the systematics of the intermetallic phases and of their applications is then discussed and compared with the history of the rise of thermodynamics and crystallochemistry.

The complexity and variability of solid state phenomena add to more practical reasons of interest in defining the peculiar approach to a systematic investigation of solid intermetallic phases.*

1.2. Identification of the intermetallic phases

The identification and crystallochemical characterization of an intermetallic solid phase requires the definition and analysis of the following points:

a) Chemical composition (and the homogeneity composition range and its temperature and pressure dependence).

* This chapter, as previously stated, will highlight the particular subject of the intermetallic solids. It may be worth reminding, however, that intermetallic substances can be found also in different aggregation states. (For the liquid state see, for instance, fig. 1). Important contributions to understanding systems in the liquid state (experimental measurements, thermodynamic properties forecasting, liquid state structure, theories and models) were brought about, for instance, by HOCH, ARPSHOFEN and PREDEL [1984], SOMMER [1982] and SINGH and SOMMER [1992]). A systematic description of the structure of amorphous and molten alloys (basic equation for the description of the structure of non-crystalline systems, experimental techniques and elements of systematics) has been presented by LAMPARTER and STEEB [1993].

References: p. 363.

b) Structure type (or crystal system, space group, number of atoms per unit cell and list of occupied atomic positions).

c) Values of a number of parameters characteristic of the specific phase within the group of isostructural phases (unit cell edges, occupation characteristics and, if not fixed, coordinate triplets of every occupied point set).

d) Volumetric characteristics (molar volume of the phase, formation volume contraction, or expansion, space filling characteristics, etc.).

e) Interatomic connection characteristics (local atomic coordination, long distance order, interatomic distances, their ratios to atomic diameters, etc.).

Clearly, not all the data relevant to the aforementioned points are independent of each other. The strictly interrelated characteristics listed under d) and e), for instance, may be calculated from the data indicated in b) and c), from which the actual chemical composition of the phase may also be obtained.

For each of the aforementioned points (and for their symbolic representation) a few remarks may be noteworthy: these will be presented in the following. *Crystallographic conventions, nomenclature and symbols* will be used. For a summary of these and of the corresponding definitions the most important reference book is "International Tables for Crystallography", HAHN [1989]. Several books, mentioned here in the reference list, contain, more or less detailed, introductions to the crystallographic notations. A few remarks on these points will be presented in this chapter (see especially table 3 and Sec. 3.1 and 3.5.5); some examples moreover have been given in chapter 1.

2. *Chemical composition of the intermetallic phase and its compositional formula*

Simple compositional formulae are often used for intermetallic phases; these (for instance, Mg_2Ge, $ThCr_2Si_2$,...) are useful as quick references, especially for simple, stoichiometric, compounds. The following remarks may be noteworthy:

Order of citation of element symbols in the formula

The symbol sequence in a formula ($LaPb_3$ or Pb_3La) is, of course, arbitrary and, in some particular cases, may be a matter of convenience. Alphabetical order has often been suggested (for example by IUPAC, LEIGH [1990]). A symbol sequence based on some chemical properties, however, may be more useful when, for instance, compounds with analogous structures have to be compared (Mg_2Ge and Mg_2Pb). Recently, in 1990, an international group of materials scientists coordinated by the Max Planck Institute for Metals Research of Stuttgart (Germany) (the so-called MSIT: Materials Science International Team) performing the critical assessment of a new series on ternary alloys edited by PETZOW and EFFENBERG [1988 *et seq.*] decided to adopt a symbol quotation order based on a parameter introduced by PETTIFOR [1984, 1986a] In fact, in order to stress the chemical character of the elements and to simplify their description, PETTIFOR [1984, 1985, 1986a, 1986b] (see also chapter 2) created a new *chemical scale* (χ) which orders the elements along a simple axis. The progressive order number of the elements in this scale (the so-called Mendeleev number) may also be considered. The Mendeleev

numbers M (which, of course, are different from the atomic numbers) start, according to Pettifor, with the least electronegative elements He 1, Ne 2,... and end with the most electronegative ones ...N 100, O 101, F 102 up to H 103. The Mendeleev Number (M) and the correlated "chemical scale χ" are shown in table 1. The chemical meaning of these parameters may be deduced not only by their relation to the Periodic Table. By using them, in fact, excellent separation of similar structures is achieved for numerous A_mB_n phases with a given stoichiometry within single two-dimensional M_A/M_B maps, (see Sec. 8.7.). Notice, however, that in subsequent papers, on the basis of a progressive improvement of the structure maps, slightly different versions of the chemical scale had been reported.

On the basis of the Pettifor's scale, the suggestion has been made that the element E with a lower value M_E (or χ_E) is quoted first in the formulae of its compounds. This will be generally adopted here.

Indication of constituent proportions

No special comments are needed for stoichiometric compounds ($LaPb_3$, $ThCr_2Si_2$,...).

More complex notation is needed for non-stoichiometric phases. Selected simple examples will be given below and more detailed information will subsequently be reported, when discussing crystal coordination formulae.

a) *Ideal formulae*

While considering a variable composition phase, it is often possible to define an "ideal composition" (and formula) relative to which the composition variations occur (or are considered to occur). This composition may be that for which the ratio of the numbers of different atoms corresponds to the ratio of the numbers of the different crystal sites in the ideal (ordered) crystal structure (as suggested by IUPAC, LEIGH [1990]). These formulae may be used even when the "ideal composition" is not included in the homogeneity range of the phase (Nb_3Al for instance, shows a homogeneity range from 18.6 at% Al which hardly reaches 25 at% Al. At the formation peritectic temperature of 2060°C the composition of the phase is about 22.5 at% Al).

b) *Approximate formulae*

A general notation which has been suggested by IUPAC when only little information has

Table 1

Chemical order of the elements, according to PETTIFOR [1986a]

1a. For the elements, arranged here in alphabetical order, the values of the so-called Mendeleev number are reported.

Ac	48	Be	77	Cm	41	Fe	61	Ho	23	Md	36	No	35	Pr	31	Sb	88	Te	92	Yb	17
Ag	71	Bi	87	Co	64	Fm	37	I	97	Mg	73	Np	44	Pt	68	Sc	19	Th	47	Zn	76
Al	80	Bk	40	Cr	57	Fr	7	In	79	Mn	60	O	101	Pu	43	Se	93	Ti	51	Zr	49
Am	42	Br	98	Cs	8	Ga	81	Ir	66	Mo	56	Os	63	Ra	13	Si	85	Tl	78		
Ar	3	C	95	Cu	72	Gd	27	K	10	N	100	P	90	Rb	9	Sm	28	Tm	21		
As	89	Ca	16	Dy	24	Ge	84	Kr	4	Na	11	Pa	46	Re	58	Sn	83	U	45		
At	96	Cd	75	Er	22	H	103	La	33	Nb	53	Pb	82	Rh	65	Sr	15	V	54		
Au	70	Ce	32	Es	38	He	1	Li	12	Nd	30	Pd	69	Rn	6	Ta	52	W	55		
B	86	Cf	39	Eu	18	Hf	50	Lr	34	Ne	2	Pm	29	Ru	62	Tb	26	Xe	5		
Ba	14	Cl	99	F	102	Hg	74	Lu	20	Ni	67	Po	91	S	94	Tc	59	Y	25		

Table 1—*Continued*

1b. The elements are arranged in the order of the Mendeleev Number M (and of the related chemical scale χ).

M	Element	χ	M	Element	χ	M	Element	χ
1	He	0.00	36	Md	0.7125	70	Au	1.16
2	Ne	0.04	37	Fm	0.715	71	Ag	1.18
3	Ar	0.08	38	Es	0.7175	72	Cu	1.20
4	Kr	0.12	39	Cf	0.72	73	Mg	1.28
5	Xe	0.16	40	Bk	0.7225	74	Hg	1.32
6	Rn	0.20	41	Cm	0.725	75	Cd	1.36
7	Fr	0.23	42	Am	0.7275	76	Zn	1.44
8	Cs	0.25	43	Pu	0.73	77	Be	1.50
9	Rb	0.30	44	Np	0.7325	78	Tl	1.56
10	K	0.35	45	U	0.735	79	In	1.60
11	Na	0.40	46	Pa	0.7375	80	Al	1.66
12	Li	0.45	47	Th	0.74	81	Ga	1.68
13	Ra	0.48	48	Ac	0.7425	82	Pb	1.80
14	Ba	0.50	49	Zr	0.76	83	Sn	1.84
15	Sr	0.55	50	Hf	0.775	84	Ge	1.90
16	Ca	0.60	51	Ti	0.79	85	Si	1.94
17	Yb	0.645	52	Ta	0.82	86	B	2.00
18	Eu	0.655	53	Nb	0.83	87	Bi	2.04
19	Sc	0.66	54	V	0.84	88	Sb	2.08
20	Lu	0.67	55	W	0.88	89	As	2.16
21	Tm	0.675	56	Mo	0.885	90	P	2.18
22	Er	0.6775	57	Cr	0.89	91	Po	2.28
23	Ho	0.68	58	Re	0.935	92	Te	2.32
24	Dy	0.6825	59	Tc	0.94	93	Se	2.40
25	Y	0.685	60	Mn	0.945	94	S	2.44
26	Tb	0.6875	61	Fe	0.99	95	C	2.50
27	Gd	0.69	62	Ru	0.995	96	At	2.52
28	Sm	0.6925	63	Os	1.00	97	I	2.56
29	Pm	0.695	64	Co	1.04	98	Br	2.64
30	Nd	0.6975	65	Rh	1.05	99	Cl	2.70
31	Pr	0.70	66	Ir	1.06	100	N	3.00
32	Ce	0.7025	67	Ni	1.09	101	O	3.50
33	La	0.705	68	Pt	1.105	102	F	4.00
34	Lr	0.7075	69	Pd	1.12	103	H	5.00
35	No	0.71						

to be conveyed and which can be used even when the mechanism of the variation in composition is unknown, is to put the sign ≈ (read as circa or approximately) before the formula; for instance ≈CuZn.

c) *Variable composition formulae*

(Ni,Cu) or Ni_xCu_{1-x} $(0 \leq x \leq 1)$ are the equivalent representations of the continuous solid solution between Ni and Cu, homogeneous in the complete range of compositions; other examples are: $Ce_{1-x}La_xNi_5$ $(0 \leq x \leq 1)$; $(Ti_{1-x}Cr_x)_5Si_3$ $(0 \leq x \leq 0.69)$; etc....

Similar formulae may also be used in more complicated cases to convey more information: $A_{m+x}B_{n-x}C_p$ $(... < x < ...)$ (phase involving substitution of atoms A for B).

$A_{1-x}B$ may indicate that there are A-type vacant sites in the structure.

$LaNi_5H_x$ ($0 < x < 6.7$) indicates the solid solution of H in $LaNi_5$.

d) *Site occupation formulae*

According to the Recommendations by the Commission on the Nomenclature of Inorganic Chemistry, (LEIGH [1990]), additional information may be conveyed by using a more complicated symbolism; suggestions have also been made about the indication of site occupation and of their characterization. These points will be discussed in more detail in the following sections; in the meantime we may mention that, for the indication of site occupation, the following criteria have been suggested by the Commission:

The site and its occupancy is represented by two right lower indexes separated by a comma. The first index indicates the type of site, the second one indicates the number of atoms in this site. (A_A, for instance, means an atom A on a site occupied by A in the ideal structure, whereas A_B represents an atom A in a site normally (ideally) occupied by B).

A formula such as:

$M_{M,1-x}N_{M,x}M_{N,x}N_{N,1-x}$ or $(M_{1-x}N_x)_M(M_xN_{1-x})_N$ represents a disordered alloy (whereas the ideal composition is MN with an ideal M_MN_N structure). In this notation vacant sites may be represented by □ or by v_.

The following examples of alloy formulae have been reported:

$Mg_{Mg,2-x}Sn_{Mg,x}Mg_{Sn,x}Sn_{Sn,1-x}$ shows a partially disordered alloy with some of the Mg atoms on Sn sites, and vice versa;

$(Bi_{2-x}Te_x)_{Bi}(Bi_xTe_{3-x})_{Te}$ shows the composition changes from the ideal Bi_2Te_3 formula;

$Al_{Al,1}Pd_{Al,x}Pd_{Pd,1-x}\,□_{Pd,2x}$ which shows that in the phase (corresponding to the ideal composition PdAl), every Al is on an Al site, but x Pd atoms are on Al sites (1–x Pd atoms in Pd sites) and 2x Pd sites are vacant.

This type of formula may be especially useful when discussing thermodynamic properties of the phase and dealing with solid solution models and quasi-chemical equilibria between point defects.

e) *Polymorphism descriptors*

Several substances may change their crystal structure because of external conditions such as temperature and pressure. These different structures (polymorphic forms) may be distinguished by using special designators of the stability conditions. (If the various crystal structures are known, explicit structural descriptors may obviously be added). A very simple, but systematic notation has been introduced by the MSIT (see before) which in the meanwhile has been adopted worldwide (see Introduction of all volumes on "Ternary Alloys" edited by PETZOW and EFFENBERG, [1988 *et seq.*]). The different temperature modifications are indicated by lower case letters in parenthesis behind the phase designation, with (h) = high temperature modification, (r) = room temperature modification and (l) = low temperature modification; (h_1, h_2, etc. represent different high temperature modifications). In the description of a number of modifications which are stable at different temperatures, the letters are used in the sequence h_2, h_1, r, l_1, l_2,..., in correspondence to the decreasing stability temperature.

Table 2, taken from Volume 3 of the series edited by PETZOW and EFFENBERG [1988], shows a few examples of this notation. (In this case, of course, the temperature and composition ranges of stability explicitly indicated for all the phases give additional, more detailed information).

References: p. 363.

Table 2
An example of crystallochemical description of alloy system.
Binary solid phases in the Ag–Al system
(from PETZOW and EFFENBERG [1988 *et seg.*] and MASSALSKI [1990]).

Phase Trivial Name, Ideal Formula, Temperature Range (°C)	Pearson Symbol/ Prototype	Lattice Parameters (pm)	Maximum Composition Range (at% Al)
(Ag) < 961.93	cF4 Cu	a = 408.53 (23°C)	0 to 20.4 (at ≈ 450°C)
β-Ag_3Al (h) 778–605	cI2 W	a = 330.2 (700°C)	20.5 to 29.8 (at 726°C)
μ-Ag_3Al (r) < 448	cP20 β-Mn	a = 693	≈21 to 24
δ-Ag_2Al < 726	hP2 Mg	a = 287.1 (27at%Al) c = 466.2 a≈ 288.5 (Al-rich c≈ 458.2 limit)	22.9 to 41.9
(Al) < 660.45	cF4 Cu	a = 404.88 (24°C)	76.5 to 100 (at 567°C, Al-rich eutectic temperature)

In connection with this group of descriptors we may perhaps remember indicators such as (am), (vt), etc. for amorphous, vitreous substances. For instance:
SiO_2(am) amorphous silica; Si(am)H_x amorphous silicon doped with hydrogen.

3. *Crystal structure of the intermetallic phase and its representation*

3.1. Unit cell description (general remarks, lattice complexes)

The characterization of a phase requires a complete and detailed description of its structure. As examples of such a description, we may consider the data (as obtained, for instance, from X-ray diffraction experiments) reported in table 3 for stoichiometric and variable composition phases. (For an explanation of the various symbols used in the table see the International Tables of Crystallography (HAHN [1989]. See also the examples reported in chapter 1).

Following information is included in the table:
— *Crystallographic system*, that is the coordinate system (and metrical relationships between the lattice parameters of the adopted unit cell: for instance, cubic: $a = b = c$, $\alpha = \beta = \gamma = 90°$; tetragonal: $a = b \neq c$, $\alpha = \beta = \gamma = 90°$, etc.); and the specific values (in picometers) of the *unit cell dimensions*.

Table 3
Examples of crystallographic description of phase structures
(from VILLARS and CALVERT [1991]).

$CsCl$ (stoichiometric compound);
Primitive cubic; a = 411.3 pm; space group $Pm\bar{3}m$, No. 221,
1 Cs in a): 0,0,0;
1 Cl in b): $\frac{1}{2},\frac{1}{2},\frac{1}{2}$;
(The two special a) and b) Wyckoff positions have no free coordinate parameter.) The two occupancy parameters are 100%.

Mg_2Ge (stoichiometric compound):
Face-centered cubic; a = 638.7 pm; space group $Fm\bar{3}m$, N. 225,
Equivalent positions (0,0,0; $0,\frac{1}{2},\frac{1}{2}$; $\frac{1}{2},0,\frac{1}{2}$; $\frac{1}{2},\frac{1}{2},0$) +
4 Ge in a): 0,0,0
8 Mg in c): $\frac{1}{4},\frac{1}{4},\frac{1}{4}$; $\frac{1}{4},\frac{1}{4},\frac{3}{4}$
(No free parameters in the atomic positions of Mg and Ge. In this case the two occupancy parameters have been found to be 100%.)

$MoSi_2$ (nearly stoichiometric compound):
body-centered tetragonal; a = 319.6 to 320.8 pm and c = 787.1 to 790.0 pm, according to the composition; space group I4/mmm, No. 139,
Equivalent positions (0,0,0; $\frac{1}{2},\frac{1}{2},\frac{1}{2}$) +
2 Mo in a): 0,0,0
4 Si in e): 0,0,z; 0,0,−z ; z = 0.333
(The Si position has the free parameter z, for which, in this particular case, the value 0.333 has been determined; the two occupancy parameters are 100%.)

≈ Ce_2NiSi_3 (disordered structure):
hexagonal; a = 406.1 to 407.1 pm; c = 414.9 to 420.2 pm; space group P6/mmm, N. 191
1 Ce in a): 0,0,0,
2 (Ni + Si) (in a ratio 1:3) in d): $\frac{1}{3},\frac{2}{3},\frac{1}{2}$; $\frac{2}{3},\frac{1}{3},\frac{1}{2}$;
(In this case the atomic sites corresponding to the d) Wyckoff position are randomly occupied by Ni and Si atoms in the given ratio and the overall composition correspond to 1Ce + 2 × (0.25 Ni + 0.75Si)).

$Cr_{12}P_7$ (simple structure showing partially occupied sites):
hexagonal; a = 898.1 pm; c = 331.3 pm; space group $P6_3/m$, No. 176.
2 P in a): $0,0,\frac{1}{4}$; $0,0,\frac{3}{4}$; (occupancy 50%)
6 P in h): $x,y,\frac{1}{4}$; $-y,x-y,\frac{1}{4}$; $-x+y,-x,\frac{1}{4}$; $-x,-y,\frac{3}{4}$; $y,-x+y,\frac{3}{4}$; $x-y,x,\frac{3}{4}$ (x= 0.2851, y = 0.4462); (occupancy 100%)
6 Cr in h): $x,y,\frac{1}{4}$; $-y,x-y,\frac{1}{4}$; $-x+y,-x,\frac{1}{4}$; $-x,-y,\frac{3}{4}$; $y,-x+y,\frac{3}{4}$; $x-y,x,\frac{3}{4}$ (x= 0.5109, y = 0.3740); (occupancy 100%)
6 Cr in h): $x,y,\frac{1}{4}$; $-y,x-y,\frac{1}{4}$; $-x+y,-x,\frac{1}{4}$; $-x,-y,\frac{3}{4}$; $y,-x+y,\frac{3}{4}$; $x-y,x,\frac{3}{4}$ (x= 0.2108, y = 0.0144); (occupancy 50%)
6 Cr in h): $x,y,\frac{1}{4}$; $-y,x-y,\frac{1}{4}$; $-x+y,-x,\frac{1}{4}$; $-x,-y,\frac{3}{4}$; $y,-x+y,\frac{3}{4}$; $x-y,x,\frac{3}{4}$ (x= 0.2638, y = 0.0137); (occupancy 50%)

In this case several groups of atoms have the same type of Wyckoff positions: the h) position which has free parameters. These, of course, have different values for the different groups of atoms. The parameter values experimentally determined in this case for each atom group are reported.

The partial occupancies found for the different positions are also reported. In this case in the a) Wyckoff position, for instance, only half of the sites are randomly occupied by P atoms; the others are vacant. The total number of atoms in the unit cell is: P: 0.5×2 + 6 = 7; Cr: 6 + 0.5×6 + 0.5×6 = 12.

— Bravais point lattice and *space group* (this describes the spatial symmetry of the structure on a microscopic (atomic) level, and is represented by means of the Hermann–Mauguin symbol, composed by a letter representing the lattice type (P = primitive, I = body centered, etc., see table 4) followed by the symbols of the symmetry elements

Table 4
Pearson Symbols

System symbol	Lattice symbol
a triclinic (anorthic)	**P** primitive
m monoclinic	**I** body centred
o orthorhombic	**F** all-face centred
t tetragonal	**C** side face centred *
h hexagonal (and trigonal and rhombohedral)	**R** rhombohedral
c cubic	

* Instead of **C**, in the future, the symbol **S** will probably be adopted according to the recommendation of the International Union of Crystallography.

ordered according to their positions relative to the axes (for instance $Pm\bar{3}m$ is the symbol of the space group of the CsCl structure).

As usual, the space group is also identified by the *serial number* (221 for $Pm\bar{3}m$) reported in several compilations such as the "International Tables" which is the fundamental reference book for crystallography (HAHN [1989]).

A *list* of the *atoms* contained in the unit cell and their *coordinates* (fractional coordinates related to the adopted system and unit cell edges) are then reported. These are usually presented in a format as *M El in n: x,y,z*. In the $MoSi_2$ structure, also reported in table 3, we have, for instance, four silicon atoms (that is: M El = 4 Si) in the position set coded as *e* and corresponding to the 4 coordinate triplets 0,0,0; 0,0,z; $\frac{1}{2},\frac{1}{2},\frac{1}{2}+z$; $\frac{1}{2},\frac{1}{2},\frac{1}{2}-z$. Such entries correspond to the so-called *Wyckoff positions* characterized by a well-defined site symmetry and by a *multiplicity M*. For each Wyckoff position M, is the number of equivalent points (positions) in the unit cell with the same site symmetry. The highest multiplicity M_{max} of the given space group corresponds to the lowest site symmetry (each point is mapped onto itself only by the "identity operation"). This is the "*general position*": the coordinate triplets of the M_{max} sites include the reference triplet indicated as x,y,z (having *three variable parameters*). In a given space group, moreover, it is possible to have several *special positions*. In this case points are considered which are located on symmetry elements (without translations) or at the intersection of several such symmetry elements. Each point will be mapped onto itself by at least one of these symmetry operations: we will have as a consequence a reduction in the number of different equivalent points in the unit cell generated by all the characteristic symmetry operations. The multiplicity of these positions will be lower than M_{max} (M in a special position is a divisor of that of the general position). We may also say that specific costraints are imposed on the coordinates of each point of a special position leading to triplets such as x,y,0 (that is z = 0) or x,x,z (that is x = y), with two variable parameters, or $x,\frac{1}{2},\frac{1}{2}$ or x,x,0 (with one variable parameter) or 0,0,0 or $\frac{1}{2},\frac{1}{2},0$ (with no variable parameter). In the International Tables of Crystallography, for each of the 230 space groups, the list of all the positions is reported. For each of the positions (the general and the special ones) the coordinate triplets of the equivalent points are also given. The different positions are coded by means of the Wyckoff letter, ***a***, ***b***, ***c***, etc., starting with ***a*** for the position with the lowest multiplicity and continuing in alphabetical order up to the general position.

In the examples reported in table 3 it is also shown that for the positions with *free parameters* the specific values of the parameters themselves have to be experimentally determined in order to present a complete description of the structure.

Notice that, for instance, in the case of the $MoSi_2$ structure the different atomic positions in the unit cell are the following: 2 Mo in 0,0,0, and in $\frac{1}{2},\frac{1}{2},\frac{1}{2}$ and 4 Si in 0,0,z; in 0,0,−z; in $\frac{1}{2},\frac{1}{2}$, $\frac{1}{2}+z$ and in $\frac{1}{2},\frac{1}{2},\frac{1}{2}-z$ (corresponding, on the basis of the experimental value z=0.333, to 0,0,0.333; 0,0,0.667; $\frac{1}{2},\frac{1}{2}$,0.833; $\frac{1}{2},\frac{1}{2}$,0.167). These positions have been described, according to the International Tables of Crystallography conventions, explicitly indicating the centring translations $(0,0,0;\ \frac{1}{2},\frac{1}{2},\frac{1}{2})+$ before the coordinate triplets. The symbol + means that, in order to obtain the complete Wyckoff position the components of these centring translations have to be added to each of the listed triplets.

A similar presentation has been used for the Mg_2Ge structure description. Notice that the coordinates are formulated modulo 1: thus, for instance, −x,−y,−z is written rather than 1−x,1−y,1−z.

Finally, in the table, some more examples are reported as an introduction to more complex, partially disordered structures (random distribution of different atom types in the same positions, partially occupancy of certain positions).

Considering now the simple structure of CsCl as an example we see that the "crystallographic description" reported in table 3 corresponds to the atom arrangement presented (with alternative representations) in fig. 3 and, in more details, in sec. 6.1.2).

More generally, we may say that, from descriptions, such as those reported in table 3, the interatomic distances may be computed and, consequently, the coordinations and grouping of the various atoms may be derived: an example of this computation will be presented in sec. 3.5.5. (A systematic listing of the crystal data relevant to all the known phases has been reported in a number of fundamental reference books such as (PEARSON [1967], LANDOLT–BÖRNSTEIN [1971], VILLARS–CALVERT [1985], VILLARS–CALVERT [1991], etc).

For the criteria to be followed, especially when complex structures are involved, in the preparation and presentation of coordinate lists see PARTHE and GELATO [1984]. Their paper describes a proposal for a standardized presentation of inorganic crystal structure data with the aim of recognizing identical (or nearly identical) structures from the similarity of the numerical values of the atom coordinates. Different, equivalent (but not easily recognizable) descriptions could, in fact, be obtained by shift of origin of the coordinate system, rotation of the coordinate system, inversion of the basis vector triplet. (See also PARTHE *et al.* [1993]).

A description which in some simple cases could in a way be considered alternative to those exemplified in table 3 is based on the *lattice complex concept.* (Listing the symbols of the lattice complexes occupied by the different atoms in a structure, for instance, symbol P for the point 0,0,0, and its equivalent points, provides in fact a means of describing and classifying structures. This may be especially convenient for relatively simple structures particularly in the cubic system).

A *lattice complex* may be defined as an arrangement of equivalent points that are related by space group symmetry operations including lattice translations (PEARSON [1972]). The same lattice complex may occur in different space group types and may have more than one location in regard to a chosen origin for the unit cell. The number

References: p. 363.

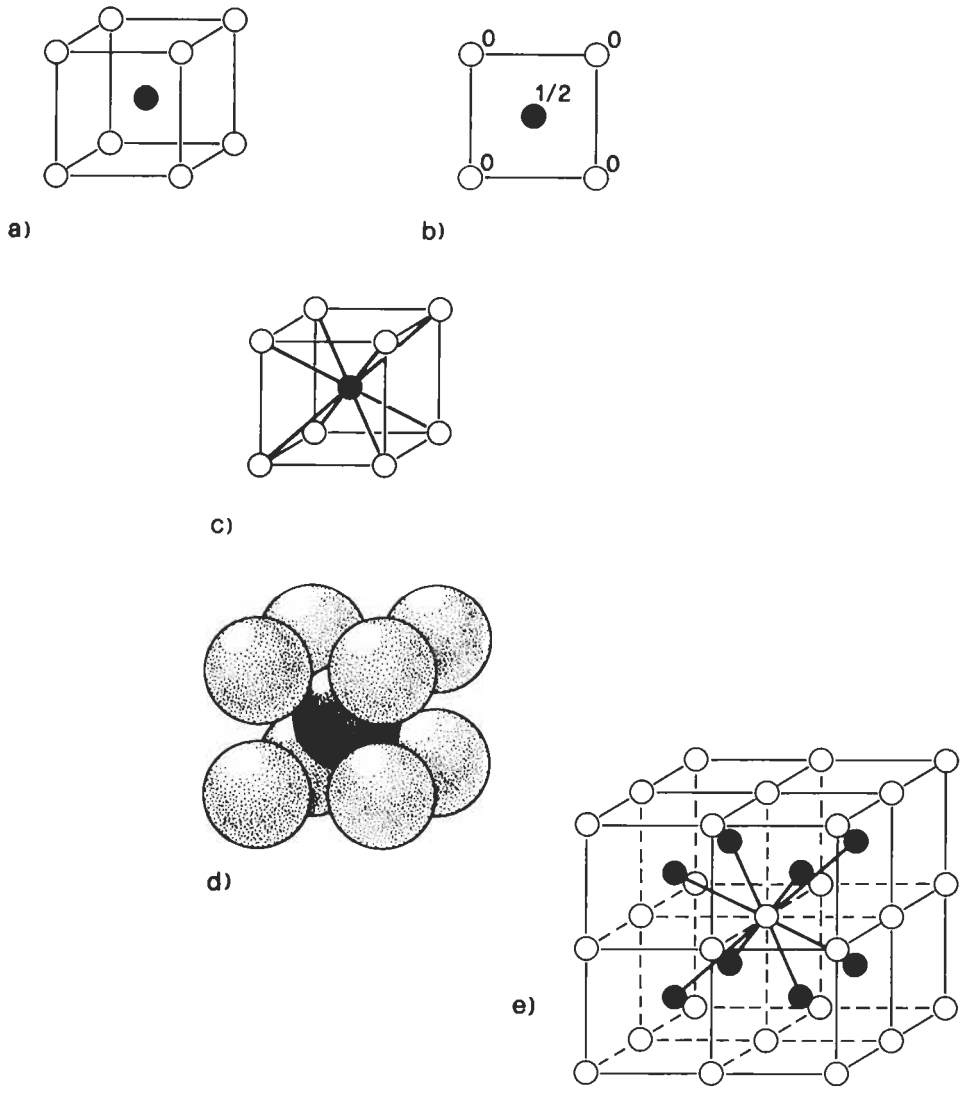

Fig. 3. Alternative representations of the unit cell of the CsCl compound. The two types of atoms are represented by means of the differently coloured spheres.

a) the positions of the centers of the atoms in the unit cell are indicated.
b) projection of the unit cell on the base plane. The values of the 3rd (vertical) coordinate are given.
c) the shortest interatomic distances are presented.
d) packed spheres model.
e) a group of 8 cells is represented in order to show that the actual structure of CsCl corresponds to a three-dimensional infinite repetition of unit cells. Notice the coordination around the white atom; it is similar to that around the black atom shown in c).

of *degrees of freedom* of a lattice complex, normally, is the same as that of any of its Wyckoff positions and is the number of coordinate (free) parameters x,y,z, that can vary independently. According to its number of degrees of freedom a lattice complex is called invariant, uni-, bi-, or trivariant.

The *invariant lattice complexes* in their characteristic Wyckoff positions are represented mainly by capital letters. Those with equipoints at the nodes of the Bravais lattice are designated by their appropriate lattice symbols. (Lattice complexes, from different crystal families that have the same coordinate description for their characteristic Wyckoff positions, receive the same symbol: for instance, lattice complex P corresponding to coordinate 0,0,0. In such a case, unless it is obvious from the context which lattice is meant, the crystal family may be stated by a small letter, preceding the lattice-complex symbol as follows: c = cubic, t = tetragonal, h = hexagonal, o = orthorhombic, m = monoclinic, a = anorthic = triclinic). Other invariant complexes are designated by letters that recall some structural features of a given complex, for instance D from the diamond structure, E from the hexagonal close-packing. Examples of two-dimensional invariant complexes are G (from graphite layer) and N (from kagomé net). (See table 4 and sec. 3.5.2.)

A short list of invariant lattice complex symbols is reported in the following. (For a complete list, for a more systematic description and formal definition, see chapter 14, Vol. A, of the International Tables of Crystallography, HAHN [1989]).

— *Lattice complex P*: (multiplicity, that is the number of equivalent points in the unit cell, 1);
coordinates 0,0,0;
(crystal families: c, t, h, o, m, a).
— *Lattice complex I*: (multiplicity 2);
coordinates 0,0,0; $\frac{1}{2},\frac{1}{2},\frac{1}{2}$;
(crystal families: c, t, o).
— *Lattice complex J*: (multiplicity 3);
coordinates $0,\frac{1}{2},\frac{1}{2}$; $\frac{1}{2},0,\frac{1}{2}$; $\frac{1}{2},\frac{1}{2},0$;
(crystal families: c).
— *Lattice complex F*: (multiplicity 4);
coordinates 0,0,0; $0,\frac{1}{2},\frac{1}{2}$; $\frac{1}{2},0,\frac{1}{2}$; $\frac{1}{2},\frac{1}{2},0$;
(crystal families: c, o).
— *Lattice complex D*: (multiplicity 8);
(D from "Diamond", see sec. 6.3.1)
coordinates 0,0,0; $\frac{1}{2},\frac{1}{2},0$; $\frac{1}{2},0,\frac{1}{2}$; $0,\frac{1}{2},\frac{1}{2}$; $\frac{1}{4},\frac{1}{4},\frac{1}{4}$; $\frac{3}{4},\frac{3}{4},\frac{1}{4}$; $\frac{3}{4},\frac{1}{4},\frac{3}{4}$; $\frac{1}{4},\frac{3}{4},\frac{3}{4}$;
(crystal families: c, o).
— *Lattice complex E*: (multiplicity 2);
coordinates $\frac{1}{3},\frac{2}{3},\frac{1}{4}$; $\frac{2}{3},\frac{1}{3},\frac{3}{4}$;
(crystal families: h).

— *Lattice complex G*: (multiplicity 2);
(G fom "Graphite" layer, see sec. 6.3.4).
coordinates $\frac{1}{3},\frac{2}{3},0$; $\frac{2}{3},\frac{1}{3},0$;
(crystal families: h).
— *Lattice complex R*: (multiplicity 3);
coordinates 0,0,0; $\frac{1}{3},\frac{2}{3},\frac{2}{3}$; $\frac{2}{3},\frac{1}{3},\frac{1}{3}$;
(crystal families: h).

The coordinates indicated in the reported (partial) list of invariant lattice complexes correspond to the so called "standard setting". Some of the non-standard settings of an invariant lattice complex may be described by a shifting vector (defined in terms of fractional coordinates) in front of the symbol. The most common shifting vectors have also abbreviated symbols: P′ represents $\frac{1}{2}\,\frac{1}{2}\,\frac{1}{2}$ P (coordinates $\frac{1}{2},\frac{1}{2},\frac{1}{2}$), J′ represents $\frac{1}{2}\,\frac{1}{2}\,\frac{1}{2}$ J (coordinates $\frac{1}{2},0,0,$; $0,\frac{1}{2},0$; $0,0,\frac{1}{2}$); F″ represents $\frac{1}{4}\,\frac{1}{4}\,\frac{1}{4}$ F (coordinates $\frac{1}{4},\frac{1}{4},\frac{1}{4}$; $\frac{1}{4},\frac{3}{4},\frac{3}{4}$; $\frac{3}{4},\frac{1}{4},\frac{3}{4}$; $\frac{3}{4},\frac{3}{4},\frac{1}{4}$) and F‴ represents $\frac{3}{4}\,\frac{3}{4}\,\frac{3}{4}$ F. (The following notation is also used J∗ = J + J′ (complex of multiplicity 6). It can be seen, moreover, that the complex D corresponds to the coordinates F + F″.

Simple examples of structure descriptions in terms of combination of invariant lattice complexes, may be: **Cs**Cl type **P** + P′ (Cs in 0,0,0; Cl in $\frac{1}{2},\frac{1}{2},\frac{1}{2}$), see table 3 and sec. 6.1.2.; **Na**Cl type structure: **F** + F′, see sec. 6.4.1; **Zn**S type structure: **F** + F″, see sec. 6.3.2.; **Na**Tl type structure: **D** + D′, see sec. 6.1.4.

Such combination of, original or transformed, invariant lattice complexes, are also indicated as *connection patterns* or *construction patterns* or *frameworks* (or *Bauverbände* in the German literature, according to LAVES [1930]). These patterns are *homogeneous* if they may be described by the parameters of one point position, *heterogeneous* if, for their description, the parameters of two or more independent point positions are necessary. This terminology may give a short informative description of the crystal structure and is specially useful for cubic substances. (For its use in a systematic description and classification of cubic structures see HELLNER [1979]). For non-invariant complexes and/or in crystal systems with symmetry lower than cubic, the geometrical configuration of the complex (and the coordination) may change significantly with free parameter value and with axial ratios and angles between the crystal axes.

3.2. Structural types

Several intermetallic phases are known which have the same (or a similar) stoichiometry and crystallize in the same crystal system and space group with the same occupied point positions.

Such compounds are considered as belonging to the same structure type. The reference to the structure type may be a simpler and more convenient way of describing the structure of the specific phase. The *structure type is generally named after the formula of the first representative* identified: the "*prototype*". Trivial names and symbols are also used in some cases (see sec. 3.4.).

The various representatives of a specific structure type generally have different unit cell edges, different values of the occupancy parameters and of the free coordinates of

the atomic positions and, in the same atomic positions, different atoms (see, for instance, sec. 3.5.5.).

If these differences are small, we may consider the general pattern of the structure unaltered.

On the other hand, of course, if these differences become larger, it might be more convenient to describe the situation in terms of a "family", instead of a single structural type, of different (more or less strictly interrelated) structural (sub) types. According to PARTHE and GELATO [1984], some structures may not really be *isotypic* but only *isopointal*, which means that they have the same space group and the same occupation of Wyckoff positions with the same adjustable parameters but *different unit-cell ratios* and *different atom coordinations* (and/or different values of Wyckoff free parameters).

An interesting example may be given by the structures of $MoSi_2$, reported in table 3, and CaC_2. In this compound, Ca and C are respectively in the same positions as Mo and Si in the same space group I4/mmm:
2 Ca in a): 0,0,0; $\frac{1}{2},\frac{1}{2},\frac{1}{2}$;
4 C in e): 0,0,z; 0,0,$-$z; $\frac{1}{2},\frac{1}{2},\frac{1}{2}+z$; $\frac{1}{2},\frac{1}{2},\frac{1}{2}-z$.
The unit cell dimensions, however, correspond to a = 388 pm, c = 638 pm (c/a = 1.644 instead of 2.463 as in $MoSi_2$) and the free parameter z has the value 0.4068 (instead of 0.333). These differences result in two different space arrangements (see fig. 4). Diatomic groups, such as C_2, clearly evident in CaC_2 (and in a number of isostructural dicarbides and peroxides) are not formed in $MoSi_2$.

Very interesting general comments and definitions on this question have been proposed, for instance, by PEARSON [1972], and more recently by LIMA DE FARIA *et al.* [1990] According to these authors, two structures are *isoconfigurational* (configurationally isotypic) if they are isopointal and are similar with respect to the corresponding Wyckoff positions and their geometrical interrelationships (same or similar positional coordinates, same or similar values of the unit cell axial ratios, c/a, a/b, b/c and cell angles α, β, γ).

Isotypism is found particularly with inorganic compounds. This behaviour has been discussed by PARTHE *et al.* [1993]. It has been underlined that to explain why two compounds adopt the same atom arrangement is not always simple. Following examples have been presented:
— The isotypism of $Gd_4Ni_6Al_{23}$ and $Y_4Ni_6Al_{23}$ may be easily explained because Gd and Y (elements of the same group of the Periodic Table) have comparable electron configuration and nearly the same atomic dimensions.
— Li_2SiO_3 and $LiSi_2N_3$ are isotypic (even if not in a rigorous sense owing to slightly different distorsions of the coordination polyhedra). They adopt an adamantine structure type (see sec. 6.3. and 7.2.1.) for which particular values of the electron concentration may be relevant even if obtained with elements from different parts of the Periodic Table.
— GdNi and NiB represent another couple of isotypic compounds. The role (the position in the crystal structure), however, of the same atom, Ni, in the two compounds is exchanged. In NiB, the Ni atoms are those centring the trigonal prism (formed by Gd atoms). A reason for the existence of this structure type could possibly be related to the

References: p. 363.

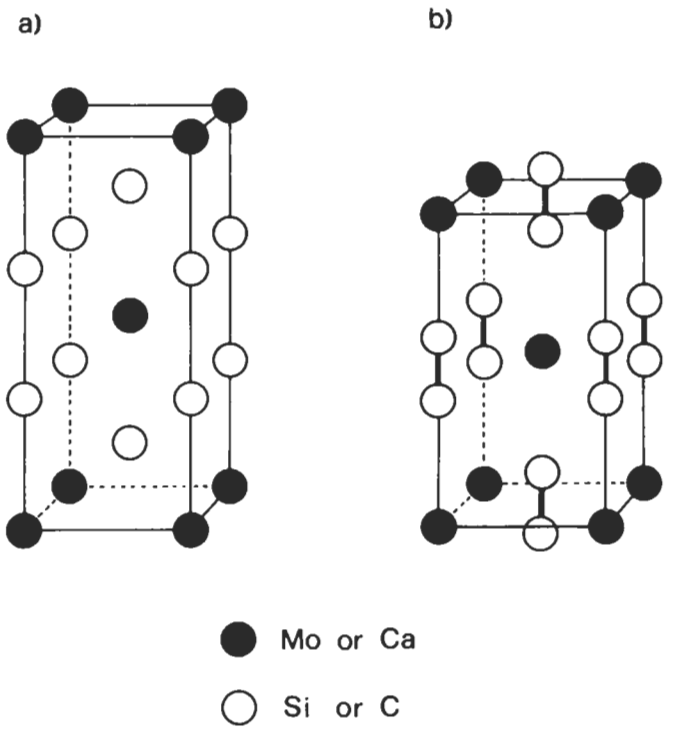

Fig. 4. $MoSi_2$ (a) and CaC_2 (b) type structures: an example of isopointal structures. Notice that, due to the different values of the c/a ratios and of the z parameters, there are different coordinations and atomic groupings (formation in CaC_2 of C–C, dumb-bell, discrete groups).

atomic size difference of the elements involved (or, perhaps, to their relative position in Pettifor's chemical scale).

— The last (and most intriguing) example reported by PARTHE *et al.* [1993] is the couple of compounds $Pu_{31}Rh_{20}$ and $Ca_{31}Sn_{20}$. For the present, the isotypism of these compounds of unusual stoichiometry cannot be expected and explained.

As a conclusion to these comments, we may mention that two structures are defined *crystal-chemically isotypic* if they are isoconfigurational and the corresponding atoms (and bonds) have similar chemical/physical characteristics.

Those interested in these concepts and in their historical development may refer also to a contribution by LAVES [1944], translated and reported by HELLNER [1979]. Conditions to be defined for calling crystal structures "equal" (isotypism), "similar" (homeotypism) or "different" (heterotypism) were suggested, discussed and exemplified.

We have finally to observe that, when considering phases having certain polar characteristics (salt-like "bonding"), the concept *type* and *antitype* may be useful. Antitypic phases have the same site occupations as the typic ones, but with the cation-anion positions exchanged (or more generally some important physical/chemical

characteristics of the corresponding atoms interchanged). As examples the structure types CaF_2 and CdI_2 and their antitypes reported in sec. 6.4.2. and 6.5.2. may be considered. Notice, however, that for a structure such as the CsCl type, it does not matter whether we describe it as 1 Cs in 0,0,0 and 1 Cl in $\frac{1}{2},\frac{1}{2},\frac{1}{2}$, or as 1 Cs in $\frac{1}{2},\frac{1}{2},\frac{1}{2}$, and 1 Cl in 0,0,0. In this case the two descriptions are undistinguishable (see fig. 3): they correspond to a mere shift of the origin of the reference axes. The CsCl type is its *own antitype*. Similar considerations are valid also for other structures such as the NaCl, ZnS types, etc.

3.3. Unit cell Pearson symbol

The use of the so-called Pearson notation (PEARSON, [1972]) is highly recommended (IUPAC, LEIGH [1990], "Ternary Alloys", PETZOW and EFFENBERG [1988 *et seg.*]) for the construction of a compact symbolic representation of the structure of the phase. As far as possible, it should be completed by a more detailed structural description by using the prototype formula which defines (as previously mentioned) a certain structure type.

The Pearson symbol is composed of a sequence of two letters and a number. The first (small) letter corresponds to the crystal system of the structure type involved; the second (capital) letter represents the lattice type (see table 4). The symbol is completed by the number of the atoms in the unit cell. A symbol as tP10, for example, represents a structure type (or a group of structure types) corresponding to 10 atoms in a primitive tetragonal cell.

In this chapter, the Pearson symbol will be used throughout; the convention has been adopted indicating in every case the number of atoms contained in the chosen unit cell. *In the case*, therefore, *of rhombohedral substances* for which the data of the (triple primitive) hexagonal cell are generally reported, the number of atoms is given which is in the hexagonal cell and *not* the number of atoms in the equivalent rhombohedral cell (FERRO and GIRGIS [1990]). So, for instance, at variance with VILLARS and CALVERT [1985, 1991], hR9 (and not rP3 or hR3) for the Sm-type structure.

If the structure is not known exactly, the prototype indication cannot be added to the Pearson symbol. In some cases, moreover, only incomplete Pearson symbols (such as o?60, cF?, etc.) can be used.

A criterion similar to Pearson's for the unit cell designation was used by SCHUBERT [1964] in his detailed and systematic description of the structural types of the intermetallic phases and of their classification.

A slightly more detailed notation, moreover, for the unit cell of a given structure has been suggested by FREVEL [1985]. Four items of information are coded in Frevel's notation:
— the number of different elements contained in the compound,
— the total number of atoms given by the chemical formula,
— the appropriate space group expressed in the HERMANN–MAUGUIN notation and
— the number of formulae for unit cell.
The notation for the CaF_2 structure, for instance, is:
2,3 $Fm\bar{3}m$ (4).

Possible augmentation of the notation has been discussed by Frevel and its use for classification and cataloguing the different crystal structures suggested.

References: p. 363.

According to PARTHE *et al.* [1993], a standardization procedure is at first necessary in the presentation of the relevant data characteristic of a crystal structure (see also PARTHE and GELATO [1984]). A convenient description of the structure types is then possible using the "*Wyckoff sequence*" (the letters of the occupied Wyckoff sites). This allows a finer classification of structure types and offers suggestions not only for recognizing isotypic structures but also possible structural relationships (substitution, formation of vacancy or filled-in structure variants).

3.4. Structure trivial names and symbols

A number of trivial names and symbols have been used (and are still in use) both as indicators, of a single phase in specific systems or as descriptors of certain structural types (or of families of different interrelated structural types).

Among the trivial symbols, we may mention the use of Greek (and Roman) letters to denote phases. These have often been used to indicate actual phases in specific systems, for instance in a given binary system, phase α, β, γ, etc., in alphabetical order according to the increasing composition from one component to the other, while in a unary system the α, β, etc., symbols have often been used to denote different allotropic forms.

Obviously this notation (or other similar ones such as τ_1, τ_2, τ_3, denoting "1st", "2nd", etc., phase) may be useful as a quick reference code while discussing and comparing phase properties of alloys in a single specific system, but in general cannot be used as a rational criterion for denoting structural types. In a few cases, however, certain Greek (and Roman) letters have assumed a more general meaning (as symbols of groups of similar phases): for instance, the name "γ-phases" which is an abbreviation of a sentence such as phases having the γ-brass (the γ-Cu–Zn) type structure. A short list, taken from LANDOLT–BÖRNSTEIN [1971], of (Greek and Roman) letters which have also been used as descriptors of structural types, may be the following:

γ : γ-brass type or similar structures
ε : Mg type
ζ : Mg type
η : W_3Fe_3C or Ti_2Ni type
μ : W_6Fe_7 type
σ : σ phase or σ-CrFe type
χ : α-Mn or Ti_5Re_{24} type
ω : ω_2 -(Cr,Ti) type (similar to the AlB_2 type)
E : $PbCl_2$ or Co_2Si type
G : G phase, Th_6Mn_{23} or $Cu_{16}Mg_6Si_7$
P : P phase or P-(Cr, Mo, Ni)
R : R phase or R-(Co, Cr, Mo)
T_1 : W_5Si_3 type
T_2 : Cr_5B_3 type

In a number of cases, names of scientists are used as descriptors. We may mention the following groups of structures (some of which will be described in more detail later).

Chevrel phases. A group of compounds having a general formula such as $M_xMo_3S_4$

(M = Ag, As, Ca, Cd, Zn, Cu, Mn, Cr, etc.). Many representatives of these structure types are superconducting with critical T_c as high as 10–15 K.

Frank–Kasper phases. (For all of which the structure can be described as composed of a collection of distorted tetrahedra which fill the space: see sec. 6.6). This family of phases includes those of the structural types: *Laves phases* (a family of polytypic structures including the hP12–$MgZn_2$, cF24–Cu_2Mg and hP24–Ni_2Mg types), *tP30 σ–phases*, *oP56–P phases* and *hR39–W_6Fe_7 type phases*.

Hägg phases. According to HÄGG [1931], a number of compounds of the transition metals with small non-metal atoms (H, B, C, N) have structures which can be described as "*interstitial*". These correspond, generally, to a simple structures in which the small non metal atoms occupy interstices in a face centered cubic or body centered cubic framework of metal atoms or, the interstices in other close packed structures. In the Hägg interstitial phases the relative atomic size of the two elements is of particular importance to the stability of the structure.
See sec. 6.2.2. for a classification of the interstices ("holes") in close packed structures, sec. 6.4.1. for NaCl-type related phases and sec. 6.5.5. for WC-type phases.

Heusler phases. Magnetic compounds of the cF16–$MnCu_2Al$-type. (See sec. 6.1.3. on this structure which can be considered "derivative" of the CsCl type).

Hume–Rothery phases. These designations can be connected to the research carried out as far back as 1926 by HUME–ROTHERY, WESTGREN and PHRAGMEN, etc. They observed that several compounds (electron compounds) crystallize in the same structural type if they have the average number of valence electrons per atom (the so-called VEC: valence electron concentration) included within certain well-defined ranges. Some groups of these phases (brasses, etc.) will be presented in sec. 6.1.5. and 7.2.2. (See also ch. 3, § 8.1.)

Nowotny phases. Chimney-ladder phases (see sec. 4.4.).

Samson phases. Complex intermetallic structures with giant unit cells, based on framework of fused truncated tetrahedra (see sec. 6.6.5.)

Zintl phases. This term was first applied to the binary compounds formed between the alkali or alkaline-earth elements and the main group elements from group 14 on, that is to the right of the "Zintl boundary" of the Periodic Table. These combinations not only yield some Zintl anions (homopolyatomic anions) in solution but also produce many rather polar or salt-like phases. A simple example may be a classical valence compound in which the more "noble" member achieves a filled "octet" and an 8–N oxidation state in salt-like structure (for example Na_3As, Mg_2Sn) (CORBETT [1985]). An important intermetallic structure discovered by Zintl (ZINTL and WOLTERSDORF [1935]) was that of the cF16–NaTl-type (superstructure of the bcc lattice, see sec. 6.1.4.). The Na and Tl atoms are arranged according to two (interpenetrating) diamond type sublattices; each atom is tetrahedrally coordinated by four like neighbours on the same sublattice and has four unlike neighbours on the other sublattice. This could be interpreted as a Tl^- array, isoelectronic with carbon in the limit of complete charge transfer. For a critical discussion on the NaTl-type structure, its stability, the role of the size factor, the comparative trend of the stabilities of CsCl and NaTl type structures, the application of modern

band-structure techniques, see HAFNER [1989]. Subsequent applications of the term "Zintl Phases" have been based on the structural characteristic of such polar phases. A review on this subject has been published by CORBETT [1985]. In this paper several phases are mentioned: starting from compounds such as hR18–$CaSi_2$ (containing rumple double layers of Si atoms resembling those of the As structure), mP32–NaGe and mC32–NaSi (respectively containing Ge, or Si atom, tetrahedra with the Na atoms arranged in the intervening spaces), up to complex alkali metal-gallium compounds exhibiting complex structures containing large interconnected usually empty gallium polyhedra, reminiscent of boron chemistry. It may be added that the concept of Zintl ions has been used also in the description of selected liquid alloys. It was proposed (VAN DER LUGT and GEERTSMA [1984], REIJERS *et al.* [1990]) that in the equiatomic liquid alkali alloys with Sn and Pb the liquid consists of poly-anion clusters, such as Pb_4^{4-} tetrahedra, formed by covalent bonding which are separated by alkali ions.

Within the group of trivial names we may also include a few "*personal*" *names* such as *austenite* (solid solution of C in γ-Fe), *ferrite* (solid solution of C in α-Fe), *martensite* (see sec. 6.1.5.), etc., and a few *mineralogical names* such as pyrite, blende, cinnabar, etc. According to the IUPAC recommendations (LEIGH [1990]), mineralogical names should be used to designate actual minerals and not to define chemical composition. They may, however, be used to indicate a structure type. They should be accompanied by a representative chemical formula:
cF8–ZnS sphalerite, hP4–ZnS wurtzite, cF8–NaCl rock salt, cP12–FeS_2 pyrite, etc.

In closing this section we have to mention the *Strukturbericht designation* adopted from pre-war time by the editors of the Strukturbericht publications (and later Structure Reports) in abstracting crystal-structure determination. This designation is no longer recommended by the International Union of Pure and Applied Chemistry, but it is still used.

According to this designation, each structure type is represented by a symbol generally composed of a letter (**A**, **B**, **C**,etc.) and a number (possibly in some cases followed by a third character). The letter was related to the stoichiometry according to the following form: **A**: unary phases (or believed to be unary), **B**: binary compounds having 1:1 stoichiometry, **C**: binary 1:2 compounds, **D**: binary m:n compounds, **E**...**K** types: more complex compounds; **L**: alloys, **O**: organic compounds and **S**: silicates.

In every class of stoichiometries, the different types of structures were distinguished by a number and/or a letter. (For instance, in the element class the frequently encountered fcc structure, cF4–Cu-type, was called A1, in the 1:1 group the common cF8–NaCl type was represented by B1, etc.). Equivalence tables between the Strukturbericht designation and the Pearson symbol-prototype may be found in PEARSON [1972], MASSALSKI [1990].

The following is a partial list of these old *Strukturbericht symbols* for some types frequently occurring in metallic systems:

A1: cF4–Cu; **A2**: cI2–W; **A3**: hP2–Mg; **A3'**: hP4–αLa; **A4**: cF8–C (diamond); **A5**: tI4–βSn; **A6**: tI2–In; **A7**: hR6–αAs;...; **A9**: hP4–C (graphite);...; **A12**: cI58–αMn; ... ; **A15**: cP8–Cr_3Si; ....The A15 structure was previously considered to be that of a W

modification (and therefore a unary structure): later on the substance concerned was recognized to be a W oxide: W_3O (isostructural with Cr_3Si); ...; $\mathbf{A_b}$: tP30–βU;...; $\mathbf{A_h}$: cP1–αPo;...; $\mathbf{A_i}$: hR3–βPo; ...

B1: cF8–NaCl; **B2**: cP2–CsCl; **B3**: cF8–ZnS (sphalerite or zinc blende); **B4**: hP4–ZnS (wurtzite);...; $\mathbf{B8_1}$: hP4–NiAs; $\mathbf{B8_2}$: hP6–Ni_2In; ... ; **B11**: tP4–γCuTi;...; **B19**: oP4–AuCd; **B20**: cP8–FeSi; ... ; **B27**: oP8–FeB;...; **B31**: oP8–MnP; **B32**: cF16–NaTl; ...; **B35**: hP6–CoSn;...; $\mathbf{B_a}$: cI16–UCo;...; $\mathbf{B_f}$: oC8–CrB;...; $\mathbf{B_h}$: hP2–WC;...; $\mathbf{B_i}$: hP8–TiAs;...

C1: cF12–CaF_2; $\mathbf{C1_b}$: cF12–AgMgAs; **C2**: cP12–FeS_2 (pyrite); ... ; $\mathbf{C11_a}$: tI6–CaC_2; $\mathbf{C11_b}$: tI6–$MoSi_2$, (the two $\mathbf{C11_a}$ and $\mathbf{C11_b}$ structures are closely interrelated, see fig. 4); ...; **C14**: hP12–$MgZn_2$; **C15**: cF24–Cu_2Mg; $\mathbf{C15_h}$: cF24–$AuBe_5$ (this structure is a derivative structure of the cF24–Cu_2Mg, C15 type, see figs. 42 and 44); **C16**: tI12–$CuAl_2$; ...; **C22**: hP9–Fe_2P;...; **C32**: hP3–AlB_2; ...; **C36**: hP24–Ni_2Mg; ...; **C38**: tP6–Cu_2Sb;...; $\mathbf{C_a}$: hP18–$NiMg_2$; $\mathbf{C_b}$: oF48–$CuMg_2$; $\mathbf{C_c}$: tI12–$ThSi_2$;...

$\mathbf{D0_2}$: cI32–$CoAs_3$; ... ; $\mathbf{D0_{18}}$: hP8–Na_3As; ... ; $\mathbf{D1_a}$: tI10–$MoNi_4$; $\mathbf{D1_b}$: oI20–UAl_4;...; $\mathbf{D1_3}$: tI10–$BaAl_4$;...; $\mathbf{D2_b}$: tI26–$ThMn_{12}$;...; $\mathbf{D8_1}$: cI52–Fe_3Zn_{10}; $\mathbf{D8_2}$: cI52–Cu_5Zn_8; $\mathbf{D8_3}$: cP52–Cu_9Al_4; $\mathbf{D8_4}$: cF116–$Cr_{23}C_6$; ...

$\mathbf{E1_a}$: oC16–$MgCuAl_2$;...;$\mathbf{E9_a}$: tP40–$FeCu_2Al_7$;..

$\mathbf{H2_4}$: cP8–Cu_3VS_4;..

$\mathbf{L1_0}$: tP2–AuCu (I); $\mathbf{L1_2}$: cP4–$AuCu_3$; $\mathbf{L2_1}$: cF16–$MnCu_2Al$; $\mathbf{L1_a}$: cF32–$CuPt_3$;...; $\mathbf{L2_a}$: tP2–δCuTi;...; $\mathbf{L6_0}$: tP4–$CuTi_3$.

3.5. Rational crystal structure formulae

We know that all of the requisite structural information for a solid phase is contained (either explicitly or implicitly) in its unit cell and this can be obtained from the Pearson symbol-prototype notation (complemented, if necessary, by data on the values of lattice parameters, atomic positions, etc.). A number of features, however, which are especially relevant for chemical-physical considerations, such as local coordination geometries, the existence of clusters, chains or layers, etc., are not self-evident in the aforementioned structural descriptions and can be deduced only by means of a more or less complicated series of calculations. It should, moreover, be pointed out that the same structure can be differently viewed and described (FRANZEN [1986], PARTHE and GELATO [1984]). The simple rock-salt structure, for instance, (see sec. 6.4.1.) can be viewed as cubic close packed anions with cations in octahedral holes, as XY_6 octahedra sharing edges, as a stacking sequence of superimposed alternate triangular nets respectively of X and Y atoms or as a cubic-close packed structure of a metal with non-metals in octahedral interstices. As a further example we may consider the Cu structure which, for instance, could be conveniently compared with those of Mg, La and Sm, or from another point of view, with the AuCu and $AuCu_3$ structures. In the two cases, as we will see in sec. 6.2, one would choose a different description and representation of the aforementioned Cu structure.

In the different cases, some criteria may therefore be useful in order to give (in a systematic and simple way) explicit information on the characteristic structural features.

References: p. 363.

In the following sections some details will be given on a few complementary, alternative notations.

3.5.1. Coordination and dimensionality symbols in the crystal coordination formula

Several attempts have been carried out in order to design special formulae (crystal coordination formulae) which (in a convenient linear format) may convey explicit information on the local coordination geometry. A detailed discussion of these attempts and of their development (through the work, inter alios, of NIGGLI [1945, 1948], MACHATSCHKI [1938, 1953], LIMA DE FARIA and FIGUEIREDO [1976, 1978], PARTHE [1980a] and JENSEN [1984]) may be found in a review by JENSEN [1989], who presented and systematically discussed a flexible notation for the interpretation of solid-state structures. A short description of Jensen's notation will be given below. The different symbols used will be briefly presented. For the notation concerning the common coordination geometries a summary is reported in table 5. A report by the International Union of Crystallography Commission on Crystallographic Nomenclature (LIMA DE FARIA *et al.* [1990]) presents a concise description of similar alternative notations, a summary of which is also presented in table 5.

The symbols suggested by Jensen, based on Niggli's proposals, indicate the local coordination environments by means of *coordination number ratios*. For instance, a *formula* $AE_{m/n}$ will indicate a binary compound where m is the coordination number (the nearest neighbour number) of atoms E around A and n will be considered the coordination number of E by A. The ratio m/n will be equal to the stoichiometric compositional ratio. For instance, we will write $NaCl_{6/6}$ to represent the hexa-coordination

Table 5
Suggested notations for common coordination geometries.

a)	from JENSEN [1989]		
1	Terminal	7″	Monocapped trigonal prism
2	Bent CN 2	8	Cube
2′	Linear CN 2	8′	Square antiprism
3	Pyramidal or in general non-planar CN 3	8″	Dodecahedron
3′	Trigonal planar	8‴	Bicapped trigonal prism
3″	T-planar	$\hat{8}$	Hexagonal bipyramid
4	Tetrahedral	9	Tricapped trigonal prism
4′	Square planar	10	Bicapped square antiprism
4″	Base of a square pyramid with the central atom as the apex	11	Monocapped pentagonal antiprism
		12	Cubic closest-packed or cuboctahedron
5	Trigonal bipyramid	12′	Hexagonal close-packed or twinned cuboctahedron
5′	Square based pyramid with the central atom inside	12″	Isocosahedron
		$\hat{12}$	Hexagonal prism
6	Octahedron or trigonal antiprism	$\tilde{n}$	Complex, distorted n-hedron
6′	Trigonal prism	$\bar{n}$	Disordered structure in which it is possible to define only an average coordination number n
6″	Hexagonal planar		
7	Pentagonal bipyramid		
7′	Monocapped octahedron		

Table 5—*Continued*

b) from LIMA DE FARIA *et al.*[1990]

Coordination polyhedron around atom A	Complete Symbol		Alternative simplified symbols	
Single neighbour	[1l]		[1]	
Two atoms collinear with atom A	[2l]		[2]	
Two atoms non-collinear with atom A	[2n]		[2]	
Triangle coplanar with atom A	[3l]		[3]	
Triangle non-coplanar with atom A	[3n]		[3]	
Triangular pyramid with atom A in the centre of the base	[4y]		[4]	
Tetrahedron	[4t]	[t]	[4]	t
Square coplanar with atom A	[4l] or [4s]	[s]	[4]	s
Square non-coplanar with atom A	[4n]		[4]	
Pentagon coplanar with atom A	[5l]		[5]	
Tetragonal pyramid with atom A in the centre of the base	[5y]		[5]	
Trigonal bipyramid	[5by]		[5]	
Octahedron	[6o]	[o]	[6]	o
Trigonal prism	[6p]	[p]	[6]	p
Trigonal antiprism	[6ap]	[ap]	[6]	ap
Pentagonal bipyramid	[7by]		[7]	
Monocapped trigonal prism	[6p1c]		[7]	
Bicapped trigonal prism	[6p2c]		[8]	
Tetragonal prism	[8p]		[8]	
Tetragonal antiprism	[8ap]		[8]	
Cube	[8cb]	[cb]	[8]	cb
Anticube	[8acb]	[acb]	[8]	acb
Dodecahedron with triangular faces	[8do]	[do]	[8]	do
Hexagonal bipyramid	[8by]		[8]	
Tricapped trigonal prism	[6p3c]		[9]	
Cuboctahedron	[12co]	[co]	[12]	co
Anticuboctahedron (twinned cubooctahedron)	[12aco]	[aco]	[12]	aco
Icosahedron	[12i]	[i]	[12]	i
Truncated tetrahedron	[12tt]		[12]	
Hexagonal prism	[12p]		[12]	
Frank-Kasper polyhedra with				
14 vertices	[14FK]		[14]	
15 vertices	[15FK]		[15]	
16 vertices	[16FK]		[16]	

(in this case octahedral coordination) of Cl around Na (and vice versa) in sodium chloride. Similarly we will have: $ZnS_{4/4}$; $PH_{3/1}$; $CsCl_{8/8}$; $CaF_{8/4}$; $UCl_{9/3}$; etc. According to one of Jensen's suggestions it is possible to add *modifiers* to the coordination numbers in order to specify not only *topological* but also *geometrical* characteristics of the primary coordination sphere. (For examples, 6: octahedral; 6′: trigonal prismatic; 6″: hexagonal planar; etc., see table 5a.

Similar symbols were proposed by DONNAY *et al.* [1964] who suggested adding to the coordination number, one or two letters to indicate the geometry: y, pyramidal; l, planar; c, cubic; etc. Detailed descriptions of the coordination polyhedra are obtained by means of the LIMA DE FARIA *et al.* [1990] symbols presented in table 5b. An advantage of the

References: p. 363.

Lima de Faria symbolism may be the existence of two alternative sets of symbols: complete and simplified. The simplified symbols give only a numerical indication, without any distinction between different geometries; the complete symbols (clearly distinguishible from the previous ones) contain beside the numeric indication a description of the coordination polyhedron. A selection of the Lima de Faria symbols, together with the Jensen's suggestions, will be used here.

According to Jensen, the *dimensionality* of a structure (or of a substructure of the same) is indicated by enclosing its compositional formula in *square brackets* and prefixing an appropriate *symbol* $\underset{\sim}{d}$. The dimensionality index, d, may be d = 0 for a discrete molecular (cluster, ring) structure, d = 1 for a one-dimensional, infinite chain structure, d = 2 for a two-dimensional, infinite layer structure and d = 3 for an infinite three dimensional, framework structure. These are the Machatschki symbols (MACHATSCHKI [1947]).

More complex symbols such as $\underset{\sim}{d}\text{-}\underset{\sim}{d}$ or $d'\underset{\sim}{d}''d$ will represent intermediate dimensionality (between d and d') or, second, the dimensionality indexes of different substructures (d' and d'') followed by that of the overall structure (d). A few examples:

Molecular structures	$\underset{\sim}{0}$[HI], $\underset{\sim}{0}$[CO_2],
Linear structures	$\underset{\sim}{1}$[$BeCl_2$]
Layer structures	$\underset{\sim}{2}$[C] graphite, $\underset{\sim}{2}$[As]
Framework structures	$\underset{\sim}{3}$[C] diamond,
Substructures	$\underset{\sim}{0}$Ca[CO_3] (finite ions);
	$\underset{\sim}{1}$K[PO_3] (infinite anionic PO_3^- chain)

etc.....

If, in a A–B structure, one wishes to show not only the A/B coordination but also the B/B, or A/A, self-coordinations this is done, according to the suggestion by Jensen via the use of a composite dimensionality index and the relative positions of the various ratios and brackets in the formula, with the last unbracketed ratio always referring to the B/A coordination. So, for instance, $\underset{\sim}{0}\underset{\sim}{3}$[$(H_2O)_{4/4}$] is a compact form for $\underset{\sim}{0}\underset{\sim}{3}$[$(H_2O)(H_2O)_{4/4}$] to indicate the molecular packing in the ice structure. The formula $\underset{\sim}{2}\underset{\sim}{3}$Al[$B_{3/3}$]$_{12/6}$ or $3\underset{\sim}{2}\underset{\sim}{3}$[$Al_{8by/8by}$][$B_{3l/3l}$]$_{12p/6p}$ correspond to a more or less detailed description of the AlB_2 type structure where the coordination of B around Al is 12 (12p: hexagonal prismatic) and that of Al around B is 6 (6p: trigonal prismatic). The self-coordinations are bipyramidal for Al/Al (8by: hexagonal bipyramidal) and trigonal-planar (3l) for B/B (the B atoms form a two-dimensional net).

Considering as a further example the compounds AB having the CsCl type structure, we may mention that according to Jensen, the two descriptions $3\underset{\sim}{3}\underset{\sim}{3}$[$A_{6/6}$][$B_{6/6}$]$_{8/8}$ and $\underset{\sim}{3}$[$AB_{8/8}$] (with and without the indication of the self-coordination) may also be used to suggest the bonding type (metallic if the A–A and B–B interactions contribute to the overall bonding, ionic, or covalent, if only A–B interactions have to be considered).

More complex examples of the use of this notation may be given by the structures of typical fluorides for which ionic type, coordination formulae are here reported:

oP16 YF_3 : $\underset{\sim}{3}$[$YF_{8/3}F_{1/3}$];
hP8 LaF_3 : $\underset{\sim}{3}$[$LaF_{8/4}F_{3/3}$];
cF16 BiF_3: $\underset{\sim}{3}$[$BiF_{8/4}F_{6/6}$].

In all these cases the sum of the numerators of the coordination ratios gives the total coordination (of two groups of F atoms) around the metal atom. (The sums of the ratios give, of course, the stoichiometric coefficients).

Another example may be represented by the hP6–Ni_2In structure ($^{3}_{\infty}[InNi_{6/6}Ni_{5/5}]$) described in sec. 6.5.3.

A detailed example ($AuCu_3$) of the application of the aforementioned notation to the description of a simple intermetallic structure will be presented in sec. 3.5.5. (with the pertinent figs. 12 to 15).

A few more examples will be reported in the following descriptions of a number of typical structures.

In conclusion to this description of "crystal coordination formulae" we have, however, to notice that the term "*coordination number*" (CN) may be used in two ways in crystallography (FRANK and KASPER [1958]). According to the first the coordination number, as previously mentioned, is the number of nearest neighbours to an atom. According to the other way, the definition of the coordination should be based on an "*interpretation*" *of the structure* which depends not only on an evaluation of the interatomic distances to assign bonding versus non-bonding contacts but on considerations on the bonding mechanism (JENSEN [1989]). These considerations are particularly important when thinking of metallic phases where it may be difficult to make distinctions between X–X, X–Y or Y–Y contacts. So, for instance, when considering the bc cubic structure of the W type, some authors define the coordination number as 8 (in agreement with the nearest-neighbours definition) but others prefer to regard it as 14 (including a group of 6 atoms at a slightly higher distance). Further considerations on this subject is delayed to a discussion, in sec. 7.2.6., on alternative definitions of coordination numbers (weighted coordination number, effective coordination number). In sec. 7.2.7., on the other hand, the *atomic-environment types* will be introduced, their codes presented and the results of their use in the classification of the selected groups of intermetallic structure types summarized.

3.5.2. Layer stacking sequence representation

A large group of structures of intermetallic phases can be considered to be formed by the successive stacking of certain polygonal nets of atoms (or, in more complex cases, by the successive stacking of characteristic "slabs"). These structural characteristics can easily be described by using specific codes and symbols, which can be very useful for a compact presentation and comparison of the structural features of several structures. Many different notations have been devised to describe the stacking pattern (for a summary see PARTHE [1964], PEARSON [1972]). A few of them will be presented here. *As an introduction to this point* we may consider figs. 5–7 where typical simple close-packed structures are shown and presented as built from the superimposition of close-packed atomic layers. If spheres of equal sizes are packed together as closely as possible on a plane surface they arrange themselves as shown in fig. 5. (Their centres are in the points of a triangular net.) Each sphere is in contact with six others. Such layers may be stacked to give three-dimensional close packed arrays. If we label the positions of the (centres of the) spheres in one layer as A, then an identical layer may be superimposed

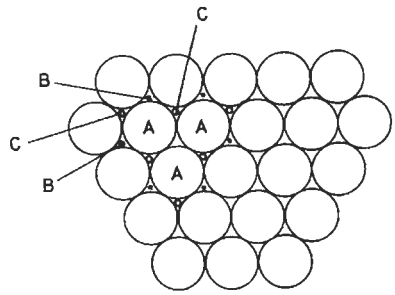

Fig. 5. Close-packed bidimensional arrangement of equal spheres. The A, B, C coding used to indicate different relative positions is shown. (See also fig. 8.)

on the first so that the centres of the spheres of the second layer are vertically above the positions B (for two layers, it is insignificant whether we choose the positions B or the equivalent position C). When we superimpose a third layer above the second (B) we have two alternatives: the centres of the spheres may be above either the A or the C positions. The two simplest sequences of layers correspond to the superimpositions ABABAB... and ABCABCABC... (more complex sequences may of course be considered). The sequence ABAB..., corresponding to the so-called hexagonal close-packed structure (Mg-type structure) is shown in fig. 6. The sequence ABCABC... having a cubic symmetry, is shown in fig. 7. It is the cubic (face-centered cubic) close-packed structure (also described as cF4–Cu type structure).

A more complete representation of different layer sequences (which can be used not only for the description of close packed structures) may be obtained by using *stacking symbols* such as those shown in fig. 8, together with layer stacking indications. Fig. 8a

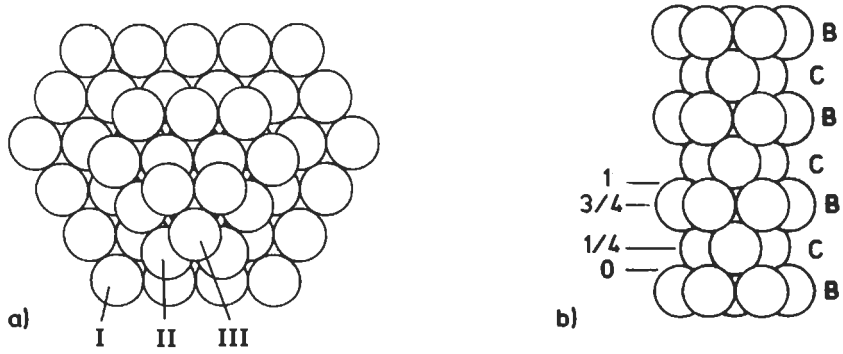

Fig. 6. Hexagonal close-packing.

a) A few spheres of three superimposed layers are shown. In this structure, the spheres of the layer III are just above those of the first one.

b) Lateral view of the same arrangement. The stacking symbols corresponding to the Mg unit cell description reported in sec. 6.2.6. (Mg in $\frac{1}{3},\frac{2}{3},\frac{1}{4}$ and $\frac{2}{3},\frac{1}{3},\frac{3}{4}$) are shown. (The ...BCBCBC... sequence description is identical to a ...ABABAB... or ...CACACA... symbol). The heights of the layers are reported as fractions of the repeat unit along the z axis of the hexagonal cell (that is of the distance between levels 0 and 1).

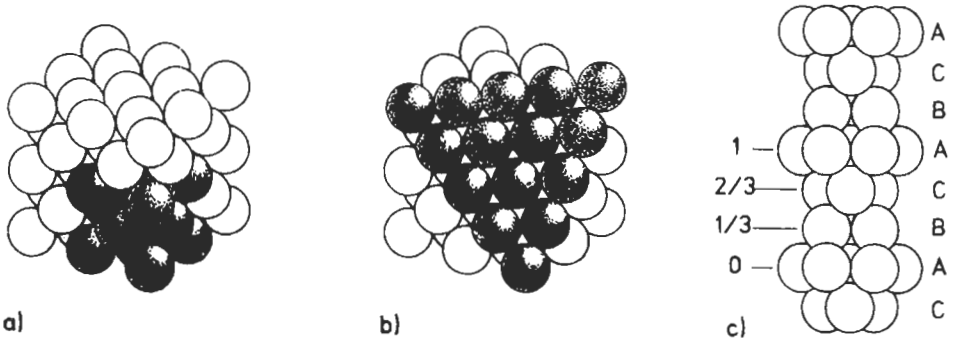

Fig. 7. Face-centered cubic close-packed structure of equal spheres.

a) Sphere-packing: a group of eight cubic unit cells is shown. (One of the unit cell is indicated by the black atoms).

b) A section of the same structure shown in a) is presented; it corresponds to a plane perpendicular to the cube diagonal. The typical arrangement of layers similar to that shown in fig. 5 is evidenced.

c) A lateral view of the stacking of the layers in the fcc structure is presented. The layer positions along the superimposition direction (which corresponds to the cubic cell diagonal) are shown as fractions of the repeat unit (cell diagonal)).

shows a network of atoms which can be considered as a triangular net, T net, that is the 3^6 net. We may incidentally notice that this notation, the Schläfli notation P^N, describes the characteristics of each node in the network, that is the number N of P-gon polygons surrounding the node. In the reported 3^6 net all the nodes are equivalent: their polygonal surrounding corresponds to 6 triangles. (More complex symbols are used for nets containing non equivalent nodes: for instance, the symbol $3^2434 + 3^24^2$ (2:1) means that, in the given net, two type of nodes, 3^2434 and 3^24^2, occur with a relative 2:1 frequency. A symbol such as 3^24^2 means that the given node is surrounded, in this order, by 2 triangles and 2 squares).

In the case of the simple, *3^6, triangular net* the aforementioned *stacking symbols A, B, C,* as can be seen in fig. 8c relate the positions of the nodes to the origin of the cell (which is defined as in fig. 8b). In the *layer stacking sequence full symbol*, the component atoms occupying the layers are written on the base line, with the stacking symbols as exponents and the layer spacings in the form of suffixes, denoting the fractional height of the repetition constant along the direction perpendicular to the layers. In the case of Mg, for instance, with reference to the standard choice of the unit cell origin (two equivalent atomic positions for the two Mg atoms in $\frac{1}{3},\frac{2}{3},\frac{1}{4}$ and $\frac{2}{3},\frac{1}{3},\frac{1}{4}$), the symbol will be $Mg^B_{1/4}Mg^C_{3/4}$ (which, with a zero point shift, is equivalent to $Mg^A_0Mg^B_{1/2}$). The symbol $Cu^A_0Cu^B_{1/3}Cu^C_{2/3}$, on the other hand, represents the cubic Cu structure as a stacking sequence of triangular layers viewed along the direction of the unit cell diagonal (which is perpendicular to the layers themselves).

A few other nets, based on the hexagonal cell, are of frequent structural occurrence. Following Pearson's suggestions, the corresponding sequences of stacking symbols which have a wide application are here presented. Fig. 9 shows the *hexagonal* (honeycomb) *net*

References: p. 363.

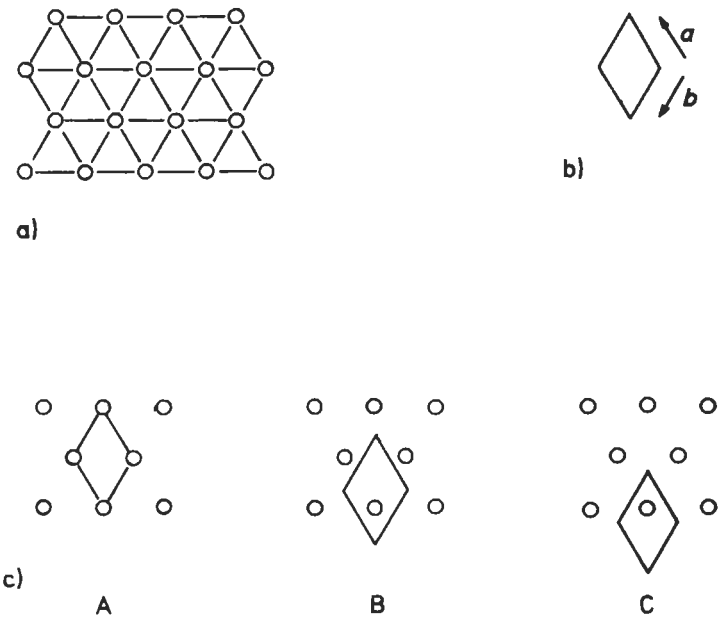

Fig. 8. Triangular net of points.

a) and b) The 3^6 net and the corresponding (bidimensional) cell are shown. Notice that, in this case, the selected coordinate system corresponds to an interaxial angle of 120°.

c) Different point positions (relative to the cell origin) and corresponding coding:
A) the representative point, in the x,y plane (a, b plane with a = b), has the coordinate 0,0;
B) with reference to the a, b constants the coordinate "doublet" of the representative point is $\frac{1}{3}, \frac{2}{3}$;
C) the representative point is in $\frac{2}{3}, \frac{1}{3}$.

(H net) and the stacking symbols (a, b, c) used for relating the different positions of the nodes to the cell origin. (Notice that two nodes are contained in the unit cell.)

A simple structure which can be described in terms of superposition of (even if far away, not close-packed) hexagonal layers is that of graphite: $C^{b}_{1/4}C^{c}_{3/4}$. The hexagonal net is also called "graphitic" net. (see sec. 6.3.4. and fig. 33).

Fig. 10 shows the three-ways bamboo weave net, known as *kagomé*, a net of triangles and hexagons (*K net*, the *3636 net* of points). The different positions of the nodes (three nodes in the unit cell) are represented by the symbols (α, β, γ) shown in fig. 10b.

Several (especially hexagonal, rhombohedral and cubic) structures may be conveniently described in terms of stacking triangular, hexagonal and/or kagomé layers of atoms. Examples will be given in the following sections. The specification of the spacing between the layers is useful in order to compare different structures, to recognize the close-packed ones (A, B, C symbols with appropriate layer distances) and to deduce atomic coordinations.

We have to notice, however, that the A, B, C notation previously described is not the

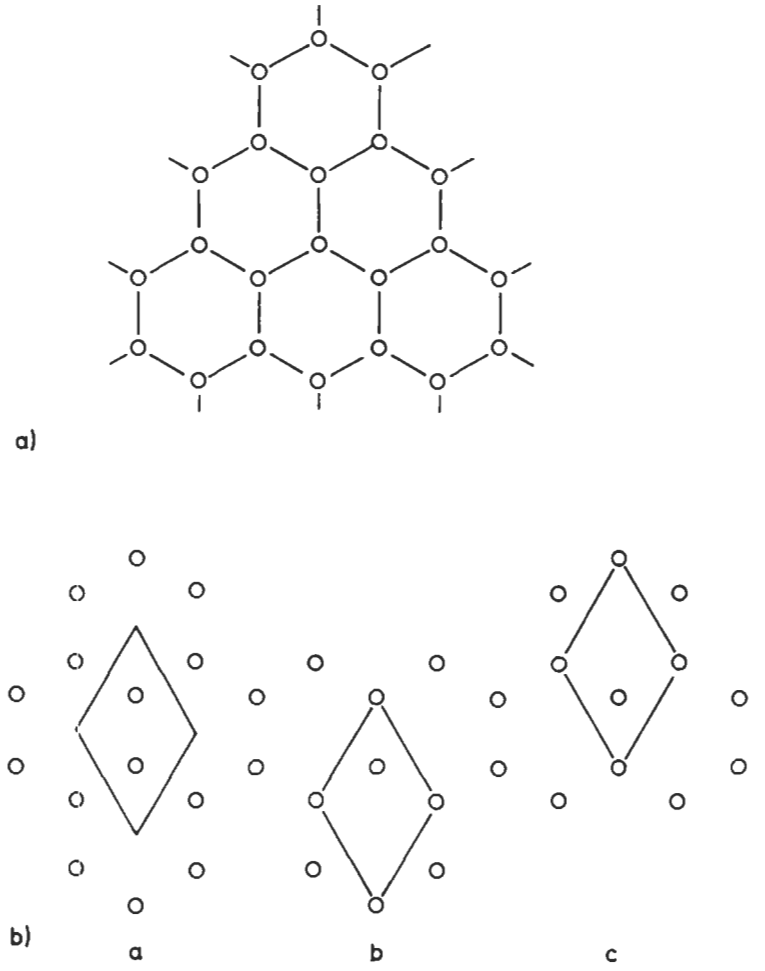

Fig. 9. Hexagonal (6^3) net of points.
The net is shown in a). In b) the different positions of the points in the unit cell are indicated with the stacking symbols a, b, c. Notice that the unit cell contains two points. (Every point in the corner is in common with (belongs to) four adjacent hexagonal cells).

only one devised. Several different symbols have been suggested to describe stacking patterns. (For a description of the more frequently used notations see PARTHE [1964], PEARSON [1972]).

A very common *notation* is that by JAGODZINSKI [1954]. This notation involving *h and c symbols* is applicable only to those structure type groups which allow not more than three possible positions of the unit layer (or more generally of the "unit slabs". See sec. 4.3. on polytypic structures). The h, c notation cannot therefore be applied, for instance, to disilicide types. The letters h and c have the following meaning:

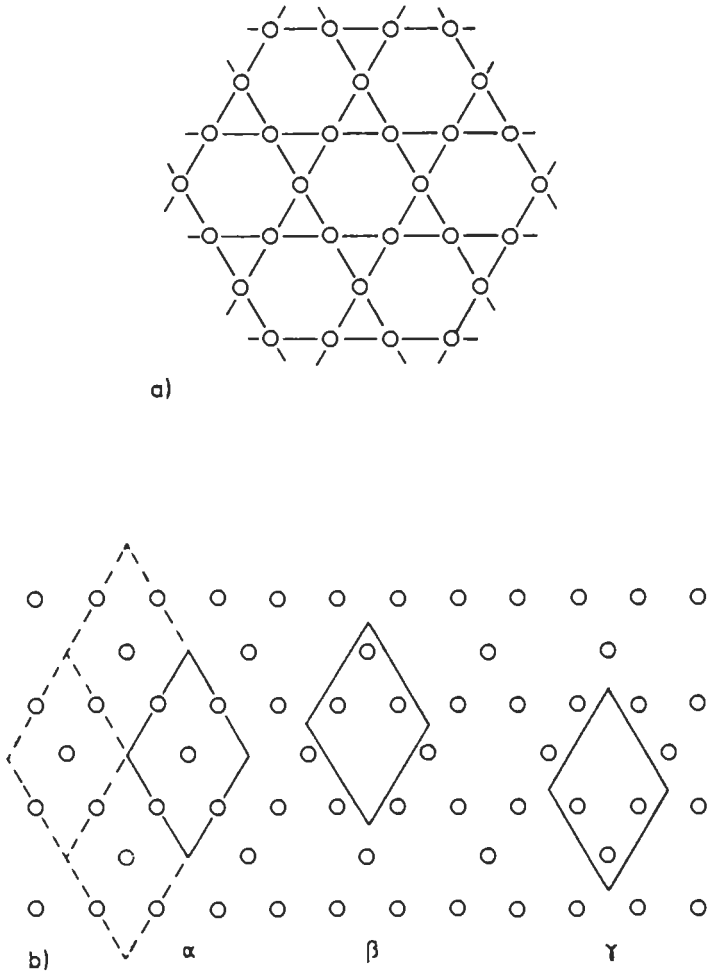

Fig. 10. The 3636 (kagomé) net of points.
The net is shown in a). In b) the different positions (relative to the hexagonal cell origin) are indicated by the symbols α, β, γ. Three points of the net are contained in the unit cell: notice that every point in an edge belongs to two adjacent cells.

— the *letter h* is assigned to a unit slab, whose neighbouring (above and below) unit slabs are displaced sideways, in the same direction for the same amount:
for instance ABABA or CBCBCB
hhh hhhh
(h comes from *hexagonal*: this is the stacking sequence of simple hexagonal structures such as hP2–Mg, hP4–ZnS wurtzite and hP12–$MgZn_2$ types).
— the *letter c*, on the other hand, is assigned to unit slabs whose neighbouring slabs

have different sideways displacements:
for instance ABCABC or CABCAB
cccc cccc
(c comes from *cubic*: this is the stacking sequence found in cubic structures such as cF4–Cu, cF8–ZnS sphalerite and cF24–Cu_2Mg types).

To denote the stacking sequence of the different structures it is sufficient to give only one identity period of the *h, c symbol series*. For instance:
cF4–Cu, c (instead of ABC); cF8–ZnS sphalerite, c; hP4–ZnS wurtzite, h; hP4–La, hc; hR9–Sm, hhc.

As can be seen from the previously reported examples, the identity period of the h, c symbols is generally shorter than the A, B, C... letter sequence. The h, c...symbols may be condensed, e.g., hcchcchchc to $(hcc)_2(hc)_2$. (If the number of c letters in a Jagodzinski symbol is divided by the total number of letters one obtains the percentage of "cubic stacking" in the total structure).

Another, common, *notation* for describing stacking of close-packed 3^6 nets (T nets) is that devised by ZHDANOV [1945] (a number notation equivalent to Jagodzinski's notation). A short description of the Zhdanov symbol is the following: a "+" is assigned if the order between a layer and its previous partner follows the sequence corresponding to any two subsequent layers in the face-centered cubic type structure, that is
A → B, B → C, C → A. Otherwise a "–" is assigned. For instance, the sequence "+++– – –" (shortened $3\underline{3}$) corresponds to ABCACB.

Finally, as another simple example of description (and symbolic representation) of structures in terms of layer stacking sequence we may now examine structures which can be considered as generated by *layer networks containing squares*. A typical case will be that of structures containing 4^4 *nets* of atoms (*Square net: S net*). The description of the structures will be made in term of the separation of the different nets (along the direction perpendicular to their plane) and of the origin and orientation of the unit cell).

Fig. 11 shows the different symbols (in this case numbers) suggested by PEARSON [1972] which will be used to indicate origin and orientation of the nets. These numbers will be reported as exponents of the symbols of the atoms forming the different nets. In this case too the relative height of the layers will be indicated by a fractional index. A few symbols of square net stacking sequences are the following:

Po_0^1: the simple cubic cell of Po (containing 1 atom in the origin) corresponds to a stacking sequence of type 1 square nets.

$W_0^1W_{1/2}^4$: the body-centered cubic structure of W (1 atom in 0,0,0 and 1 atom in $\frac{1}{2},\frac{1}{2},\frac{1}{2}$) corresponds to a sequence of type 1 and type 4 square nets at the heights 0 and $\frac{1}{2}$, respectively.

For more *complex polygonal nets*, their symbolic representation and use in the description, for instance, of the Frank-Kasper phases, see FRANK and KASPER [1958] and PEARSON [1972]. (Brief comments on this point will be reported in sec. 6.6.)

3.5.3. Assembly of polyhedra

A complementary approach to the presentation and analysis of the intermetallic phase

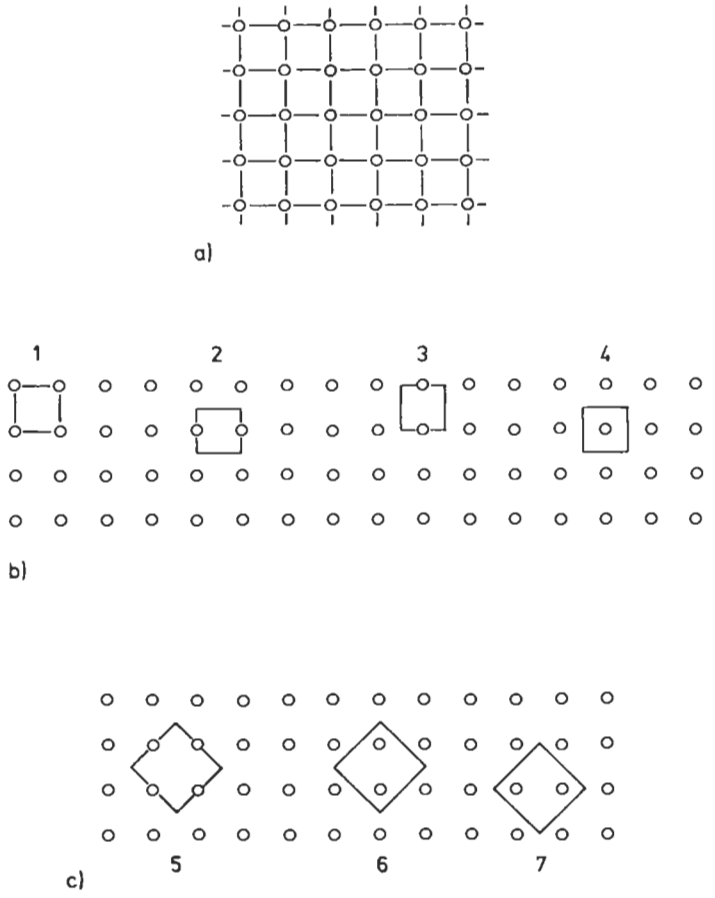

Fig. 11. A bidimensional square (4^4) net is shown in a).
b) Different positions of the representative point in the unit square are presented and coded (net of points aligned parallel to the cell edge).
c) Codes used for different positions of a square net of points referred to a larger square cell with axes at 45° to the net alignment (and edges equal to $\sqrt{2}$ times the repeat unit of the net).
In b) one point of the net is contained in the unit square, in c) there are two.

structures consists of their description with *coordination polyhedra* as *building blocks*.

A classification of types of intermetallic structures based on the coordination number, configurations of coordination polyhedra and their method of combination has been presented by KRIPYAKEVICH [1963].

According to Kripyakevich, a coordination polyhedron of an atom is the polyhedron, the vertices of which are defined by the atoms surrounding this atom: a coordination polyhedron should have a form as close as possible to a sphere, that is, it should be convex everywhere and have the maximum number of triangular faces. At the vertices of a coordination polyhedron of a given atom (in addition to atoms of different elements)

there can also be atoms of the same kind. A considerable variety of coordination polyhedra exists. In some cases, plane coordination polygons have to be considered. The number of vertices may vary from, say, 3 to 24. Generally, the structure consists of atoms with different coordination numbers; according to Kripyakevich, structures are most conveniently classified considering the type of coordination polyhedron of the atoms with the lowest coordination number. (For a general approach to the classification of atomic environment types and their description and coding in terms of coordination polyhedra see also sec. 7.2.7.).

An important contribution to the structure analysis of intermetallic phases in terms of the coordination polyhedra has been carried out by FRANK and KASPER [1958]. They described several structure types as the result of the *interpenetration* of a group of *polyhedra*, which give rise to a distorted tetrahedral close-packing of the atoms. (The Frank–Kasper structures will be presented in sec. 6.6).

In particular, SAMSON [1967, 1969] developed the analysis of the structural principles of intermetallic phases having giant unit cells. These structures have been described as arrangements of fused polyhedra rather than the full interpenetrating polyhedra (see a short description in sec. 6.6.5.).

The principles of describing structures in terms of *polyhedron-packing* has been considered by GIRGIS and VILLARS [1985]. To this end they consider, in a given structure, the coordination polyhedra of all the atomic positions; structures are then described by *packing* the *least* number of polyhedra types. All the atoms in the unit cell are included in the structure-building polyhedra. The *polyhedra considered should not penetrate each other.*

According to GIRGIS and VILLARS [1985] structures are then classified mainly on the basis of the following criteria:

— *Number of polyhedra types* employed in the description of the structure,
— *Characteristics of the polyhedra* (number of vertices, symmetry),
— *Types of polyhedra packing* (either *three-dimensional distribution of discrete polyhedra sharing corners, edges or faces,* or *layer-like distribution of polyhedra).*

As examples of structures described by *packing of one polyhedron type* we may mention:
cP4–$AuCu_3$ type, three-dimensional arrangement of cubooctahedra (coordination number, CN, 12);
tP30–σ(Cr,Fe) type, layer-like arrangement of icosahedra (CN 12).

For a general approach to the problem of *structure descriptions in term of polyhedron packing* a paper by HAWTHORNE [1983] should also be consulted. The following hypothesis is proposed: crystal structures may be ordered or classified according to the polymerization of those coordination polyhedra (not necessarily of the same type) with the higher bond valences. *The linkage of polyhedra to form "clusters"* is then considered from a graph-theoretic point of view. Different kinds of isomers are described and their enumeration considered. According to Hawthorne, moreover, it has to be pointed out that many classifications of complex structures recognize families of structures based on different arrangements of a fundamental building block or module (see the sec. 3.5.4. and

References: p. 363.

4.5. on recombination structures). *If this* building *module is a tightly bound unit* within the structure it could be considered, for instance, as the analogue of a molecule in an organic structure. Such *modules* can be considered the *basis of structural hierarchies* that include, for instance, simple and complex oxides and complex alloy structures. These modules may be considered as formed by polymerization of those coordination polyhedra that are most strongly bonded and may be useful for a classification and systematic description of crystal structures.

As a conclusion to this section we may mention also the "environment polyhedra", defined and coded by DAAMS *et al.* [1992]. A short decsription of this topic will be presented in sec. 7.2.7.

3.5.4. Modular aspect of crystal structure

A very general, mainly geometric, approach to the description and classification of the different inorganic structures may be based on a systematic "*construction of complex structural types" by means of a few operations applied to some building units*. As has been suggested by ANDERSSON and HYDE [1982, 1989] a formal description and classification of the various crystal structures could be obtained in terms of a classification of the *building units* and of the *construction mechanism*. Building units may correspond to *packets of points* (atoms) (blocks, clusters, bounded in three dimensions) or to *groups of lines* (rods, columns bounded in two dimensions, infinite in the third) or to *groups of planes* (slabs, sheets, layers, lamellae bounded in only one dimension, infinite in the other two). Structures may then be constructed from such portions by (discontinuous) symmetry operations (translation, reflection, or their combinations) repeated in a *parallel way* or by similar symmetry operations repeated in a cyclic way (involving rotation) (see, for instance, fig. 36).

Emphasis to similar approach has been given by ZVYAGIN [1993]. He pointed out that many crystal structures can be represented as a composite of certain standard "*construction modules*" and various combinations, distributions and arrangements of them. The simplest example of a modular structures is the densest packing of identical atoms (the atomic planes represent the construction modules forming various structures owing to a variation of the two possible placements of the successive plane relative to the preceding one).

A classification of the different structures may be based on:

— *module types* (sheets, rods, blocks),
— *dimension* of the modules,
— *variety* of module type (single or mixed-module structures),
— *relative number* of module types,
— *arrangement* of adjacent modules (*variations* in these arrangements, *periodicity/aperiodicity* of successive variations, etc.).

Strictly related to this kind of description may be the concepts of "*Recombination Structures*" and of "*Intergrowth Structure Series*" which will be presented in sec. 4.5.

3.5.5. An exercise on the use of alternative structural notations ($AuCu_3$ type as an example)

In the following, data concerning a few selected structures, will be presented. In this section, by using a simple structural type (cP4–$AuCu_3$, $3^3_\infty3[Au_{6/6}][Cu_{8/8}]_{12/4}$, or, in more detail, $3^3_\infty3[Au_{6o/6o}][Cu_{8p/8p}]_{12co/4l}$) a presentation will be given on the different ways of describing the structure.

$AuCu_3$ is primitive, cubic. The space group is $Pm\bar{3}m$ (N. 221 in the International Tables for Crystallography, HAHN [1989]). In the unit cell there are 4 atoms in the following positions:

1 Au in a) 0,0,0;
3 Cu in c) $0,\frac{1}{2},\frac{1}{2}$; $\frac{1}{2},0,\frac{1}{2}$; $\frac{1}{2},\frac{1}{2},0$;

Several phases are known which have this structure; in the VILLARS and CALVERT compilation [1991] there are around 450 listed: 1.7 % of all the reported phases. This structural type is the 8th in the frequency rank order (see sec. 7.1.). A short selection is presented in the following list:

≈$HfPt_3$ a = 398.1 pm	Pt_3Al a = 387.6 pm.
$LaIn_3$ a = 473.21 pm	Ti_3Hg a = 416.54 pm
La_3In a = 509.0 pm	$TiZn_3$ a = 393.22 pm
Mn_3Pt a = 383.3 pm	UPb_3 a = 479.3 pm
$MnZn_3$ a = 386 pm	YAl_3 a = 432.3 pm
Ni_3Al a = 357.0 pm	Y_3Al a = 481.8 pm

(Note that, in this structure type, in some cases, according to the phase stoichiometry, the same element may occupy either the a) or the c) Wyckoff position).

In the reported list the unit cell edges have been given. In the following, while discussing the characteristics of this structural type, we will consider the data referring to the prototype itself (a = 374.84 pm).

The structure is shown in fig. 12, where the tridimensional sequence of the atoms is suggested by presenting a small group (eight) of contiguous cells. The unit cell itself is shown in figs. 13a and 13b, by using two different drawing styles.

The subsequent figures 14a, 14b, 14c, 14d correspond to an analysis of the structure carried out in order to show the different local atomic arrangements (coordinations around the atoms in the two crystal sites).

In the analysis of a structure, however, it is also necessary to take into consideration the values of the *interatomic distances*. It may be useful to consider both absolute and so called "reduced" values of the interatomic distances. In the case of the $AuCu_3$ phase, the minimum interatomic distance corresponds to the Au-Cu distance (Au in 0, 0, 0 and Cu in $0,\frac{1}{2},\frac{1}{2}$) which is the same as the Cu–Cu distance between Cu in $0,\frac{1}{2},\frac{1}{2}$ and Cu in $\frac{1}{2},0,\frac{1}{2}$. This distance is given by $a\sqrt{2}/2$.

For the $AuCu_3$ phase a = 374.8 pm and, therefore, d_{min} = 265.0 pm. This value could be compared, for instance, to the value 272 pm, sum of the radii of Cu and Au (as defined for a coordination number of 12) or to the value 256 pm of the Cu–Cu distance in the metal (Cu atom "diameter"). *Reduced interatomic distances* ($d_r = d/d_{min}$) may be defined as the ratios of the actual distance values to the minimum value.

References: p. 363.

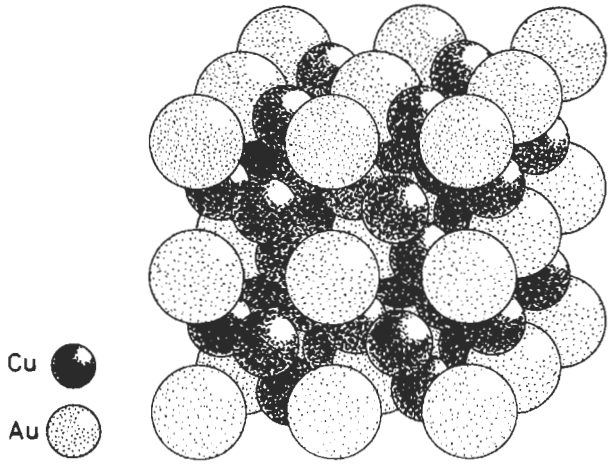

Fig. 12. cP4–$AuCu_3$ type structure. A group of eight cells is shown. The light spheres represent Au atoms. In order to get a better view of the structure inside, the atomic diameters are not to scale.

A first set of interatomic distances (and coordination) which can be considered in the $AuCu_3$ phase is that corresponding to the Au coordination around Au atoms (see fig. 14a):

Considering as the *reference atom*, the atom Au in 0,0,0, the next neighbours Au atoms are the six Au shown in fig. 14a, corresponding to the same Wyckoff position and having, in comparison with the reference atom, the coordinates 0,0,1; 0,0,$\bar{1}$; 0,1,0; 0,$\bar{1}$,0; 1,0,0; $\bar{1}$,0,0; all at a distance $d = a = 374.8$ pm, corresponding to a reduced distance $d_r = d/d_{min} = 1.414$.

In the same group of Au–Au interatomic distances a subsequent set is represented by distances such as those between $Au_{0,0,0}$ and $Au_{0,\bar{1},1}$ (or $Au_{0,\bar{1},\bar{1}}$, $Au_{0,1,\bar{1}}$, $Au_{1,0,1}$, etc.). This set corresponds to a group of 12 atoms (all at an absolute distance of $a\sqrt{2} = 530.1$ pm, that is, at a reduced distance $d_r = d/d_{min} = 2.000$).

A compact representation of these data is given by means of the bar-graph in fig. 15a).

A second set of interatomic distances (and coordination) corresponds to the Cu coordination around Au atoms:

Considering as the *reference atom*, the atom Au in 0,0,0, the next neighbours Cu atoms are the 12 Cu reported in fig. 4–14b, in the coordinates: $0,\frac{1}{2},\frac{1}{2}$; $0,\frac{1}{2},\frac{\bar{1}}{2}$; $0,\frac{\bar{1}}{2},\frac{1}{2}$; $0,\frac{\bar{1}}{2},\frac{\bar{1}}{2}$; $\frac{1}{2},0,\frac{1}{2}$; $\frac{1}{2},0,\frac{\bar{1}}{2}$; $\frac{\bar{1}}{2},0,\frac{1}{2}$; $\frac{\bar{1}}{2},0,\frac{\bar{1}}{2}$; $\frac{1}{2},\frac{1}{2},0$; $\frac{1}{2},\frac{\bar{1}}{2},0$; $\frac{\bar{1}}{2},\frac{1}{2},0$; $\frac{\bar{1}}{2},\frac{\bar{1}}{2},0$; all at a distance $d = a\sqrt{2}/2 = 265.1$ pm, corresponding to a reduced distance $d/d_{min} = 1.000$.

Considering also the subsequent sets of Au–Cu distances, 24 atoms at $d = 459.1$ pm ($d_r = d/d_{min} = \sqrt{3} = 1.732$), 24 Cu at $d = 592.7$ pm ($d_r = 2.236$), etc. we obtain the histogram reported in fig. 15b.

A third group of interatomic distances (and coordination) which has to be considered is that corresponding to the Cu coordination around Cu atoms (see fig. 14c):

Considering as the *reference atom*, the atom Cu in $\frac{1}{2},\frac{1}{2},0$, the next neighbours Cu

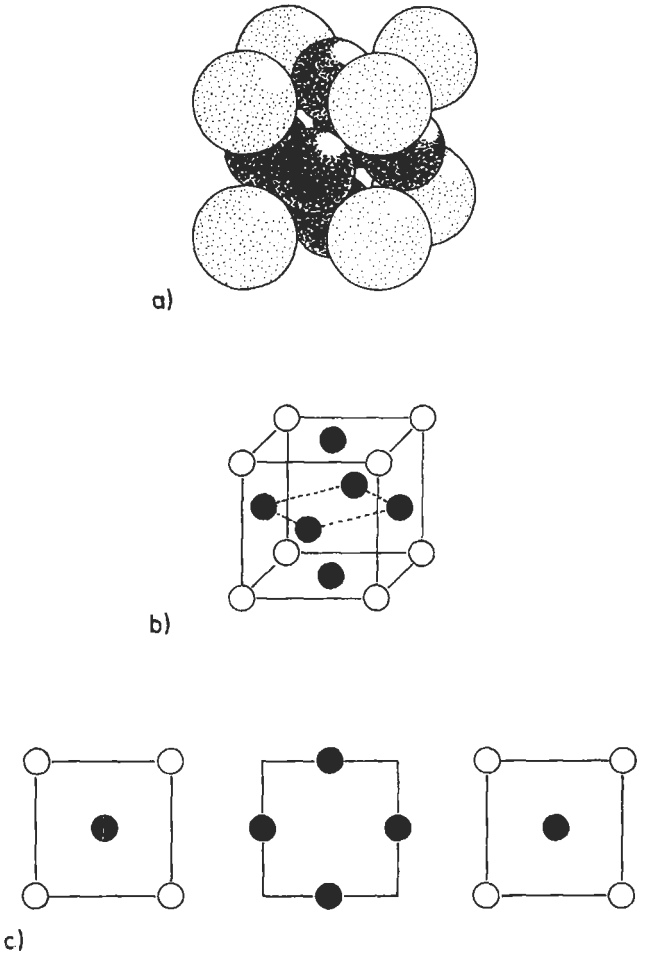

Fig. 13. The cP4–$AuCu_3$ unit cell is presented in different drawing styles. In a) an (approximate) indication of the packing and space filling is given. In b) the positions of the different atoms are reported in a perspective view of the unit cell and in c), in some typical sections of the same at different heights: notice the square net arrangement. The first (and the third) section corresponds to the height 0 or 1 * c. The second to the height $\frac{1}{2}$ * c. For the first section the position codes of the two atoms, in the square net, are 1 and 4; for the second the code is 5. (Compare with fig. 11.)

atoms are the 8 Cu atoms in $\frac{1}{2},0,\frac{1}{2}$; $0,\frac{1}{2},\frac{1}{2}$; $1,\frac{1}{2},\frac{1}{2}$; $\frac{1}{2},1,\frac{1}{2}$; $\frac{1}{2},0,\bar{\frac{1}{2}}$; $0,\frac{1}{2},\bar{\frac{1}{2}}$; $1,\frac{1}{2},\bar{\frac{1}{2}}$; $\frac{1}{2},1,\bar{\frac{1}{2}}$; all at a distance $d = a\sqrt{2}/2 = 265.1$ pm, corresponding to a reduced distance $d/d_{min} = 1.000$.

The subsequent sets of Cu–Cu distances correspond to 6 Cu atoms (in coordinates such as $\frac{1}{2},\frac{1}{2},1$; $\frac{1}{2},\frac{1}{2},\bar{1}$; $\frac{3}{2},\frac{1}{2},0$; etc.) at a distance $d = 374.8$ pm ($d_r = 1.414$), 16 Cu atoms at $d = 459.1$ pm ($d_r = 1.732$), 12 Cu atoms at $d = 530.1$ pm ($d_r = 2.000$), 16 Cu atoms at 592.7 pm ($d_r = 2.236$), etc. The corresponding histogram is presented in fig. 15c).

References: p. 363.

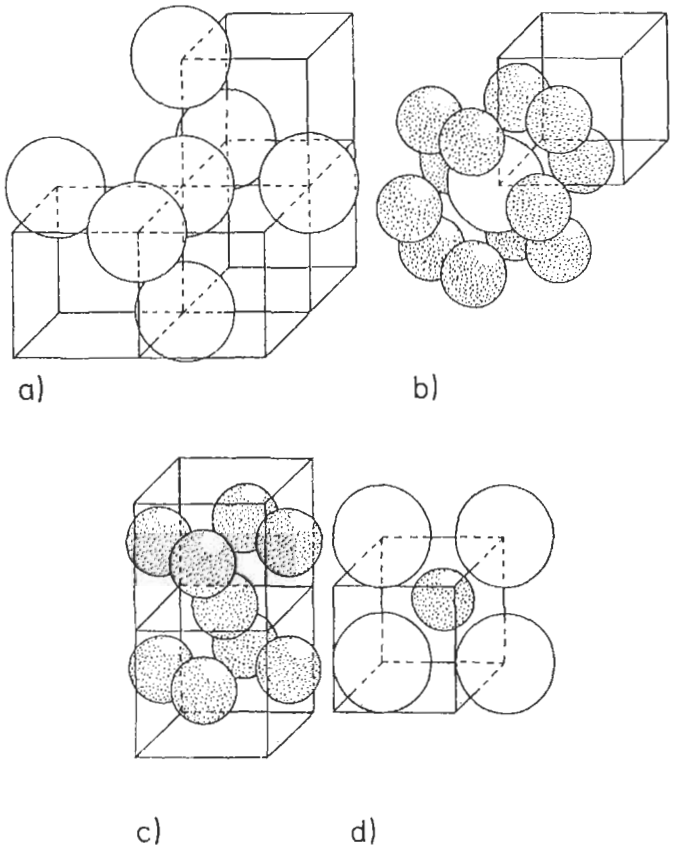

Fig. 14. cP4–$AuCu_3$ type structure. Different fragments of the structure (of a few unit cells) are presented in order to show the various typical coordinations. (Cu atoms are represented by small dotted spheres)
a) Au – 6 Au (octahedral); b) Au – 12 Cu (cuboctahedral);
c) Cu – 8 Cu (tetragonal prismatic); d) Cu – 4 Au (square).
The 8 Cu+4 Au at the same distance from Cu form a heterogeneous cuboctahedron. (Compare also with fig. 25.)

The fourth (and last) type of interatomic distances (and coordination) characteristic of the $AuCu_3$ structure is given by Au coordination around Cu atoms (see fig. 14d).

Considering as the *reference atom* one of the three equivalent atoms Cu in c), for instance, the atom in $0,\frac{1}{2},\frac{1}{2}$, the next neighbours Au atoms are 4 Au in 0,0,0; 0,0,1; 0,1,0; 0,1,1, respectively; all at a distance $d = a\sqrt{2}/2 = 265.1$ pm, corresponding to a reduced distance $d/d_{min} = 1.000$.

Subsequent sets of Cu–Au distances correspond to a group of 8 Au atoms (in coordinates such as 1,0,0; 1,0,1; 1,1,0; etc.) at a distance $d = 459.1$ pm (reduced distance $d/d_{min} = 1.732$), to a group of 8 Au (in coordinates such as $0,0,\bar{1}$; $0,1,\bar{1}$; 0,0,2; etc.), at a